DAMPING OF LAYERED AND JOINTED BEAMS WITH RIVETED JOINTS

Ramesh Chandra Mohanty

DEPARTMENT OF MECHANICAL ENGINEERING
NATIONAL INSTITUTE OF TECHNOLOGY
ROURKELA - 769008, ORISSA, INDIA

AUGUST 2010

DAMPING OF LAYERED AND JOINTED BEAMS WITH RIVETED JOINTS

A THESIS SUBMITTED TO THE
NATIONAL INSTITUTE OF TECHNOLOGY, ROURKELA
IN PARTIAL FULFILMENT OF THE REQUIREMENTS
FOR THE DEGREE OF

DOCTOR OF PHILOSOPHY

IN

MECHANICAL ENGINEERING

BY

Ramesh Chandra Mohanty
(Roll- 50703001)

UNDER THE GUIDANCE OF

Prof. Bijoy Kumar Nanda

DEPARTMENT OF MECHANICAL ENGINEERING
NATIONAL INSTITUTE OF TECHNOLOGY
ROURKELA - 769008, ORISSA, INDIA

AUGUST 2010

Department of Mechanical Engineering
National Institute of Technology
Rourkela-769008, Orissa, India

Certificate

This is to certify that the thesis titled "**Damping of Layered and Jointed Beams with Riveted Joints**" being submitted to the National Institute of Technology Rourkela by **Mr. Ramesh Chandra Mohanty** for the award of the degree of **Doctor of Philosophy (Mechanical Engineering)** is a record of bonafide research work carried out by him under my supervision and guidance. Mr. Mohanty has worked for more than three and half years on the above problem and the work has reached the standard fulfilling the requirements and regulations for the degree. To the best of my knowledge, the work incorporated in this thesis has not been submitted in part or full to any other University or Institute for the award of any degree or diploma.

Rourkela (Prof. Bijoy Kumar Nanda)
Date: Supervisor

Acknowledgement

First and foremost, I express my deep sense of indebtedness and gratitude to Dr. B.K. Nanda, Professor, Department of Mechanical Engineering, National Institute of Technology, Rourkela for kindly providing me an opportunity to work under his supervision and guidance. His keen interest, invaluable guidance and immense help have helped for the successful completion of the thesis.

I express my sincere thanks to Prof. S.K. Sarangi, Director, NIT, Rourkela for creating healthy working environment in the campus and giving permission to use the facilities available in the institute for this study.

I would also like to thank Prof. R.K. Sahoo, Head of the Department, Prof. K.P. Maity, Prof. K.B. Mohanty, Prof. N. Kavi, Prof. C.K. Biswas, Prof. Alok Satapathy, Prof. R.K. Behera and other faculty and staff members of the department for their help and cooperation during the progress of the work. I am immensely grateful to Dr. S.C. Mohanty, Professor-in-charge of Dynamic Laboratory and his staffs for their cooperation and support in conducting the experiments.

I also acknowledge the help extended by my colleagues Mr. Bhagat Singh, Mr. A.K. Rout, Mr. B.N. Padhi and Mr. L.N. Patra of the department for providing friendship, moral support and good times during the course of this work.

Special thanks to my parents and uncle for their love, affection and understanding.

I wish to thank my wife Lisa for sharing all the good and bad moments and for her love, sacrifice and understanding. Without her full support and encouragement, this thesis would not have been brought to completion.

Last but not the least, I owe to God for giving me strength in overcoming the pain for the brain hemorrhage incurred to my wife during the course of the research work.

This thesis is dedicated to my beloved son Suryansh. I love him more than I can express.

(Mr. Ramesh Chandra Mohanty)

Abstract

The present investigation highlights the effect of interfacial slip on the damping of layered cantilever beams jointed with rivets undergoing free vibration. The inclusion of mechanical joints bears a strong influence in the overall system performance and behavior, particularly the damping level of the structures. In fact, the damping and its improvement in machines or structures are one of the biggest challenges to the practicing engineers. Usually, such structures inherently possess low structural damping necessitating the introduction of additional measures to improve their damping characteristics in order to control the harmful effects of vibration in normal operating conditions. Monolithic structures can be used as an alternative, but unfortunately these are very poor in damping capacity and are not cost-effective. One of the techniques used in the present problem for improving damping is fabricating these structures in layers by means of riveted joints. The incorporation of such joints is the major source of energy dissipation through frictional effects associated with relative shear displacements at the interfaces of the various structural members. Most of the damping in built-up structures is thus attributed to micro-slip at the interfaces. The contribution of the micro-slip on the overall system damping is always significant in spite of its low magnitude.

This thesis consists of two different parts: a theoretical analysis of the problem and an experimental work. The theoretical analysis proposes two different methods to calculate damping: *classical method* and *finite element method*. The analyses are based on the assumptions of Euler-Bernoulli beam theory as the dimensions of test specimens satisfy the criterion of thin beam theory. In the first case, a continuous model is characterized by a partial differential equation with respect to spatial and time coordinates. An analytical exact solution is obtained for the above differential equation from which the dynamic characteristics of the structure are represented accurately. In the latter case, the model is represented by one-dimensional beam elements with each element consisting of two nodes with two degrees of freedom, i.e. transverse displacement and rotation at each node. This model is approximate and characterized by stiffness and mass matrices from which natural frequencies and mode shapes are obtained by modal analysis. As the direct evaluation is not easy, an alternate energy approach has been used to derive the damping matrix.

It is a general fact that the theoretically computed results will differ from the actual values due to the assumptions made in the theoretical analyses. In view of this discrepancy in results, experiments are conducted for different set of mild steel and aluminium specimens under different vibrating conditions. The logarithmic decrement technique has been used for measuring the damping from the time history curve of the decaying signals recorded on the screen of digital storage oscilloscope. The experimental results are compared with the corresponding theoretical ones for establishing the authenticity of the theory developed. Finally, useful conclusions have been drawn from both the theoretical and experimental results.

The damping characteristics in jointed structures are influenced by the intensity of pressure distribution, micro-slip and kinematic coefficient of friction at the interfaces and the effects of all these parameters on the mechanism of damping have been extensively studied. All the above vital parameters are largely influenced by the thickness ratio of the beam and thereby affect the damping capacity of the structures. In addition to this, number of layers, cantilever length and diameter of connecting rivet also play key roles on the damping capacity of the jointed structures quantitatively. The effects of all these parameters are studied vividly in the present investigation. It is established that the damping capacity can be enhanced appreciably using larger cantilever length and rivet diameters as well as lower thickness ratio of the beams. Further improvement in damping is possible with the use of more number of layers compared to its equivalent solid one. This design concept of using layered structures with riveted joints can be effectively utilized in trusses and frames, aircraft and aerospace structures, bridges, machine members, robots and many other applications where higher damping is required.

CONTENTS

List of Figures

List of Tables

Nomenclature

English Symbols

A	Area of cross-section of the beam
A_o	Area of cross-section of the rivet
A'	Area under a connecting rivet head
d	Diameter of connecting rivet
$\boldsymbol{d}^e$	Nodal displacement vector of an element
$\boldsymbol{D}$	Global displacement vector
$\ddot{\boldsymbol{D}}$	Global acceleration vector
E	Static bending modulus of elasticity
E_f	Energy loss per cycle due to friction at joints
E_{loss}	Total energy loss per cycle
E_n	Energy stored in the system per cycle
E_o	Energy loss per cycle due to material and support friction
F_{rM}	Maximum frictional force at the interfaces
$2h_1$, $2h_2$	Thickness of each layer of the cantilever specimen
I	Second moment of area
k	Static bending stiffness of the layered and jointed beam
k'	Static bending stiffness of the solid beam
$\mathbf{k}^e$	Element stiffness matrix
$\mathbf{K}$	Global stiffness matrix
l	Length of individual elements
L	Free length of the layered and jointed beam
m	Number of layers in a jointed beam

$\mathbf{m}^e$	Element mass matrix
$\mathbf{M}$	Global mass matrix
n	Number of finite elements
N	Total normal force under each connecting rivet
p	Interface pressure
P	Preload on a rivet
q	Number of rivets
R	Any radius within influencing zone
R_B	Radius of the connecting rivet
R_M	Limiting radius of influencing zone
S_1, S_2, S_3, S_4	Cubic shape functions
t	Time coordinate
u_o	Relative dynamic slip between the interfaces at a riveted joint in the absence of friction
u_r	Relative dynamic slip between the interfaces at a riveted joint in the presence of friction
u_{rM}	Relative dynamic slip between the interfaces at the maximum amplitude of vibration
v_1, v_2	Transverse displacement at the nodes of an element
w	Galerkin's weighting function
W	Static load
x_1, x_{z+1}	Amplitude of first cycle and last cycle, respectively
$y(l, 0)$	Initial free end displacement
z	Number of cycles

Greek Symbols

α	Dynamic slip ratio (u_r/u_o)
δ	Logarithmic decrement of the system
δ_f	Logarithmic decrement due to interface friction
δ_o	Logarithmic decrement due to internal and support friction
Δ	Deflection due to static load
μ	Kinematic coefficient of friction
ω_n	Natural frequency of vibration
ω_d	Damped frequency of vibration
$\boldsymbol{\phi}$	Eigenvector or modal displacement
ρ	Mass density
σ_o	Initial stress on a rivet
σ_S	Surface stress on the jointed structure
θ_1, θ_2	Slope at the nodes of an element
ξ	Damping ratio

Superscripts

e	Element

Operators

‘.’	$\frac{d}{dt}$
‘,’	$\frac{d}{dx}$
T	Transpose of a matrix

CHAPTER 1

INTRODUCTION

1.1Background

Problems involving vibration occur in many areas of mechanical, civil and aerospace engineering. Engineering structures are generally fabricated using a variety of connections such as bolted, riveted, welded and bonded joints etc. The dynamics of mechanical joints is a topic of special interest due to their strong influence in the performance of the structure. Further, the inclusion of these joints plays a significant role in the overall system behavior, particularly the damping level of the structures. However, the determination of damping either by analysis or experiment is never straightforward owing to the complexity of the dynamic interaction of components. The estimation of damping in beam-like structures with passive damping approach is the essential problem addressed by the present research.

Although the vibration is an age old problem, the demands for today's engineering have led to a steady increase of interest in recent years. In some structures, such as vibratory conveyors and compactors, vibration is encouraged, but these are special cases. However, in most structures, the vibration is not desirable and the interest lies in reducing it by dissipating the vibration energy. This is because uncontrolled vibration creates dynamic stresses and strains which can cause fatigue failure in structures, fretting corrosion between contacting elements and noise in the environment [1]. Also it can impair the function and life of the structures or its components.

The knowledge of structural dynamics is very essential to make accurate predictions under a variety of circumstances. The final purpose of the structural design is to control the vibration of structures at a desirable level. In most cases, the vibration level should be kept as low as possible so that the performance and the cost of the structure are not severely affected. In practice, the excitation can only be reduced, but it is almost impossible to eliminate completely. When a structure with low inherent damping is excited at one of its natural frequencies, violent vibration is inevitable. This causes serious problems leading to ultimate failure of the structures. Therefore,

an engineering structure must be designed so that the response of a structure under external excitation does not exceed a permitted level.

If the frequency of the external force coincides with one of the natural frequencies of the system, a condition known as *resonance* occurs resulting in undesirable large oscillations. Failures of most structures are associated with the occurrence of resonance. In case of free vibration, the amplitude is maximum at the start of motion and goes on decreasing to zero with the passage of time. The rate of decrease in the amplitude depends on the amount of damping. Immediately after the free vibration is initiated, higher modes are damped out leaving the system to vibrate especially at its fundamental mode and the damping for this mode can be computed from the decay rate of vibration amplitudes. In practice, all infinite number of natural frequencies and mode shapes are not significant and typically higher modes are neglected [2].

The damping and its improvement in structural applications poses the biggest challenge to the practicing engineers. Usually, such structures possess both low structural weight and damping. This situation calls for use of additional measures to improve the damping characteristics by dissipating more energy. However, increasing the damping in a structure is not always easy and may cause waste of energy during normal operating conditions. The monolithic structures can be used as a replacement, but unfortunately these are very poor in damping capacity and are not cost-effective. One of the techniques used for improving damping is fabricating these structures in layers by means of joints which provide suitable means of energy dissipation. The introduction of joints promotes the flexibility of the assembled structure and contributes adequately to the damping properties. The low material damping of assembled structures are thus compensated. Therefore, the use of joints is becoming increasingly significant in most of the engineering applications.

However, the use of joints has its own drawbacks causing fretting corrosion at the interfaces, reducing stiffness and presenting difficulty in analysis due to nonlinearity [2, 3]. Beards [4] has pointed out that any loss of static stiffness of a structure will not necessarily affect the integrity of the structure if the joints are carefully designed. The effect of friction joints on the reduction of vibration level have attracted great interests from many researchers in the past and present [5-12] and a detailed discussion is corroborated in the next chapter.

Friction damping takes place whenever two surfaces experience relative motion in the presence of friction. In case of a jointed structure, the relative motion between contacting layers is a function of normal load which arises from the tightening of the joints holding the components. When the joint is very loose, the normal load is insignificant and the contact surface experiences pure slip. Since no work is required to be done against friction, no energy is dissipated. On the other hand, when the joint is very tight, high normal loads cause the whole contact interface to stick. This results in no energy dissipation again since no relative motion is allowed at the interfaces. For normal loads lying between these two extremities, energy is dissipated and the maximum value of energy dissipation occurs within this range.

A feature common to all joints is that they dissipate energy when subjected to vibration. In practice, the joint effects can be very significant on the response of a fabricated structure. As pointed out by Beards [4], up to 60% of the deformation and 90% of the damping in a fabricated structure arises from various joints. Neglecting these effects can make the prediction on the property of the whole structure inaccurate or even unreasonable. Clearly, establishment of proper joint models is of great importance in accurate prediction of the dynamic behavior of the structures. Even though most of the inherent damping occurring in real structures arises in the structural joints, little effort has been made to study this source of damping. This is because the energy dissipation mechanism is a complex phenomenon being largely influenced by the interface pressure, coefficient of friction and relative slip at the interfaces. Proper assessment of these influencing parameters is very much essential in determining the damping capacity correctly.

The contact pressure between the surfaces is generated by the clamping action of the joints and plays a vital role in the joint properties. Under such circumstances, the profile of the interface pressure distribution assumes a significant role, especially in the presence of slip for dissipation of vibration energy. This pressure is not uniform across the interface; rather it is maximum at the joint and decreases radially with the distance away from the joint. Due to this uneven pressure distribution, a local relative motion termed as micro-slip occurs at the interfaces of the connecting members.

The presence of friction in connecting joints has a strong impact on the system dynamics and largely contributes to the majority of the damping capacity of the

system. It is understood that the joint friction arises only when the contacting layers tend to move relatively under the action of transverse vibration and serves as a catalyst for energy dissipation. For most analyses, the Coulomb's friction law is widely used to represent the dry friction at the contacting surfaces. Many authors have carried out an elaborate review of research on the effects of joint friction on structural damping in built-up structures [13-18].

Micro-slip is the normal mechanism by which mechanical joints dissipate energy and therefore, a better understanding of its phenomenon is required for the study of damping effects in the jointed structures. The micro-slip at the interfaces of the connecting members as shown in Fig. 1.1 occurs only at lower excitation levels. When the excitation level is increased, both micro- and macro-slips occur at the jointed interfaces. Usually, the macro-slip is avoided as it leads to structural damage of the joints. The contribution of the micro-slip on the overall system damping is significant in spite of its low magnitude and is generally promoted in structural joint designs.

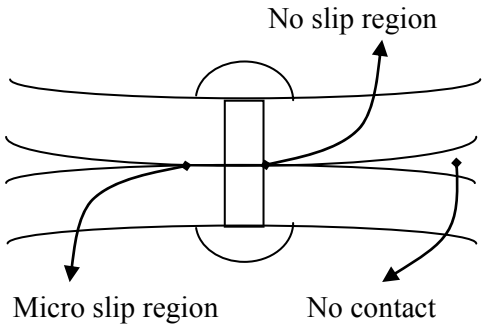

Fig. 1.1 Mechanism of micro-slip at the jointed interface

The energy dissipated in most real structures is often very small, so that an un-damped analysis is sometimes realistic. When the damping is significant, its effect must be included in the analysis particularly when the dynamic study of a structure is required. The origin and mechanism of damping are complex and sometimes difficult to comprehend. The energy of the vibrating system is dissipated by various mechanisms and often more than one mechanism may be present at the same time. Although the knowledge on the friction joint is limited, efforts have been put in the present investigation to study the damping aspect of the friction joints in built-up structures.

1.2 Motivation

Built-up structures are generally fabricated using many types of fasteners such as bolted, riveted and welded joints. It is the well known fact that the improvement in damping due to the provision of welded joints is not appreciable compared to the use of bolted or riveted joints [19]. Therefore, the use of welded joints is usually avoided in structural applications where higher damping is the main criterion. In case of bolted and riveted joints, the fundamental mechanism of damping may be same, but they differ in their functional aspects. For example, the parameters such as interface pressure distribution characteristics, zone of influence and preload are not same in both cases. Since the zone of influence differs in both cases, the relative spacing among the joints will be different thereby changing the relative dynamic slip at the interfaces. These facts suggest that the damping action for both cases is not same. Further, the axial load on a bolt can be varied by applying the tightening torque as per the clamping requirements of the structure whereas the preload in a rivet is constant and cannot be changed in the latter part of the design.

Although, a lot of analytical, computational and experimental works have been carried out by several researchers in the recent past on the damping of bolted structures, but no substantial work has been reported till date on the damping capacity of riveted structures. The motivation for the present investigation lies in estimating the damping in jointed beams connected with rivets through the analytical and experimental studies and exploring the possibilities of improving the damping.

1.3 Linear Problem

Most structural problems are studied based on the assumption that the structure to be analyzed is either linear or nonlinear. In linear systems, the excitation and response are linearly related and their relationship is given by a linear plot as shown in Fig. 1.2. For many cases, this assumption is more often valid over certain operating ranges. Working with linear models is easier from both an analytical and experimental point of view. For a linear system, the principle of superposition holds which means that doubling the excitation will double the levels of the response. For beams undergoing small displacements, linear beam theory is used to calculate the natural frequencies, mode shapes and the response for a given excitation.

It is very clear from Fig. 1.2 that the linear and nonlinear systems agree well at small values of excitation, while they deviate at higher levels. The nonlinear beam theory is used for larger displacements where the superposition principle is not valid [20]. The linear vibration theory is used when the beam is vibrated at small amplitudes and lower modes of vibration [2]. The present investigation mainly focuses on the study of damping of jointed cantilever beams at lower excitation levels which can be well considered as linear.

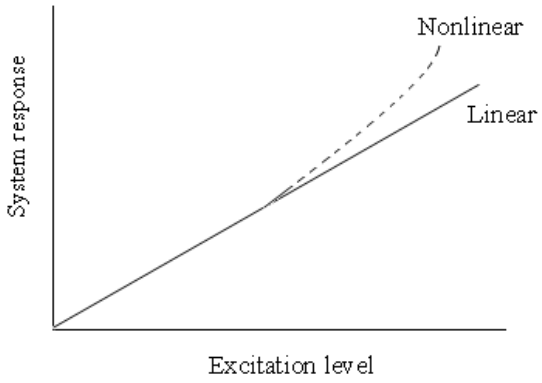

Fig. 1.2 Comparison of Linear and nonlinear systems

1.4 Beam Theories

The beam is one of the fundamental elements of an engineering structure and finds application in structural members like helicopter rotor blades, spacecraft antennae, flexible satellites, airplane wings, gun barrels, robot arms, high-rise buildings, long-span bridges, etc. These beam-like structures are typically subjected to dynamic loads. Therefore, studying the static and dynamic response, both theoretically and experimentally, of these structural components under various loading conditions would help in understanding and explaining the behavior of more complex and real structures.

The popular beam theories in use today are: (a) Euler-Bernoulli beam theory and (b) Timoshenko beam theory. Dynamic analysis of beams is generally based on one of the above beam theories. If the lateral dimensions of the beam are less than one-tenth of its length, then the effects of shear deformation and rotary inertia are neglected for the beams vibrating at low frequency [21]. The no-transverse-shear assumption means that the rotation of cross section is due to bending alone. A beam based on such conditions is called Euler-Bernoulli beam or thin beam.

If the cross-sectional dimensions are not small compared to the length of the beam, the effects of shear deformation and rotary inertia are to be considered in the analysis. Timoshenko [22-24] included these effects and obtained results in accordance with the exact theory. The procedure presented by Timoshenko is known as thick beam theory or Timoshenko beam theory.

The present investigation is based on the assumptions of Euler-Bernoulli beam theory as the beam is vibrated at low frequency and the dimensions of test specimens are much smaller in the lateral directions compared to length, thus satisfying the condition of thin beam theory.

1.5 Modeling of a Structure

It is essential to have a theoretical model to represent a structure in order to study its dynamic characteristics. Theoretical modeling of the present problem considers two approaches using the Euler-Bernoulli beam theory: *continuous model* approach and *finite element model* approach. Both these approaches are used in the present investigation.

A continuous model is characterized by a partial differential equation with respect to spatial and time coordinates which is often used for studying simple structures such as a uniform beam. Exact solutions of such equations are possible only for a limited number of problems with simple geometry, boundary conditions and material properties.

However, real-life engineering structures are generally very complex in geometry, boundary conditions and material properties. For this reason, normally some kind of other approximate method is needed to solve a general problem. In contrast to the continuous model, the system is characterized by a finite element model which consists of many one-dimensional small elements with each element consisting of two nodes with two degrees of freedom, i.e. transverse displacement and rotation at each node. In this case, the equations of motion are expressed by a set of coupled *ordinary-differential equations*.

For a linear structure, the model is to be established by using experimental measures besides theoretical modeling. Several experimental techniques are in use to quantify

the level of damping in a structure. The most popular experimental techniques are the frequency and time domain approaches. The frequency domain analysis is based on frequency response and forced vibration is the main concept behind this method [25]. The time domain methods are based on the observation of the time history of energy dissipation which results in the decay of amplitude of oscillation and applied equally to free as well as forced vibration problems. As the time domain approach for measuring damping has been used in the present analysis, more elaborative discussion is presented for this method in the succeeding chapters.

The classical logarithmic decrement method is very popular for measuring damping in the time domain. This method is mostly used for free vibration response of a lightly damped linear system having low and medium frequency range [26]. In this method, the damping is measured for a single frequency oscillation directly from the decay of the system response. It is established that this method is equally applicable to single as well as multiple degrees of freedom systems. In case of multiple degrees of freedom systems, the damping for each mode is separately determined if the decay of initial excitation takes place primarily in one mode of vibration [27]. Many authors have conveniently used this technique for estimating damping in their research works in the past and present [28-31].

1.6 Aims and Objectives of this Research

Damping is an important issue in analyzing the dynamic systems. The estimation of damping in engineering structures has been interesting and promising topic in both analytical and experimental aspects and its improvement poses the biggest challenge to the practicing engineers. Usually, most structures possess low structural damping necessitating the introduction of additional measures to improve their damping characteristics. The technique used in the present investigation is by fabricating the structure in layers incorporating joints for improving the damping. The inclusion of joints is the major source of energy dissipation through frictional effects associated with relative shear displacements at the interfaces of the structural members.

The research presented in this thesis is devoted to the problem of damping estimation in engineering structures, typically layered cantilever beams jointed with rivets, through analytical and experimental work. The prime reason for selecting rivets as compared to welding or bolting is that the riveted connections are largely used in

structural designs. For example, trusses, aircraft, pressure vessels, robots and many other applications use riveted joints in one form or another. The analyses are based on the assumptions of Euler-Bernoulli beam theory as the dimensions of test specimens satisfy the criterion of thin beam theory and the beam is vibrated at low frequency. Further, this study is mainly confined to the freely damped linear vibrating systems at their first mode subjected to low initial excitation.

The damping characteristics in jointed and riveted structures are influenced by the intensity of pressure distribution, relative dynamic slip and kinematic coefficient of friction at the interfaces and their correct assessment is very important to understand the mechanism of damping in such structures. All the above vital parameters being largely influenced by the thickness ratio of the beam, this aspect has been critically studied in subsequent chapters.

This thesis consists of two different parts: a theoretical analysis of the problem and an experimental work. The theoretical analysis proposes two different methods to calculate damping: *classical method* and *finite element method*. The classical method is efficiently applied to relatively simple systems producing an almost exact solution. The finite element method rendering an approximate solution is a recent development being widely used around the globe for practical problems because of its diversity and flexibility. In this method, the beam model is treated as a discrete system and the partial differential equations governing the motion are reduced to a system of ordinary differential equations. Finally, the validity of the theoretical methods has been checked from the experiments. The experimental part details how the experiments are carried out and the logarithmic decrement method is used to process the experimental data to investigate the damping characteristics. Both the numerical and experimental results are compared for authentication. Finally, useful conclusions have been drawn from both the numerical and experimental results.

1.7 General Assumptions

Certain assumptions are made in the present analysis while treating joint dynamics. These include:

(1) Each layer of the beam undergoes the same transverse deflection.

(2) The initial excitation at the free end of the beam is of small amplitude.

(3) There is no gross or macro-slip in the joint.

(4) The local mass of the joint area is not considered as significant in altering the behavior of the beam.

(5) The circular holes for inserting rivets on the test specimens are completely filled by the rivets.

(6) There is no displacement and rotation of the beam at the clamped end.

(7) The Coulomb law of friction is used.

(8) The material behaves linearly.

(9) The deflections are small compared to the beam thickness.

(10) The effects of rotary inertia and shear deformation are neglected.

1.8 Organization of the Thesis

The research presented in this thesis provides a framework to study the damping capacity and its improvement in jointed and riveted structures due to joint friction and micro-slip. The investigation as outlined in this thesis is broadly divided into seven chapters. The present chapter serves as a brief introduction to the thesis work and summarizes the importance, motivation, aims and objectives of the present investigation.

The remainder of this thesis is organized as follows:

Chapter 2: This chapter contains a detailed survey of relevant literature on various aspects of vibration analysis of layered and jointed structures. Most of the past and present important researches carried out by various investigators have been presented in detail. This chapter is divided into different sections emphasizing types of damping, mechanisms of damping, various vibration terminologies and techniques used for improving the damping.

Chapter 3: This chapter gives a detailed description of the theoretical analysis by classical approach for determining the damping capacity in layered and jointed cantilever beams. The theoretical expression for the non-uniform pressure distribution within the influencing zone under each rivet has been found out for different beam thickness ratio by curve fitting the numerical

data of Minakuchi et al. [32] using MATLAB software. This pressure distribution has been further utilized to estimate the normal and frictional forces at the interfaces, from which the expression for logarithmic decrement for two as well as multi-layered jointed beams has been formulated using the energy principle.

Chapter 4: This chapter deals with the solution of the present problem using the finite element method and extends the results of Chapter 3 to a jointed structure represented by a discrete model. The Galerkin's method of residual approach has been used to formulate the dynamic equation of free vibration of a jointed cantilever beam. In this method, the beam is discretized into finite number of one-dimensional elements and a suitable solution is assumed within each element. Two-node Euler-Bernoulli linear elements of equal length are utilized for the calculations.

Chapter 5: This chapter outlines the details of the experimental set-up, instrumentation, specimen preparation and testing procedure for the measurement of damping. In practice, the experimental measurement of vibration becomes necessary because of the fact that the theoretically computed vibration of a machine or structure may be different from the actual values due to assumptions made in the theoretical analyses. Free decay method has been used in order to measure the damping in terms of logarithmic decrement. Experimental results for different set of layered and jointed mild steel and aluminium specimens have been compared with the corresponding numerical values obtained in chapters 3 and 4 for establishing the authenticity of the theory developed. These comparative results are presented in graphical and tabular forms.

Chapter 6: This chapter elaborates the detailed discussions on the results obtained from the theoretical, numerical and experimental analyses of chapters 3, 4 and 5, respectively.

Chapter 7: This chapter concludes with a description of what has been accomplished and mentions some important remarks drawn from the observations as discussed in chapter 6. Finally, the chapter is concluded with suggestions for continuing future work in this field.

CHAPTER 2

REVIEW OF LITERATURE

2.1 Introduction

The study of damping and its improvement in many engineering structures is of paramount importance for controlling excessive vibration. Theoretical and experimental work on the measurement of damping in such structures has been extensively pursued in the past and recent years. As the main objective is concerned with the measurement of damping in the present research, the general background of damping is introduced and the mechanisms are discussed in this section. The reported literature presented in the current chapter mainly deals with the theoretical and experimental findings by various investigators on the interfacial slip damping in built-up structures.

2.2 Vibration and Damping

Most engineering structures experience unwanted vibration which results in premature failure. It is observed that all free vibrations cannot keep on going indefinitely and will die out ultimately. In other words, there is some resistance to the motion of the body. Damping characteristics represent the ability of the structure to dissipate vibration energy so that the unwanted vibration is suppressed. However, the vibration energy loss from the system is dependent on the physical mechanisms that cause the dissipation. These mechanisms are complicated processes that are not fully perceived. The types of damping that are present in the structure will depend on the mechanisms predominate in the given situation. For most vibrating systems, a significant part of the energy is dissipated as heat to the environment in an irreversible manner.

The knowledge of damping in a dynamic system is very useful in the design and operation of the system. Damping in a structural system may be either desirable or undesirable depending on the specific application. It is desirable for all structures to possess sufficient damping so that their response to the external excitation is

acceptable [33]. With the increased damping, there will be a reduction in the vibration, noise and dynamic stresses in the structure with a resulting benefit to the fatigue life. For example, a crane structure has to be heavily damped to sustain sudden loads and machine tools must have enough damping so that the cutting tool produces a good surface finish with a high cutting speed. Other structures such as chimneys, bridges, building and ships should possess adequate damping so that their response to external excitation does not produce dynamic stresses that likely cause fatigue failure. However, it should be noted that increasing the damping in a structure is not always easy; rather it is expensive and may be wasteful of energy during normal operating conditions. There are some special cases, such as vibratory conveyors, compactors and musical instruments, where the damping is discouraged for their normal performance.

Structural systems always have very low damping capacities. Hence, passive or active damping techniques are widely used in practice in order to protect structures from unwanted vibrations [34, 35]. Passive damping involves the use of add-on materials with very high damping capacities. For example, high damping viscoelastic materials are often incorporated during fabrication of many structures for the purpose of vibration control. In general, the passive damping is a well developed technique and cost-effective [36]. Among passive damping treatments, the use of layered constructions connected with mechanical joints is the most commonly used method. On the other hand, active damping refers to the energy dissipation from the system by external means such as actuators and sensors for vibration detection and control.

The origin and mechanism of damping are complex and sometimes difficult to comprehend. The energy of the vibrating system is dissipated by various mechanisms and often more than one mechanism may be present simultaneously. For convenience, damping is divided into two major groups identified as: (a) internal damping and (b) structural damping.

2.2.1 Internal Damping - of Material

Internal damping, also called solid or material damping, is related to the energy dissipation within the volume of material. This mechanism is usually associated with internal reconstructions of the micro and macro structure ranging from crystal lattice

to molecular scale effects, thermo-elasticity, grain boundary viscosity, point-defect relaxation, etc. [25, 37]. The majority of published information on material damping is of empirical nature and the underlying physical effects are not fully understood. Besides, there are two types of internal damping: hysteretic damping and viscoelastic damping.

When materials are critically stressed, energy is dissipated internally within the material itself. Experiments by several investigators indicate that for most structural systems, the energy dissipated per cycle is independent of the frequency and approximately proportional to the stiffness of the system and square of amplitude of vibration. Internal damping fitting to this classification is termed as hysteretic damping. The energy loss per cycle is expressed as $E = \pi k \lambda A^2$, where k, λ and A are the stiffness of the system, dimensionless damping factor depending on the property of the material and amplitude of vibration, respectively. The magnitude of this damping is very small as compared to other types of damping. When a body having material damping is subjected to vibration, the stress-strain diagram shows a hysteresis loop whose area denotes the energy lost per cycle due to damping. The stress (σ) and strain (ε) relations at a point in a vibrating body possess a hysteresis loop as shown in Fig. 2.1. The area of the hysteresis loop gives the energy dissipation per unit volume of the material per stress cycle [27, 38]. This is termed as specific damping capacity (Ψ) and given by the cyclic integral $\psi = \oint \sigma \, d\varepsilon$.

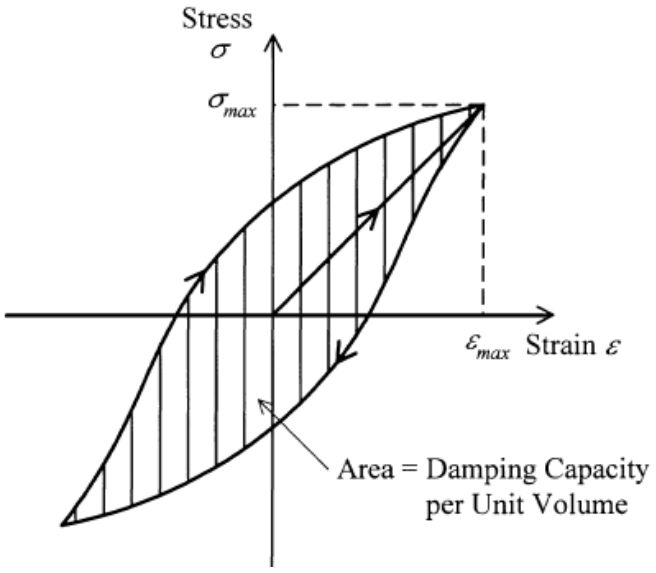

Fig. 2.1 A typical hysteresis loop for material damping [27]

Passive damping using viscoelastic materials (VEM's) is widely used in both commercial and aerospace applications. Viscoelastics are elastomeric materials whose long-chain molecules cause them to convert mechanical energy into heat when they are deformed. The relation between the stress and strain of a viscoelastic damping material is expressed through a linear differential equation with respect to time. The most widespread model used for viscoelastic damping is the Kelvin-Voigt model as it gives the most accurate results for practical purposes [27]. The stress-strain relationship given by this model is $\sigma = E\varepsilon + E^* \frac{d\varepsilon}{dt}$, where E and E^* are the Young's modulus and complex modulus of the material, respectively. The term $E\varepsilon$ represents the elastic behavior of the material with no contribution to damping, while the second term $E^* \frac{d\varepsilon}{dt}$ is responsible for damping. The damping capacity per unit volume is expressed as $d_v = E^* \oint \frac{d\varepsilon}{dt} d\varepsilon$.

2.2.2 Structural Damping – at Joints and Interfaces

Since the damping in the structural material is not significant, most of the damping in real fabricated structures arises in the joints and interfaces [27]. It is the result of energy dissipation caused by rubbing friction resulting from relative motion between components and by intermittent contact at the joints in a mechanical system. However, the energy dissipation mechanism in a joint is a complex phenomenon being largely influenced by the interface pressure and degree of slip at the interfaces. It is this slip phenomenon occurring in the presence of friction at the joint interface that causes the energy dissipation and nonlinearity in the joints.

Fretting corrosion is always present when two surfaces nominally at rest with respect to each other causing slight interfacial slip [33]. It is recognized that joint damping depends on the slip and this always occurs in association with fretting corrosion. The fear of fretting corrosion occurring in a structural joint is a serious problem for the successful joint design. Joint surface prepared from cyanide hardening and electro-discharge machining considerably reduces the fretting effect while allowing high joint damping [39].

Always, some of the stiffness of the structure is sacrificed due to the inclusion of joints, although this loss in stiffness is not allowed to be large if the joints are carefully designed. It is often unnecessary to include a special damping device to a structure to increase the friction damping. Instead, it is easy and cheap to enhance the inherent damping in a structure by utilizing damping in joints ensuring adequate stiffness. This damping mechanism is most effective at low frequencies and the first few modes of vibration because the vibration amplitudes are large enough to allow significant slip [33].

2.3 Measurement of Structural Damping

There are several ways of expressing the damping in a structure. They are time-response and frequency-response methods where the response of the system is expressed in terms of time and frequency, respectively. Depending on the mathematical model of the physical problem, the above two methods are used to measure the damping capacity of the structures. Logarithmic decrement δ is determined using time domain method and the quality factor Q by frequency domain method. However, the other nomenclatures such as; damping ratio ζ, specific damping capacity ψ and loss factor η are estimated from either of the above two methods for measuring the damping [27].

2.3.1 Logarithmic Decrement (δ)

The logarithmic decrement method is the most widely used time-response method to measure damping from the free-decay of the time history curve [27, 33, 40, 41]. When the structure is set into free vibration, the fundamental mode dominates the response since all the higher modes are damped out quickly [33]. The logarithmic decrement represents the rate at which the amplitude of a free damped vibration decreases. It is defined as the natural logarithm of the ratio of any two successive amplitudes. Thus, the logarithmic decrement δ is obtained as;

$$\delta = ln\frac{x_1}{x_2} = \frac{2\pi\zeta}{\sqrt{1-\zeta^2}}$$

where x_1 and x_2 are the successive amplitudes and ζ is the damping ratio.

For small damping, the above relation is approximated as; $\delta \simeq 2\pi\zeta$.

Generally for low damping, it is preferable to measure the amplitudes of oscillations of many cycles so that an accurately measurable difference exists. In such a case, $\delta = \frac{1}{z} ln\left(\frac{x_1}{x_{z+1}}\right)$, where x_1, x_{z+1} and z are the amplitudes of first and last cycles and number of cycles, respectively.

2.3.2 Quality Factor (*Q*)

The half-power point bandwidth method is a frequency-domain method used to determine the damping in terms of quality factor (Q). This method is based on the magnitude curve of the frequency-response function [27]. When a structure is subjected to a forced vibration by a harmonic exciting force, the ratio of maximum dynamic displacement (X_{max}) at steady-state condition to the static displacement (X_s) under a similar force is called the Q factor. Thus $Q = \frac{X_{max}}{X_s} = \frac{1}{2\zeta}$.

The above equation shows that the Q factor is equal to the reciprocal of twice the damping ratio ζ. Since a structure is excited into resonance at any of its modes, a Q factor can be determined for each mode. Systems with high Q factor have low damping and vice versa.

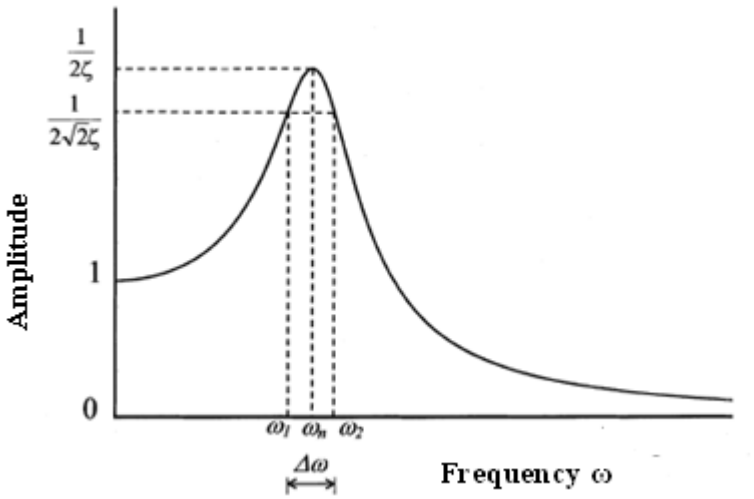

Fig. 2.2 Q-factor method of damping measurement

If the static displacement (X_s) cannot be determined, the Q factor is found out using the half-power point method [27]. The half-power points are those points on the response curve with amplitude $1/\sqrt{2}$ times the amplitude at resonance as presented in Fig. 2.2. This method requires very accurate measurement of the vibration amplitude for excitation frequencies in the region of resonance. Once the maximum dynamic displacement (X_{max}) and resonant frequency (ω_n) have been located, the so-called half-power points are determined when the amplitude is $X_{max}/\sqrt{2}$ and the corresponding frequencies on either side of resonant frequencies, ω_1 and ω_2 are determined. Since the energy dissipated per cycle is proportional to the square of amplitude, the energy dissipated is reduced by 50% when the amplitude is reduced by a factor $1/\sqrt{2}$. Thus the Q factor is modified as; $Q = \frac{1}{2\zeta} = \frac{\omega_n}{\Delta\omega}$, where $\Delta\omega$ is the frequency bandwidth at the half-power points.

2.3.3 Damping Ratio (ζ)

The damping ratio is another way of measuring damping which shows the decay of oscillations in a system after a disturbance [2]. Many systems show oscillatory behavior when they are disturbed from their position of static equilibrium. Frictional losses damp the system and cause the oscillations to gradually decay to zero amplitude. The damping ratio provides a mathematical means of expressing the level of damping in a system. It is defined as the ratio of the damping constant to the critical damping constant.

The rate at which the motion decays in free vibration is controlled by the damping ratio ζ, which is a dimensionless measure of damping expressed as a percentage of critical damping. Figure 2.3 displays the free vibration response of several systems with varying levels of damping ratios. It is observed that the amplitude of vibration decays more rapidly as the value of the damping ratio increases.

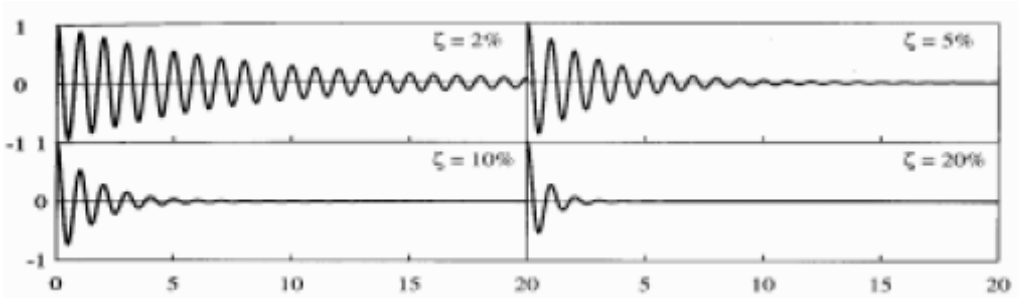

Fig. 2.3 Free vibration of systems with different levels of damping [2]

2.3.4 Specific Damping Capacity (Ψ)

The damping capacity is defined as the energy dissipated per complete cycle of vibration [42-44]. The energy dissipation per cycle is calculated from the damping force (f_d) and is expressed in the integral form as;

$$\Delta U = \oint f_d \, dx$$

This is given by the area of the hysteresis loop in the displacement force-plane. The specific damping capacity (Ψ) is defined as the ratio of energy dissipated per cycle of vibration to the total energy of the system. If the initial (total) energy of the system is denoted by U_{max}, the specific damping capacity is given by;

$$\psi = \frac{\Delta U}{U_{max}}$$

2.3.5 Loss Factor (η)

The loss factor η is the specific damping capacity per radian of the damping cycle [42-44] and is widely used in case of viscoelastic damping. This is expressed as;

$$\eta = \frac{\Delta U}{2\pi U_{max}}$$

It is noted that U_{max} is approximately equal to the maximum kinetic or potential energy of the system when the damping is low.

Finally, the general relationship among various nomenclatures of damping measurement (valid for small values of damping) is given by;

$$\frac{1}{Q} = \frac{\psi}{2\pi} = \eta = \frac{\delta}{\pi} = 2\zeta = \frac{\Delta U}{2\pi U_{max}}$$

2.4 Improvement of Damping Capacity of Structures

The problem of dissipating energy in structures so as to reduce the amplitudes of vibration is an important feature in mechanical design. It is recognized that the magnitude of material damping is always low unless and otherwise some external energy dissipating sources are incorporated to the parent system to improve the damping. As the available damping in the structural members is not sufficient, a number of techniques have been developed in practice to enhance the damping level of the structures. These include;

- Use of unconstrained and constrained viscoelastic layers
- Use of special high damping inserts
- Use of layered and jointed constructions

2.4.1 Use of Unconstrained and Constrained Viscoelastc Layers

A viscoelastic material is characterized by possessing both viscous and elastic behavior. Some of the energy stored in a viscoelastic system is recovered upon the removal of the load and the remainder is dissipated in the form of heat. Viscoelastic damping, otherwise known as passive layer damping, is the most common form of damping treatment widely used in various engineering fields [45, 46]. When exposed to vibrations, the high polymeric molecular properties exhibited by the viscoelastic materials enhance the system damping, thereby dissipating considerable amount of vibration energy. Two types of composite constructions are widely used in practice: namely, the unconstrained layer construction where the damping material is applied as a layer on the structural surface and the sandwich construction (termed as constrained layer) where the damping material is sandwiched between elastic layers. The vibratory energy is dissipated due to direct strains in case of the former and predominantly by shear strains in case of the later [1].

For the same mass of the damping material applied, sandwich constructions are known to yield significantly larger system damping compared to unconstrained layer damping treatments. Moreover, the presence of the constraining layer results in an additional mass of the sandwich panels. However, unconstrained damping treatments are preferred to sandwich panels in many practical applications due to simplicity.

2.4.1.1 Unconstrained-layer or Extensional Damping

In case of unconstrained layer damping, the damping material is applied over the entire structural surface. It is one of the simplest forms of viscoelastic material applications as shown in Fig. 2.4. The material is simply attached with a strong bonding agent to the surface of a structure. Alternatively, the structure may be dipped into a vat of heat-liquefied material that hardens upon cooling. Energy is dissipated as a result of extension and compression of the damping material under flexural stress from the base structure [47]. Damping increases with the increase in the thickness of the damping layer. Changing the composition of a damping material may also alter its effectiveness.

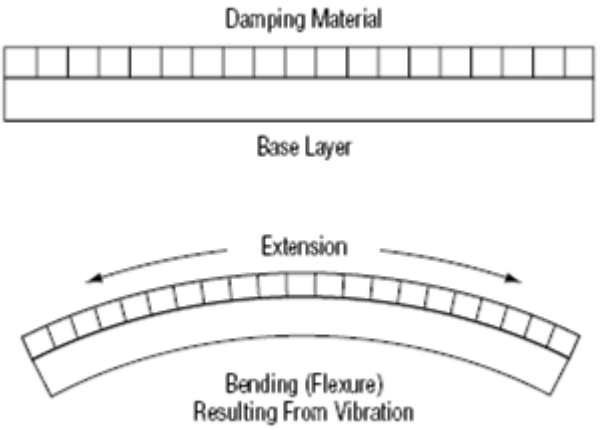

Fig. 2.4 A free-layer damping system

Such constructions have received a considerable amount of interest and extensive theoretical and experimental investigations have been reported [47, 48]. The addition of damping material implies an increase in the structural mass, which has to be viewed with caution in the design of lightweight structural configurations, especially in the aerospace industry. In view of the above considerations, the damping material is applied over a certain area of the structural surface alone, where the extensional

deformation in the layer is large. In regions of the structure where the extensional deformation of the layer is least, the presence of the damping material does not contribute much to the system damping. Reddy et al. [49] and Parthasarathy et al. [50] have evaluated the damping effectiveness of unconstrained layer damping treatment applied to rectangular plates through theoretical and experimental investigations. They have shown that the application of damping material increases the modal loss factor and decreases the modal frequencies.

2.4.1.2 Constrained-layer Damping

Sandwich beams are commonly incorporated in the design of machines and structures because of their superiority compared to homogeneous beams particularly when high strength and stiffness to weight ratios are desirable. In constrained layer damping, a "sandwich" is formed by laminating the base layer of the structure with a thin core of a high-damping viscoelastic material which is further covered by a third constraining layer as shown in Fig. 2.5. When the base structure deforms, the damping layer is loaded in shear. This type of damping system is usually recommended for stiff structural applications. When the system flexes during vibration, shear strains develop in the damping layer. Energy is lost through shear deformation, rather than extension of the material. The effect of the outer elastic layer, the constraining layer, is to increase the deformation in the viscoelastic core, thus resulting in higher energy dissipation in the viscoelastic material.

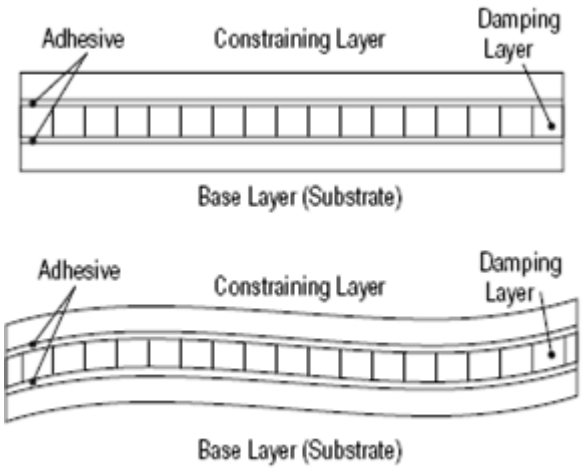

Fig. 2.5 A constrained-layer damping system

The majority of the research in this area has focused on the shear method of dissipating energy. Kerwin [51] and Di Taranto [52] have focused on the mathematical modelling of long, simply supported beams with soft viscoelastic cores and thin, stiff constraining layers. Later, Douglas and Yang [53] and Douglas [54] have presented a mathematical model for compressional damping in three-layer beams. Sylwan [55] has developed a model to combine shear and compressional damping effects in layered beams with thin damping cores showing increased losses over a wider frequency range. More recently, Lee and Kim [56] have presented mathematical results in the analysis of beams and plates with constrained viscoelastic damping layers and obtained good results with the use of very thin viscoelastic layers. The analytical work presented by Mead and Markus [57, 58] and Mead [59] shows that shearing of the viscoelastic core is the only mechanism for energy dissipation without any compressional damping. The work of Mead and Markus has been widely accepted for modeling and analyzing the damping of three-layer beams and plates.

2.4.2 Use of Special High Damping Inserts

Another way of improving the damping capacity of structural members is by using the inserts of special high damping materials [60-62]. The inserts are considered to be both welded and press-fit to the members. It has been observed that the effectiveness of the press-fit inserts is much more than that of the welded inserts. In case of the welded inserts, there exists an optimum size whereas for shrink-fit inserts best results are obtained with solid inserts. The damping capacity of a member has been considerably increased with inserts without any significant loss in static rigidity [60]. Rahmathullah and Mallik [63] have experimentally studied the damping capacity of aluminium cantilever strips by using high damping inserts of different materials namely Cast Iron, Bakelite and Perspex. They have reported that with a proper choice of insert material, considerable improvement of damping capacity can be attained by using very little amount of high damping material.

2.4.3 Use of Layered and Jointed Constructions

The control of structural vibration represents a serious problem in many engineering applications. It is advantageous for any engineering structure to possess sufficient damping capacity so that any excessive vibration is suppressed to a reasonable limit

thereby enhancing the life of the structures. One of the techniques is to make the structure more rigid and robust for preventing excessive vibration. However, rigid structures are heavy and expensive so that the costs and resources necessary for fabricating the same increase significantly making it unsuitable for many applications. Another way to reduce vibration is by making the structure in layers connected with mechanical joints. It is a general fact that the total damping in a structure is always much more than the sum of the material damping of individual elements of the structure. It is therefore recognized that the damping is largely caused due to the inclusion of mechanical joints or fasteners in the structure.

The dynamics of structures with mechanical joints is a topic of special interest because of their existence in practically all complex structures. The damping in beam type structures is increased by fabricating the same in several layers bolted or riveted together so that the interfacial slip occurs between the layers during vibration, thus giving rise to frictional damping. Many researchers in this field [64-66] have suggested that the presence of joints accounts most of the damping in a typical jointed structure and offers a major potential for passive vibration control. The energy dissipation is mainly caused due to the inclusion of bolted or riveted connections that produce local stiffness and damping in assembled structures. This energy dissipation, although undesirable when one wishes to avoid fretting corrosion, is usually desirable since it acts to limit the vibration amplitudes [67]. A great deal of research work [66, 68-71] has been reported from the theoretical and experimental studies focusing the joint damping.

The energy dissipation mechanism in a joint is a complicated phenomenon being largely influenced by the interface pressure and slip between the contacting surfaces. Although the energy dissipation is related to many physical phenomena, the friction between the layers is considered to be the most important factor [17]. It is always difficult for the theoretical assessment of damping arising in joints because of variations in the coefficient of friction under dynamic conditions. However, it is generally accepted that the friction force generated between the joint interfaces is usually dependent on the materials in contact and proportional to the normal force across the interface. At the specified joint clamping pressure, sliding takes place on a micro scale and the Coulombs law of friction is assumed to be valid.

Notwithstanding the difficulties of analysis in the estimation of damping in joints, some form of this damping always occurs in all structural applications. There is a wide range of dynamic systems and structures such as beam systems, frameworks, gas turbines and aerospace structures that would benefit from increased joint damping. The research presented in this thesis primarily emphasizes on the use of jointed connections in built-up structures so as to derive increased damping. A vast amount of relevant literature study on the interfacial joint damping is enumerated in the succeeding section.

2.5 Review of Relevant Literature on Joint Damping

Most engineering structures are built up by connecting structural components through mechanical connections. Such assembled structures need sufficient damping to limit excessive vibrations under dynamic loads. Damping in such structures mainly originates from two sources. One is the internal or material damping which is inherently low [72] and the other one is the structural damping due to joints [73]. The latter one offers an excellent source of energy dissipation, thereby adequately compensating the low material damping of structures. It is estimated that structures consisting of bolted or riveted members contribute about 90% of the damping through the joints [14, 64-66]. The work in this thesis is oriented towards the use of mechanical systems fabricated in layers jointed with rivets for achieving increased damping.

As discussed in the preceding paragraph, the provision of layers in association with joints encourages large damping in built-up structures. These connections are recognized as a good source of energy dissipation and greatly affect the dynamic behavior in terms of natural frequency and damping [13, 17, 67]. This structural damping offering excellent potential for large energy dissipation is associated with the interface shear of the joint. It is thus recognized that the provision of joints can effectively contribute to the damping of all fabricated structures. Although most of the inherent damping occurring in real structures arises in the joints, but a little effort has been made to study this source of damping because of complex mechanism occurring at the interfaces due to relative slip, coefficient of friction and pressure distribution characteristics. It is therefore important to focus the attention to study these parameters for accurate assessment of the damping capacity of structures.

An important feature of built-up structures is the existence of slip at the interfaces of the structural components. The energy in such structures is dissipated through slipping, thereby emphasizing the need to study the mechanism of slip at the interfaces. In case of mechanical joints, the dissipation of energy takes place due to both micro- and macro-slip [74]. On application of the force, small regions of the interface breaks encouraging slipping. These localized motions are termed as *micro-slip* during which no relative motion takes place between the contacting surfaces. The micro-slip between the connecting members occurs only at lower excitation levels. With the application of more and more force on the joint, the entire contact area slips giving rise to *macro-slip*. In most of the joint configurations excited at reasonable dynamic force, the micro-slip occurs but not the macro-slip. Macro-slip usually leads to the failure of the joint and is generally avoided in all structural applications. However, the micro-slip provides a good level of energy dissipation without damaging the joint and is therefore encouraged in its design. Any relative slip, whether in the form of macro- or micro-slip, always provides damping through energy dissipation. The work embedded in this thesis presents a technique based on the micro-slip approach to determine the damping capacity of fabricated structures.

Over the past few decades, most of the work has been confined in the area of micro- and macro-slip phenomena [75, 76]. These concepts are utilized to study the dynamic behavior of jointed structures having friction contact [7-12, 77-82]. Several workers [83-87] have investigated using the macro-slip approach modeling the friction interface as a rigid body. This model is generally adopted when the normal load at the interface is small. On the other hand, many researchers [10, 11, 88-91] have utilized the micro-slip concept considering the friction surface as an elastic body. In this case, the interface undergoes partial slip at high normal load. Masuko et al. [28] and Nishiwaki et al. [29, 30] have found out the energy loss in jointed cantilever beams considering micro-slip and normal force at the interfaces. Olofsson and Hagman [92] have shown that the micro-slip at the contacting surfaces occur when an optimum frictional load is applied. They have also presented a model for micro-slip between the flat smooth and rough surfaces covered with ellipsoidal elastic bodies. Ying [93] has proposed a new generalized micro-slip model to study the effect of friction in joints for controlling the dynamic response of structures.

The role of friction is of paramount importance in controlling the dynamic characteristics of engineering structures. This may be undesirable or desirable depending on the type of applications. Friction is often considered detrimental in the design of moving parts. On the other hand, this is desirable in fabricated structures for effective energy dissipation. Therefore, this concept of design is always considered in assembled structures requiring high damping. The friction at the jointed interfaces arises when the layers experience relative movement under transverse vibration. The Coulomb's law of friction is widely used to represent the dry friction at the contacting surfaces. The friction in a joint arises from shearing between the parts and is governed by the tension in the bolt/rivet, surface properties and type of materials in contact [94]. Den Hartog [95] has analytically solved the steady state response of a simple friction-damped system with combined Coulomb and viscous friction. Reviews on the effects of joint friction on structural damping in built-up structures have been presented by many researchers [16, 17, 38, 95-98]. Their findings have shown that the friction in structural joints is regarded as a major source of energy dissipation in assembled structures.

The nature of pressure distribution across a beam layer is another important aspect affecting the damping capacity of jointed structures. Several workers have tried over the years to know the actual pattern of pressure distribution at the interfaces due to the clamping action on the joint. Almost all previous researchers have idealized the joints by assuming a uniform pressure profile without considering the effects of surface irregularities and asperities [28-30, 73, 99, 100]. In fact, many authors [101-106] have conducted experiments to know the exact distribution characteristics. These experiments have confirmed that the interface pressure is hardly constant in actual situation. In particular, Gould and Mikic [107] and Ziada and Abd [108] have reported that the pressure distribution at the interfaces of a bolted joint is parabolic in nature circumscribing the bolt which is approximately 3.5 times the bolt diameter. The pressure profile is also reported to be independent of the applied tightening load. Hisakado and Tsukizoe [109] have presented a simple method for measuring the interface pressure distribution of bolted joints. Their experimental results show that the interface pressure distribution is almost independent of the surface roughness. They measured the pressure distribution of two metals in contact by using the impressions of the softer surface formed by the penetrations of harder asperities.

Recently, Nanda and Behera [31] have developed a theoretical expression for the pressure distribution at the interfaces of a bolted joint by curve fitting the earlier data reported by Ziada and Abd [108]. They have obtained an eighth order polynomial even function in terms of normalized radial distance from the centre of the bolt such that the function assumes its maximum value at the centre of the bolt and decreases radially away from the bolt. They have used Dunn's curve fitting software to calculate the exact spacing between bolts that would result in a uniform interfacial pressure distribution along the entire length of the beam. Using exact spacing of 2.00211 times the diameter of the connecting bolts, Nanda and Behera have been successful in simulating uniform interface pressure over the length of the beam. Thereafter, they have investigated the effect of interface pressure on the behavior of interfacial slip damping.

Damisa et al. [110] have also recently carried out an analysis to study the effect of non-uniform pressure distribution on the mechanism of slip damping for layered beams, but their analysis is limited to static load. Later, they have extended their analysis to realistic dynamic loading for estimating the interfacial slip damping in clamped layered beams [111]. They have shown that under the action of dynamic loads, the factors like non-uniform pressure distribution as well as frequency variation have a significant effect on both the energy dissipation and logarithmic decrement associated with the mechanism of slip damping in layered structures. They have further reported that the amount of energy dissipation through slip damping under externally applied dynamic load is less than that of the corresponding static load. Olunloyo et al. [112] have used other forms of pressure distributions such as polynomial or hyperbolic representations but the results obtained have demonstrated that the effects of such distributions in comparison with the linear profile are largely incremental in nature.

There are various measuring methods available in practice to know the contact pressure between layers. The technique of using ultrasonic waves is most capable among them as it measures the real contact pressure without changing the characteristics of the contact surface. This measurement has produced fair results using a normal probe [113, 114]. However, the angle probe used by Minakuchi et al. [32] is more convenient to measure. They have found out the contact pressure

between two layered beams of different thicknesses by establishing a relationship between the mean contact pressure and sound pressure of reflected waves. This method is widely accepted as the experimental results fairly agree with the theoretical ones. The present investigation uses the numerical data of Minakuchi et al. [32] to obtain the theoretical expressions for non-uniform pressure at the interfaces of a jointed beam by curve fitting with MATLAB software.

Energy dissipation resulting from slip and non-uniform pressure distribution in bolted joints has been the subject of many studies [28-30, 115-118]. Some researchers [13, 119, 120] have reported different mechanisms of energy dissipation that might take place depending on the clamping pressure. Typically, the normal interfacial pressure across the clamped joint is not uniformly distributed. Under high pressure, the slip is small, while under low pressure the shear due to friction is small. An optimal clamping force exists somewhere between these two limits under which a joint dissipates maximum vibration energy. Beards [121] has looked into this aspect and recognized the existence of an optimum joint force for maximum energy dissipation. Jezequel [118] has proposed an algorithm for calculating the energy loss due to slip in bolted plates. It has been found that the joint friction exhibits viscous-like damping characteristics when the normal force is allowed to vary with the relative slip [70, 122-126].

Beards and Williams [8] in their experimental investigation of a frame structure have shown that a useful increase in damping could be achieved by fastening joints tightly to prohibit translational slip, but not tightly enough to restrict rotational slip. Beards and Imam [7] have found that the frictional damping of plate-type structures is enhanced using fastened laminated plates having interfacial slip during vibration. In another study, Beards and Woodwat [82] have experimentally determined the effect of controlled frictional damping in joints on the frequency response of a frame under harmonic excitation. However, Beards [14, 65, 121, 127, 128] has concluded that the relative motion between contact surfaces should be avoided as it results in the reduction of the stiffness and creates corrosion of the joint interfaces. Researchers at Sandia National Laboratories have performed experiments to investigate the damping due to micro-slip at joints and established a power law relation between the energy dissipation and lateral load [129, 130].

More recently, Heller et al. [131] have used an experimental procedure to determine the nonlinear damping capacity of built-up structures due to friction joints. They have conducted experiments on a simple built-up structure consisting of two bolted beams to analyze the influence of interface pressure and contact area on its dynamic behavior. Their experiment has confirmed that the frictional joints are the main source of energy dissipation in built-up structures due to relative motion between the components. The recent experimental investigation of Walker et al. [132] discusses the joint parameters affecting the damping of aerospace structures. They have studied the importance of joint stiffness on the damping and found that the riveted joints result in lower energy dissipation compared to its equivalent bolted ones due to higher stiffness. They have drawn another conclusion that the damping of the plate increases with the reduction in the bolt torque.

The modeling of structural joint is very important for accurate analysis. A good knowledge of the joint characteristics is necessary to devise an efficient model considering slip associated energy dissipation. Many investigators [17, 133-135] have contributed significantly on the models with joint friction of built-up structures. Song et al. [136] have proposed the Adjusted Iwan Beam Element (AIBE) model considering nonlinearity effects of an assembled bolted structure. Hartwigsen et al. [75] have investigated experimentally to quantify the effects of nonlinearity on shear lap joints of two structures: a beam with a bolted joint at its center and a frame with a bolted joint in one of its members. Both structures are subjected to a variety of dynamical tests to determine the effects of nonlinearity of the joints. Their experimental results discuss several important parameters influencing the effective stiffness and damping of lap joints. Miller and Quinn [137] have presented a two-sided interface model based on a series-series Iwan system in which the parameters are physically motivated. This interface model is then incorporated into a large structural model to calculate the damping arising from micro-slip. Khattak et al. [138] have developed a parameter-free and physics-based model of the joint dynamics considering shear lap joints with reasonable accuracy. This model can be applied for different loading and joint parameters, i.e., different joint geometries, friction coefficients and clamping pressures.

It is very difficult to assess the joint properties correctly from the theoretical results and therefore, experiments are performed to verify the same. The damping of a structure is experimentally measured either by time or frequency domain methods. In case of the former, the damping is estimated in terms of logarithmic decrement using the free decay signal. This method is generally applied to lightly damped linear systems excited at lower amplitude and frequency. Many researchers have conveniently used this technique for estimating damping [13, 17, 31, 67]. Nishiwaki et al. [29] have developed an improved band-width method to measure experimentally the damping capacity in terms of logarithmic decrement of a bolted cantilever beam at first, second and third modes of vibration. Masuko et al. [28] and Nishiwaki et al. [30] have theoretically calculated the logarithmic decrement of a jointed cantilever beam considering the normal force and micro-slip at the interfaces. Recently, Olunloyo et al. [139] have analytically investigated the slip damping of layered viscoelastic beam-plate structures using the logarithmic decrement approach. Damisa et al. [111] have performed a dynamic analysis of slip damping in clamped layered beams with non-uniform pressure distribution at the interfaces. They have shown that under dynamic loads, the frequency variation and non-uniformity in pressure distribution can have significant effect on both the energy dissipation and logarithmic damping decrement.

Wang and Chuang [140] and Tsai and Chou [141] have proposed a frequency domain method to study the stiffness and damping of a single bolted joint directly from the frequency response function (FRF) of the structures. They have used FRFs in different frequency ranges to extract the joint properties so that the joint dynamic behavior is well represented over the frequency range. Yin et al. [142] have introduced a method based on the wavelet transform of FRFs for linear systems to estimate the natural frequency and damping. They have used Cauchy's integral formula for calculating the continuous wavelet transform of the FRFs for any complex function. Hwang [143] has developed a response model in frequency domain to identify the stiffness constant and damping coefficient parameters of connections using the experimental data. Ahmadian and Jalali [144] have presented a parametric model for an Euler-Bernoulli beam with bolted lap joint in the mid span. The solution provides the FRF of the beam at any desired point due to excitation at a certain location. This FRF is compared with the corresponding experimental results to identify the parameters of the bolted joint interface affecting damping.

The finite element method is one of the numerical techniques for solving many boundary and initial value engineering problems. However, its application in damping analysis is relatively recent. Gaul and Lenz [135] have worked in detail on the finite element models considering slip mechanisms to study the dynamic response of assembled structures. Sainsbury and Zhang [145] have used the finite element procedure through Galerkin element method (GEM) to make the dynamic analysis of damped sandwich beam structures. Lee et al. [146] have used the finite element model of a jointed beam to obtain the natural frequencies and mode shapes. Hartwigsen et al. [75] have found out the contact area of bolted joint interfaces using finite element analysis and further conducted experiments to verify the same. Chen and Deng [147] have carefully studied the micro-slip phenomenon using the finite element method under plane stress conditions. They have carried out investigations on two classical joint configurations for modeling: the press-fit joint and lap-shear joint. They have focused their work to evaluate the effect of dry friction and slip on the damping response of joints for quantifying the energy dissipation during cyclic loading. Oldfield et al. [148] have analyzed the effect of dynamic friction on energy dissipation of a bolted joint under harmonic loading by finite element method using Jenkins elements. They have studied the effect of preload on the interface pressure affecting the response of the joint. At high preload, little sliding occurs at the joint interface producing less frictional energy.

As evident from the preceding discussions, built-up structures are generally assembled by bolted or riveted connections representing a significant source of damping. The dynamics of bolted structures have been studied by many investigators as evidenced from the wealth of published literatures. However, a little amount of research has been reported till date on the riveted joints. Rivets are widely used in aircraft, building constructions, trusses, frames, bridges and various other applications requiring high joint strength and damping. The use of rivets in such applications is cheaper compared to other fasteners thereby giving low assembly cost. Further, rivets are not susceptible to unintended loosening which might otherwise cause joint failures and hazardous environments.

In general, the introduction of riveted joints increases the amount of damping in addition to the inherent material damping of the equivalent monolithic construction.

In the past, Pian and Hallowell [149] presented the theory of structural damping in built-up beams connected with riveted cover plates. Moreover, Pian [100] has carried out the theoretical analysis of energy dissipation of a continuously riveted spar and spar cap and found the results are in good agreement with the experimental ones. Further, Pian has established that the riveted joints are uniquely responsible for enhancing the damping levels in structures. Walker et al. [132] have experimentally investigated the effect of joint parameters influencing the damping of metal plates for aerospace applications. They have reported that the riveted joint possesses lower damping compared to an equivalent bolted joint owing to higher stiffness.

The above literature survey reveals that a great deal of work has been pursued in determining the damping capacity of bolted structures with little or no progress in the study of damping of riveted structures. In the context of the present investigation, a proper differentiation has to be made between the bolted and riveted connections in built-up structures in order to emphasize the present research. In both cases, the fundamental mechanism of damping is identical but they differ in their functional aspects. The parameters such as interface pressure distribution characteristics, zone of influence and preload are not the same. For example, the zone of interface pressure distribution circumscribing a rivet is equal to 4.125, 5.0 and 5.6 times the rivet diameter for beam thickness ratios of 1.0, 1.5 and 2.0, respectively, whereas the same in case of bolted joint is 3.5 times the diameter [150]. Since the zone of influence being different in both the cases, the relative spacing among the joints will be different thereby changing the magnitude of dynamic slip at the interfaces. Further, the axial load on a bolt can be varied by applying the tightening torque as per the clamping requirements of the structure whereas the preload in a rivet is constant and no control can be exercised over its magnitude. In other words, the tightening torque and initial stress are the controlling parameters in determining the axial load/preload on the bolt and rivet, respectively. Above observations suggest that the damping action in case of both the joints are different. The motivation for the present investigation lies in developing the theory of damping mechanism in riveted structures through classical and finite element methods. The results so obtained are validated experimentally.

2.6 Chapter Summary

Most engineering structures inherently possess less material damping thereby making them unsuitable for structural applications requiring higher damping capacity. The introduction of additional measures is therefore needed for improvement of the damping characteristics. The use of jointed construction serves this purpose to a larger extent. The efficient utilization of damping from joint configurations provides an accurate prediction of dynamic responses of assembled structures subjected to external excitation. But the damping as a dynamic characteristic is least understood and most difficult to quantify. Therefore, the prediction of damping in built-up structures is always challenging due to limited knowledge of joint physics. It is therefore necessary to analyze the damping mechanism theoretically along with the influencing parameters and authenticate the results experimentally.

It is evident from this literature survey that the presence of joints offers a major potential for passive vibration control. The damping arising from these joints is always dominant compared to the low inherent material damping. It is produced by the energy dissipation during the vibration of a structure when some relative movement takes place at the joint interfaces in the presence of friction. This energy dissipation is desirable since it acts to limit vibration amplitudes thereby enhancing the useful life of the structures. Extensive research has been carried out since many decades on the damping of bolted structures. However, the information available on the damping behavior of riveted joints is rather limited and insufficient. The research presented in this thesis mainly deals with the estimation of damping and its related mechanisms caused by the micro-slip of fabricated structures, typically layered cantilever beams jointed with rivets, through analytical and experimental work. The prime reason for selecting rivets as compared to welding or bolting is that the riveted connections are largely used in structural designs, viz. trusses, aircrafts, pressure vessels, robots and many other applications.

CHAPTER 3

THEORETICAL ANALYSIS BY CLASSICAL ENERGY APPROACH

3.1 Introduction

As already discussed in previous chapters, the incorporation of joints is the major source of energy dissipation in built-up structures. The damping is due to frictional effects associated with relative shear displacements at the interfaces of the connections. The damping characteristics are influenced by the intensity of pressure distribution, micro-slip and kinematic coefficient of friction at the interfaces and the effect of all these parameters are to be considered for accurate evaluation of energy loss in assembled structures. This chapter gives a detailed description of the theoretical analysis by classical energy approach for determining the damping capacity in layered and jointed cantilever beams with riveted joints. A cantilever beam model representing a continuous system based on the Euler-Bernoulli beam theory has been used for deriving the necessary formulations.

3.2 Types of Beam Model

Models of vibrating systems are generally divided into two classes, discrete and continuous depending on the nature of parameters. In case of *discrete or lumped parameter system*, the mass is assumed to be rigid being concentrated at individual points and the stiffness is considered to be mass less springs connecting these rigid masses. The motion of discrete systems is governed by ordinary differential equations and the number of masses generally defines the number of degrees of freedom of the system. The solution of discrete systems is approximate and has been considered in detail using finite element approach in the succeeding chapter.

In *real or continuous systems*, the mass and elasticity are considered as distributed or continuous parameters. This distribution of the mass and elasticity requires partial differential equations to describe the vibration. Systems with distributed parameters are characterized by an infinite number of degrees of freedom. If the model is linear,

the number of its natural frequencies and modes are equal to its degrees of freedom. Indeed, the displacement depends on two independent variables, i. e., spatial and time variables *x* and *t*, respectively. The time *t* is an independent variable in a dynamic response problem. As a result, the motion of continuous systems is governed by partial differential equations satisfying the whole domain. This chapter is entirely devoted to distributed-parameter systems producing exact solutions.

3.3 Dynamic Equations of Free Transverse Vibration

Figure 3.1 shows a cantilever beam undergoing free vibration with transverse displacement $y(x,t)$. In formulating the dynamic equations, Euler-Bernoulli beam theory is used on the assumptions that the rotation of the differential element is negligible compared to translation and the angular distortion due to shear is small in relation to bending deformation. This assumption is valid when the ratio of the length of beam to its depth is relatively large as in case of the present investigation.

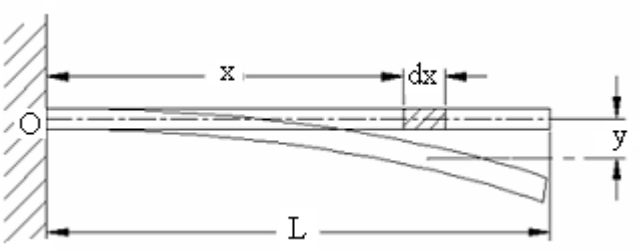

Fig. 3.1 Differential analysis of a beam

The beam vibration is governed by partial differential equations in terms of spatial variable *x* and time variable *t*. Thus, the governing differential equation for the free transverse vibration is given by;

$$c^2 \frac{\partial^4 y(x,t)}{\partial x^4} = -\frac{\partial^2 y(x,t)}{\partial t^2} \tag{3.1}$$

where $c = \sqrt{EI/\rho A}$ and *E, I,* ρ and *A* are modulus of elasticity, second moment of area of the beam, mass density and cross-sectional area, respectively. The free vibration given by Eq. (3.1) contains four spatial derivatives and hence requires four boundary conditions for getting a solution. The presence of two time derivatives again requires two initial conditions, one for the displacement and another for velocity.

The above equation is solved using the technique of *separation of variables*. In this method, the displacement $y(x,t)$ is written as the product of two functions, one depending only on *x* and the other depending only on *t*. Thus, the solution is expressed as;

$$y(x,t) = F(x)G(t) \tag{3.2}$$

where *F*(*x*) and G(t) are the space and time functions, respectively.

Substituting Eq. (3.2) into Eq. (3.1) results;

$$c^2 F''''(x)G(t) = -F(x)\ddot{G}(t) \tag{3.3}$$

Dividing Eq. (3.3) by *F*(*x*)*G*(*t*) on both the sides, the variables are separated as;

$$c^2 \frac{F''''(x)}{F(x)} = -\frac{\ddot{G}(t)}{G(t)} = \omega_n^2 \tag{3.4}$$

where the term $\omega_n{}^2$ is the separation constant representing the square of natural frequency. Because the first term in this equation is a function of *x* only and the second term is a function of *t* only, the entire equation can be satisfied for arbitrary values of *x* and *t* only if each term is a constant.

This equation yields two ordinary differential equations and the first one is given by;

$$F''''(x) - \left(\frac{\omega_n}{c}\right)^2 F(x) = 0 \tag{3.5}$$

Taking $\lambda^2 = \frac{\omega_n}{c}$, Eq. (3.5) is rewritten as;

$$F''''(x) - \lambda^4 F(x) = 0 \tag{3.6}$$

This equation can be solved in the usual way with *F*(*x*) consisting of the sum of four terms and the required solution is simplified as;

$$F(x) = A_1 \cosh \lambda x + A_2 \sinh \lambda x + A_3 \cos \lambda x + A_4 \sin \lambda x \tag{3.7}$$

where constants A_1, A_2, A_3 and A_4 are determined from the boundary conditions of the cantilever beam.

The second equation is given as;

$$\ddot{G}(t) + \omega_n^2 G(t) = 0 \tag{3.8}$$

which is the familiar free vibration expression for an undamped single degree of freedom system having the solution

$$G(t) = A_5 \cos \omega_n t + A_6 \sin \omega_n t \tag{3.9}$$

where constants A_5 and A_6 are evaluated from the initial conditions.

Substituting the expressions for space and time functions as given by Eq. (3.7) and (3.9), respectively, into Eq. (3.2), the complete solution for the deflection of a beam at any section is expressed as;

$$y(x,t) = \left(A_1 \cosh \lambda x + A_2 \sinh \mu x + A_3 \cos \lambda x + A_4 \sin \lambda x\right) \times \left(A_5 \cos \omega_n t + A_6 \sin \omega_n t\right) \tag{3.10}$$

It is to be noted here that the model of the transverse vibration of the beam presented in Eq. (3.1) ignores the effects of shear deformation and rotary inertia. If these effects are considered, more accurate *Timoshenko beam theory* is to be used. However, the same procedure is still followed except that the formula deduction may be more tedious.

3.3.1 Evaluation of Constants A_1, A_2, A_3 and A_4

Writing the expression for space function as given in Eq. (3.7) and taking the successive derivatives, the following relations are written as;

$$F(x) = A_1 \cosh \lambda x + A_2 \sinh \lambda x + A_3 \cos \lambda x + A_4 \sin \lambda x \tag{3.11a}$$

$$F'(x) = \lambda\left(A_1 \sinh \lambda x + A_2 \cosh \lambda x - A_3 \sin \lambda x + A_4 \cos \lambda x\right) \tag{3.11b}$$

$$F''(x) = \lambda^2\left(A_1 \cosh \lambda x + A_2 \sinh \lambda x - A_3 \cos \lambda x - A_4 \sin \lambda x\right) \tag{3.11c}$$

$$F'''(x) = \lambda^3\left(A_1 \sinh \lambda x + A_2 \cosh \lambda x + A_3 \sin \lambda x - A_4 \cos \lambda x\right) \tag{3.11d}$$

The four boundary conditions for a cantilever beam are given by:

At the fixed end: $x = 0$, $F(0)=0$, $F'(0) = 0$

At the free end: $x = l$, $F''(l) = 0$, $F'''(l) = 0$

Putting the above boundary conditions, Eq. (3.11) is reduced to;

$$F(0) = A_1 + A_3 = 0 \tag{3.12a}$$

$$F'(0) = A_2 + A_4 = 0 \tag{3.12b}$$

$$F''(l) = \lambda^2 \left(A_1 \cosh \lambda l + A_2 \sinh \lambda l - A_3 \cos \lambda l - A_4 \sin \lambda l \right) = 0$$

i.e., $A_1 \cosh \lambda l + A_2 \sinh \lambda l - A_3 \cos \lambda l - A_4 \sin \lambda l = 0$ (3.12c)

$$F'''(l) = \lambda^3 \left(A_1 \sinh \lambda l + A_2 \cosh \lambda l + A_3 \sin \lambda l - A_4 \cos \lambda l \right) = 0$$

i.e., $A_1 \sinh \lambda l + A_2 \cosh \lambda l + A_3 \sin \lambda l - A_4 \cos \lambda l = 0$ (3.12d)

The Eq. (3.12) can be written in a compact matrix form as;

$$\begin{bmatrix} 1 & 0 & 1 & 0 \\ 0 & 1 & 0 & 1 \\ \cosh \lambda l & \sinh \lambda l & -\cos \lambda l & -\sin \lambda l \\ \sinh \lambda l & \cosh \lambda l & \sin \lambda l & -\cos \lambda l \end{bmatrix} \begin{bmatrix} A_1 \\ A_2 \\ A_3 \\ A_4 \end{bmatrix} = \begin{bmatrix} 0 \\ 0 \\ 0 \\ 0 \end{bmatrix} \tag{3.13}$$

This vector equation can have a nonzero solution for the vector $\begin{bmatrix} A_1 & A_2 & A_3 & A_4 \end{bmatrix}^T$ only if the determinant of the coefficient matrix vanishes, i.e., singular. Setting the determinant equal to zero, the characteristic equation is given as;

$$\cos \lambda l . \cosh \lambda l = -1 \tag{3.14}$$

This transcendental equation is the required condition for the co-efficient matrix to give a non-trivial solution and can be further used to determine the frequencies of vibration.

The Eq. (3.13) can be expressed into four algebraic equations. The constants A_1, A_2 and A_3 are dependent parameters and A_4 is an independent parameter. A_4 may have any value. Taking A_4=1, the values of constants of A_1, A_2, A_3 and A_4 are found as;

$A_1 = \left(\dfrac{\sin \lambda l + \sinh \lambda l}{\cos \lambda l + \cosh \lambda l} \right)$, $A_2 = -1$, $A_3 = -\left(\dfrac{\sin \lambda l + \sinh \lambda l}{\cos \lambda l + \cosh \lambda l} \right)$ and $A_4 = 1$

The space function as given in Eq. (3.7) is modified by putting the values of various constants as;

$$F(x)=\left(\frac{\sin\lambda l+\sinh\lambda l}{\cos\lambda l+\cosh\lambda l}\right)\cosh\lambda x-\sinh\lambda x-\left(\frac{\sin\lambda l+\sinh\lambda l}{\cos\lambda l+\cosh\lambda l}\right)\cos\lambda x+\sin\lambda x$$

i.e., $$F(x)=\frac{(\cosh\lambda x-\cos\lambda x)(\sin\lambda l+\sinh\lambda l)+(\sin\lambda x-\sinh\lambda x)(\cos\lambda l+\cosh\lambda l)}{\cos\lambda l+\cosh\lambda l} \quad (3.15)$$

This equation gives different mode shapes of vibration.

3.3.2 Evaluation of Constants A_5 and A_6

The general expression for deflection at any section of the beam as given in Eq. (3.10) is rewritten as;

$$y(x,t)=F(x)(A_5\cos\omega_n t+A_6\sin\omega_n t) \quad (3.16)$$

Taking derivatives with respect to time, the above equation is reduced to;

$$\frac{dy(x,t)}{dt}=F(x)(-A_5\omega_n\sin\omega_n t+A_6\omega_n\cos\omega_n t) \quad (3.17)$$

The Eq. (3.17) represents the velocity of deflection at any section of the beam. However, from the initial condition of the cantilever beam, the velocity of deflection at the free end is zero, i.e., $\frac{dy(l,0)}{dt}=0$, which yields $A_6=0$.

Hence, the Eq. (3.16) is reduced to;

$$y(x,t)=F(x).A_5\cos\omega_n t \quad (3.18)$$

The initial deflection at the free end of the beam is taken equal to $F(l)$ and substituting the same in Eq. (3.18), the equation is modified as;

$y(l,0)=F(l).A_5$, which gives $A_5=\frac{y(l,0)}{F(l)}$

Substituting the value of A_5 in Eq. (3.18), the final equation for deflection is found to be;

$$y(x,t) = F(x)\left[\frac{y(l,0)}{F(l)}\right]\cos\omega_n t \tag{3.19}$$

This is the generalized deflection equation at any section of a cantilever beam.

3.4 Mechanisms of Micro-slip

The mechanism of micro-slip at the interfaces presents a very complicated characteristics and a thorough understanding of this phenomenon is required for correct assessment of energy dissipation. Therefore, different theories have been proposed for the possible cause of micro-slip at the interfaces of connecting members.

In practice, the interfaces are microscopically irregular and contain asperities of different size and shape. When two interfaces are pressed together and vibrate, big asperities get compressed and deform first in the tangential direction. Due to different physical properties, the nature of the deformation of the asperities is different; some deform elastically, few plastically and others break up completely. These deformations introduce a partial slippage over a small area at the interfaces. Therefore, even though there is no deformation of the component members being jointed, micro-slip can still occur. However, this may not be the only cause of micro-slip and possibly there are other mechanisms responsible for its occurrence.

Another mechanism for micro-slip takes place when the joints connecting the members are semi-rigid and a small relative motion is allowed at the interfaces. Under the action of the clamping force, no immediate slippage occurs at the riveted joint. However, the normal force away from the joint is smaller, thereby promoting slippage in this region. This slippage occurs over a fraction of the region of contact and is referred to as *micro-slip*. The occurrence of micro-slip is mainly controlled by the clamping force provided by the rivet. When the joint is rigidly clamped, no frictional sliding takes place at the interfaces and the two beam components is considered as a monolithic cantilevered structure. Moreover, when the slip occurs over the entire interface, it is termed as *macro-slip* which has not been considered in the present investigation.

Further, the contact pressure at the jointed interface is non-uniform in nature being maximum at the rivet hole and decreases with the distance away from the rivet. The

micro-slip first occurs in regions of the interface where the contact pressure is insufficient to prevent the shear stress.

From the above discussion, it is established that the cause of micro-slip is due to several effects such as; i) different properties of the asperities at the interfaces, ii) semi-rigid nature of joints joining different layers and iii) uneven pressure distribution at the interfaces. It is the micro-slip at the jointed interface which is mainly responsible for the cause of energy dissipation. Moreover, the micro-slip between the connecting members occurs only at lower excitation levels. When the excitation level is increased, both micro- and macro-slip occur at the jointed interfaces. Usually, the macro-slip is avoided because it may lead to structural damage of the joint. On the other hand, micro-slip provides a good level of energy dissipation without causing any adverse effect to the joint. The contribution of micro-slip to the overall system damping is significant in spite of its low magnitude in real applications.

3.4.1 Determination of Relative Dynamic Slip

The transverse deflection of a cantilever beam specimen undergoing vibration at any distance x from the fixed end is obtained combining Eqs. (3.15) and (3.19) as;

$$y(x,t)=\begin{bmatrix}(\cosh\lambda x-\cos\lambda x)(\sinh\lambda l+\sin\lambda l)+\\(\sin\lambda x-\sinh\lambda x)(\cosh\lambda l+\cos\lambda l)\end{bmatrix}\left[\frac{y(l,0)}{F(l)}\right]\frac{\cos\omega_n t}{\cosh\lambda l+\cos\lambda l} \tag{3.20}$$

The value of $F(l)$ is found out from Eq. (3.15) substituting $x = l$. Thus, the initial deflection at the free end is given by;

$$F(l)=\frac{(\cosh\lambda l-\cos\lambda l)(\sin\lambda l+\sinh\lambda l)+(\sin\lambda l-\sinh\lambda l)(\cos\lambda l+\cosh\lambda l)}{\cos\lambda l+\cosh\lambda l}$$

$$=\frac{2(\cosh\lambda l.\sin\lambda l-\sinh\lambda l.\cos\lambda l)}{\cos\lambda l+\cosh\lambda l} \tag{3.21}$$

The slope at any section of the beam is determined differentiating Eq. (3.19) with respect to x as;

$$\frac{\partial y(x,t)}{\partial x}=\frac{\partial F(x)}{\partial x}\left[\frac{y(l,0)}{F(l)}\right]\cos\omega_n t \tag{3.22}$$

The value of $\frac{\partial F(x)}{\partial x}$ is found out differentiating Eq. (3.15) with respect to x and is given by;

$$\frac{\partial F(x)}{\partial x} = \lambda \left[\frac{\begin{matrix}(\sinh \lambda x + \sin \lambda x)(\sin \lambda l + \sinh \lambda l) + \\ (\cos \lambda x - \cosh \lambda x)(\cos \lambda l + \cosh \lambda l)\end{matrix}}{\cos \lambda l + \cosh \lambda l} \right] \tag{3.23}$$

The slope at any section is found out substituting the values of $F(l)$ and $\frac{\partial F(x)}{\partial x}$ as;

$$\frac{\partial y(x,t)}{\partial x} = \left[\begin{matrix}(\sinh \lambda x + \sin \lambda x)(\sin \lambda l + \sinh \lambda l) + \\ (\cos \lambda x - \cosh \lambda x)(\cos \lambda l + \cosh \lambda l)\end{matrix} \right] \frac{\lambda . y(l,0) \cos \omega_n t}{2(\cosh \lambda l . \sin \lambda l - \sinh \lambda l . \cos \lambda l)} \tag{3.24}$$

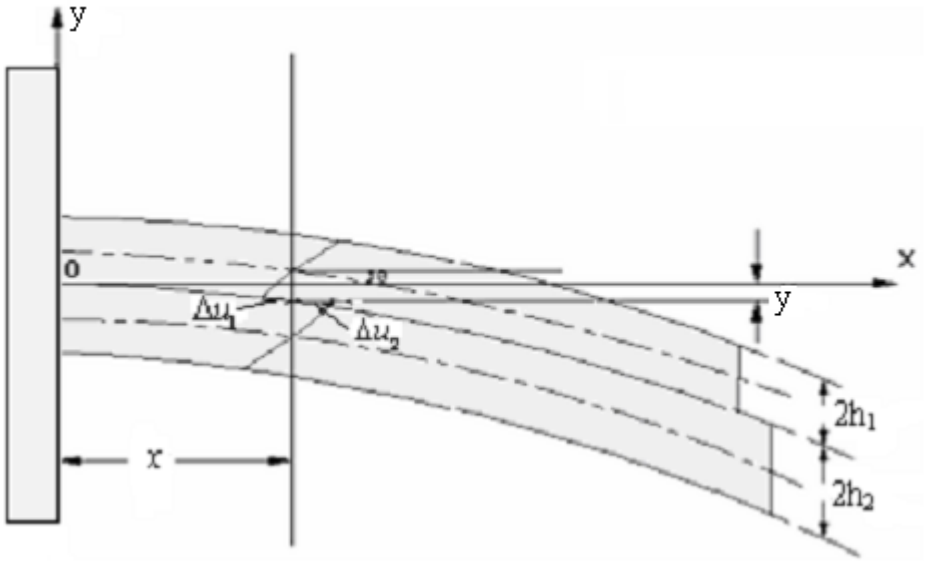

Fig. 3.2 Mechanism of dynamic slip at the interfaces

The jointed cantilever beam undergoes a relative displacement when an initial deflection is given at its free end as shown in Fig. 3.2. This relative displacement $u_0(x,t)$ at any distance x from the fixed end is equal to the sum of Δu_1 and Δu_2 and is given by;

$$u_o(x,t) = \Delta u_1 + \Delta u_2 = (h_1 + h_2)\left[\partial y(x,t)/\partial x\right] \tag{3.25}$$

The actual micro-slip $u_r(x,t)$ between the interfaces being always less than $u_o(x,t)$ is given as;

$$u_r(x,t) = \alpha u_o(x,t) \tag{3.26}$$

where α is a unknown constant called *dynamic slip ratio* and is defined as the ratio of the actual micro-slip $u_r(x,t)$ in the presence of friction to the ideal micro-slip $u_o(x,t)$ in the absence of friction. This varies with the pressure distribution and the surface condition at the jointed interface.

The maximum relative dynamic slip under a connecting rivet is found out modifying equation (3.26) and combining the same with Eq. (3.24) as;

$$u_{rM} = \left[\alpha\left(\frac{h_1+h_2}{2}\right)\right]\left[\begin{matrix}(\sinh\lambda x+\sin\lambda x)(\sin\lambda l+\sinh\lambda l)+\\(\cos\lambda x-\cosh\lambda x)(\cos\lambda l+\cosh\lambda l)\end{matrix}\right]\frac{\lambda.y(l,0)}{(\cosh\lambda l.\sin\lambda l-\sinh\lambda l.\cos\lambda l)} \tag{3.27}$$

This expression determines the relative dynamic slip under a single rivet at any distance x from the cantilever end. But the jointed cantilever beam consists of many numbers of similar rivets with definite spacing. As the centre distance of each connecting rivet changes from the fixed end of the cantilever beam, the relative dynamic slip under one rivet will differ from another. The overall dynamic slip for the entire jointed beam is determined from the contributions of all the connecting rivets. Hence, the actual overall maximum relative dynamic slip for a layered and jointed cantilever beam with 'q' number of equispaced connecting rivets is found from Eq. (3.27) as;

$$u_{rM} = \alpha\left(\frac{h_1+h_2}{2}\right)X\lambda\, y(l,0) \tag{3.28}$$

where $X = \left[\begin{matrix}(\sin\lambda l+\sinh\lambda l)\sum_{i=1}^{q}(\sinh\lambda x+\sin\lambda x)+\\(\cos\lambda l+\cosh\lambda l)\sum_{i=1}^{q}(\cos\lambda x-\cosh\lambda x)\end{matrix}\right]\times\left[\cosh\lambda l.\sin\lambda l-\cos\lambda l.\sinh\lambda l\right]^{-1}$

3.5 Pressure Distribution at the Jointed Interfaces

A layered and jointed construction is made by means of rivets that hold the members together at the interfaces. Under such circumstances, the profile of the interface pressure distribution assumes a significant role, especially in the presence of slip, to dissipate the vibration energy. Consequently, it is necessary to examine the exact

nature of the interface pressure profile and its magnitude across a beam layer for the correct assessment of the damping capacity in a jointed structure. This pressure distribution at the interfaces is due to the clamping of the rivets of the contacting members. As discussed in the previous chapter, almost all earlier analyses have examined the effect of pressure distribution on slip damping in a jointed beam with bolted joints but no significant work has been reported till date on the similar beams jointed with rivets.

When two or more members are pressed together by riveting, a circle of contact will be formed around the rivet with a separation taking place at a certain distance from the rivet hole as shown in Fig. 3.3.

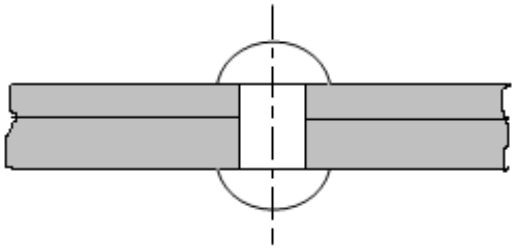

(a)

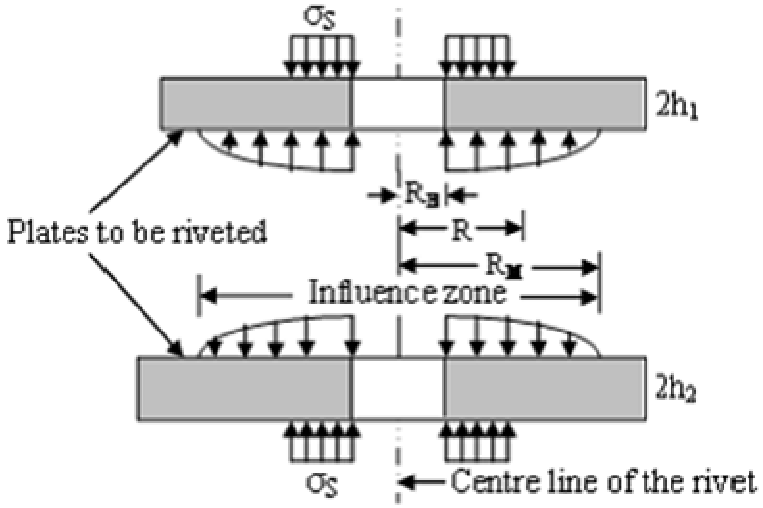

(b)

Fig. 3.3(a) Plates clamped by a rivet (b) Free body diagram of a riveted joint showing the influence zone

The contact between the connecting members develops an interface pressure whose exact nature and magnitude across the beam layer is very important for the correct assessment of damping capacity of a jointed structure. As established, the contact pressure at the jointed interface is non-uniform in nature being maximum at the rivet hole and decreases with the distance away from the rivet. This allows localized slipping at the interfaces while the overall joint remains locked. Further, this non-uniformity in contact pressure is influenced by the use of beams with different thickness ratios. Minakuchi et al. [32] have found that the interface pressure distribution due to this contact is parabolic with a circular influence zone circumscribing the rivet with diameter equal to 4.125, 5.0 and 5.6 times the diameter of the connecting rivet for thickness ratios 1.0, 1.5 and 2.0, respectively.

3.5.1 Determination of Pressure Distribution at the Interfaces

The interface pressure distribution under each rivet in a non-dimensional polynomial for layered and jointed structures is assumed as;

$$p/\sigma_S = C_1\left(R/R_B\right)^{10} + C_2\left(R/R_B\right)^{8} + C_3\left(R/R_B\right)^{6} + C_4\left(R/R_B\right)^{4} + C_5\left(R/R_B\right)^{2} + C_6 \tag{3.29}$$

where p, σ_S, R and R_B are the interface pressure, surface stress on the layered and jointed structure due to riveting, any radius within the influencing zone and radius of the connecting rivet, respectively and constants C_1 to C_6 of the polynomial are evaluated from the numerical data of Minakuchi et al. [32] by curve fitting using MATLAB software as shown in Table 3.1. The surface stress (σ_S) depends upon the initial tension on the rivet (P) and the area under a rivet head (A') and is evaluated from the relation $\sigma_S = P/A'$.

The above expression is an even function and a tenth order polynomial in terms of the normalized radial distance from the center of the rivet such that the function assumes its maximum value at the center of the rivet and decreases radially. It is evident from Table 3.1 that apart from the last two terms, values of the coefficients are relatively insignificant. This suggests for a linear profile for the pressure distribution across the interface. Damisa et al. [111] have used linear pressure profile in their analysis as an approximation. But a higher order polynomial for non-uniform interface pressure

distribution has been used in the present investigation in order to obtain a good accuracy.

Table 3.1 Values of polynomial constants for different thickness ratios

Constants	Thickness ratio = 1.0	Thickness ratio = 1.5	Thickness ratio = 2.0
C_1	0.14581228E-05	-1.737236E-07	-0.7419798E-07
C_2	-0.57951686E-04	1.398793E-05	0.74507972E-05
C_3	0.60446153E-03	-0.458813E-03	-0.29801024E-03
C_4	0.30852824E-02	0.817021E-02	0.62164809E-02
C_5	-0.95814172E-01	-0.877333E-01	-0.74592085E-01
C_6	0.53777732E+00	0.488330E+00	0.46039144E+00

Moreover, Table 3.1 establishes that the values of the polynomial constants are different for different thickness ratios for layered beams. This signifies that the pressure distribution varies and depends upon the thickness ratio of the layered beam. The pressure distribution curves as given by Minakuchi et al. [32] and obtained by curve-fitting along with their respective error as a measure of residuals are shown in Figs. 3.4 to 3.6 for different thickness ratios. Both these curves are in good agreement with a reasonable error below 1%. Figure 3.7 presents a cumulative plot showing the variation of pressure distribution at the interfaces of the jointed beams with different thickness ratios.

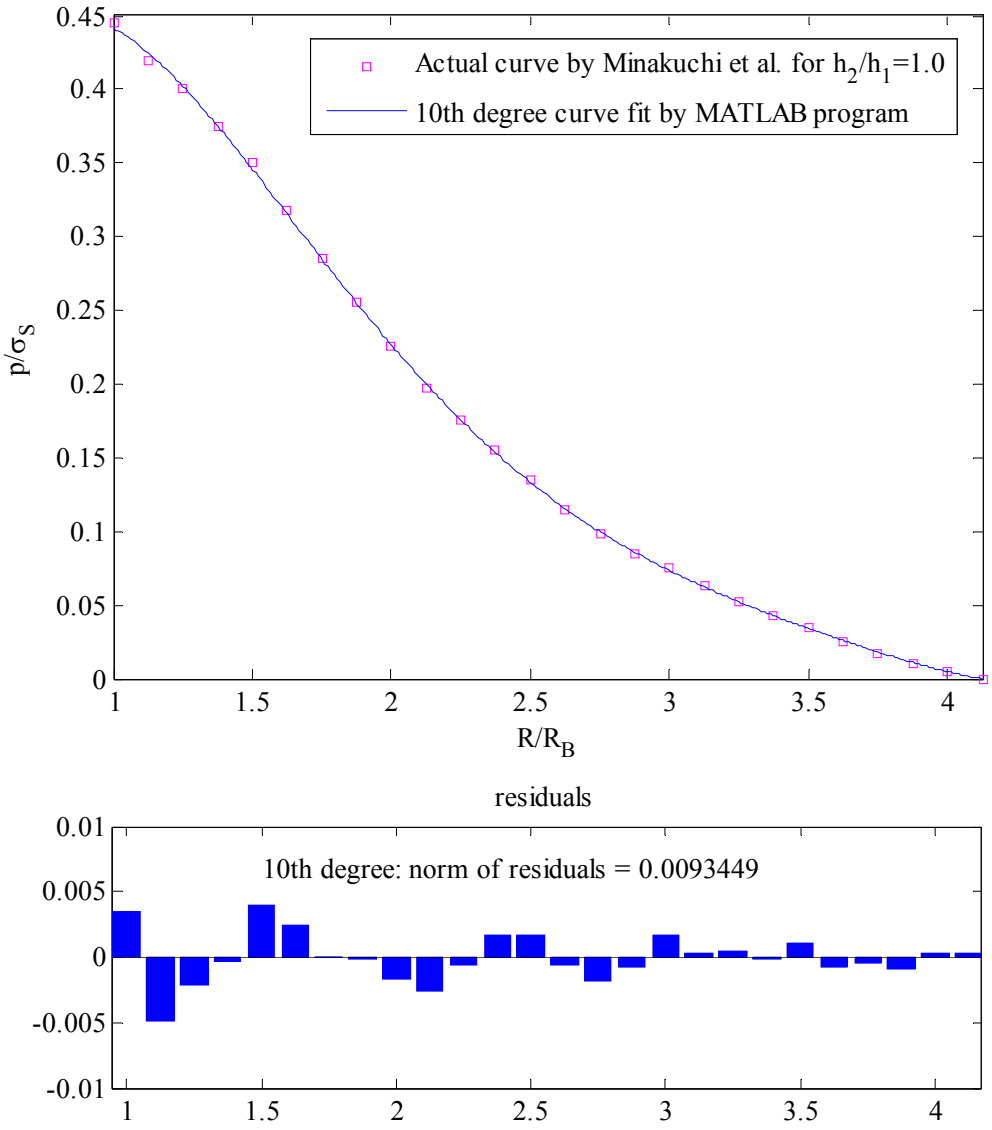

Fig. 3.4 Pressure distribution at the contact surface for thickness ratio 1.0

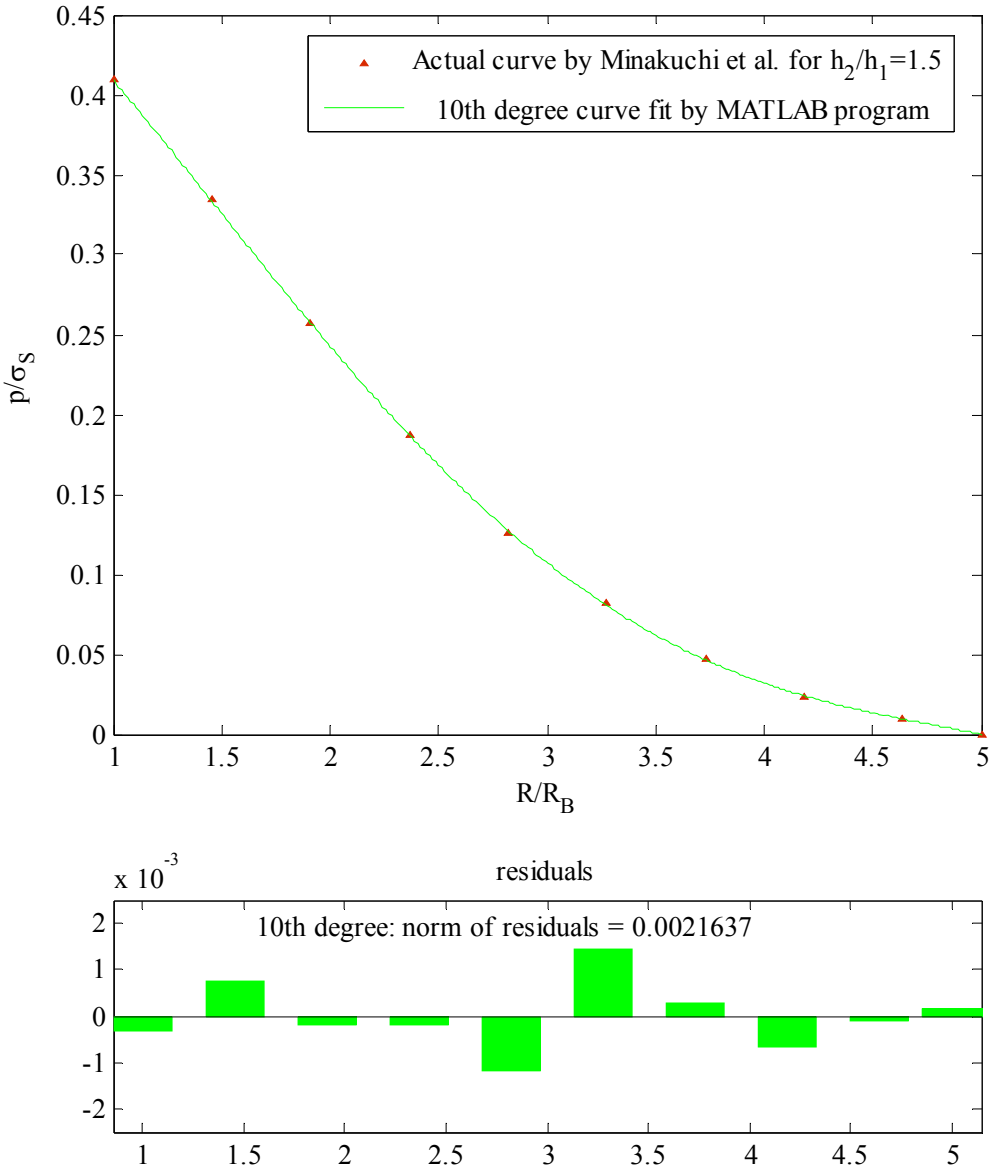

Fig. 3.5 Pressure distribution at the contact surface for thickness ratio 1.5

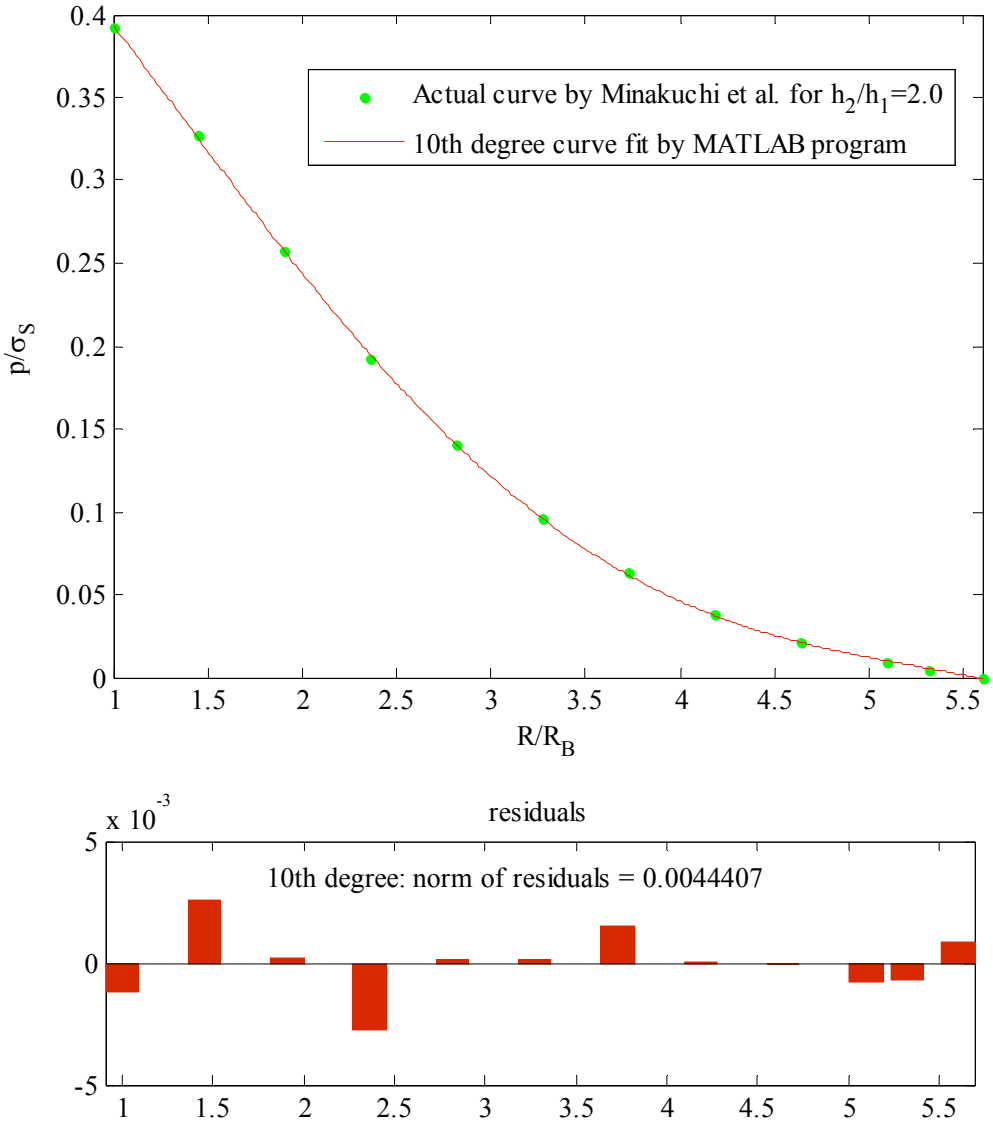

Fig. 3.6 Pressure distribution at the contact surface for thickness ratio 2.0

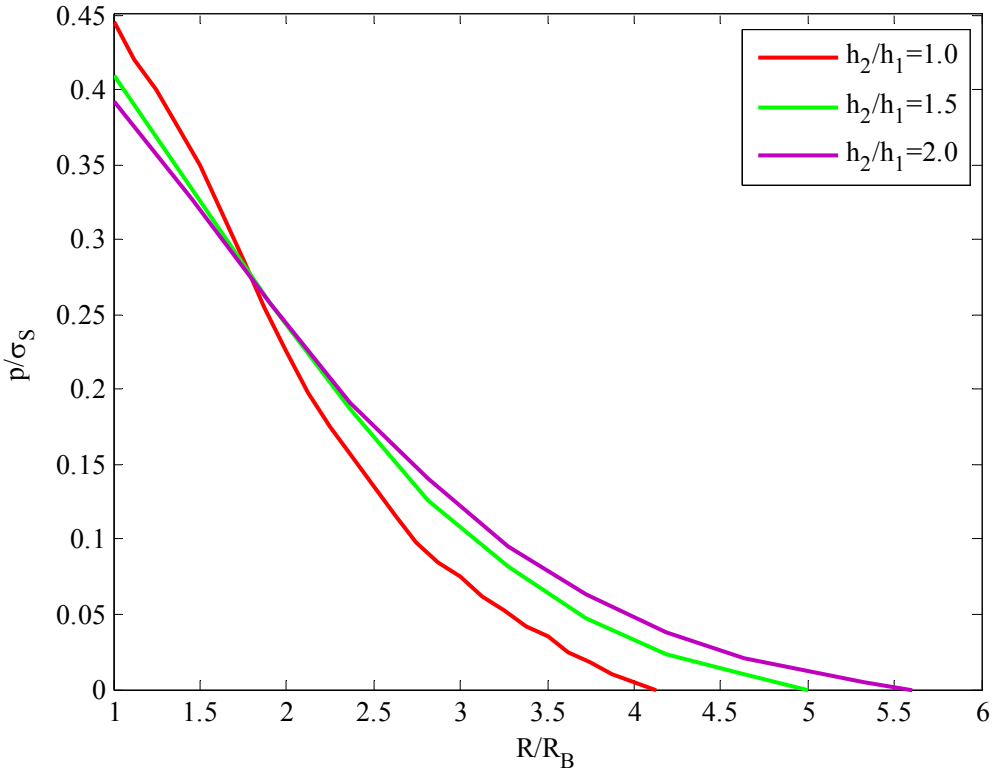

Fig. 3.7 Pressure distribution at the contact surface for thickness ratios 1.0, 1.5 and 2.0

3.6 Energy Dissipation due to Friction and Micro-slip

Structural joints are regarded as a potential source of energy dissipation in assembled structures. During vibration, a jointed beam oscillates about its mean position in the transverse direction. As a result, the different layers constituting the jointed beam undergo a small relative motion (micro-slip) at the interfaces. Friction will arise due to this relative motion of the components in contact and its presence results in the energy losses. The friction, although is viewed to have deteriorating effects on the performance of various systems, but it can also be used to enhance the system performance due to its damping properties. The energy loss of a structure is found out by measuring the area of the hysteresis loop obtained from the friction force vs. relative displacement plot.

3.6.1 Determination of Energy Dissipation per Cycle of Vibration

The components of a jointed cantilever beam are held together by riveting which further generates the pressure at the interfaces of the jointed structures as discussed in

Section 3.5.1. The normal force on the contact surface is determined from this interface pressure for accurate estimation of energy dissipation.

The interface pressure as given in Eq. (3.29) is rewritten as;

$$p = \left[C_1 \left(R/R_B \right)^{10} + C_2 \left(R/R_B \right)^8 + C_3 \left(R/R_B \right)^6 + C_4 \left(R/R_B \right)^4 + C_5 \left(R/R_B \right)^2 + C_6 \right] \times \left(P/A' \right)$$

$$= \left[C_1 \left(R/R_B \right)^{10} + C_2 \left(R/R_B \right)^8 + C_3 \left(R/R_B \right)^6 + C_4 \left(R/R_B \right)^4 + C_5 \left(R/R_B \right)^2 + C_6 \right] \times \left[P/2.0625\pi R_B{}^2 \right] \tag{3.30}$$

Taking the diameter of the rivet head equal to 1.75 times the diameter of rivet hole as per Shigley et al. [151], the area A' under rivet head is found to be $A' = \pi \left\{ \left(1.75R_B \right)^2 - \left(R_B \right)^2 \right\} = 2.0625\pi R_B{}^2$.

The direct evaluation of normal force is not possible owing to non-uniform distribution of pressure at the jointed interfaces. Instead, it is calculated considering a differential element in the form of an annular circular ring of radius R and thickness dR as shown in Fig. 3.8 whose area is given by $dA = 2\pi RdR$.

The normal force on the element of the circular ring is given as;

$$dN = p \times dA = 2p\pi RdR$$

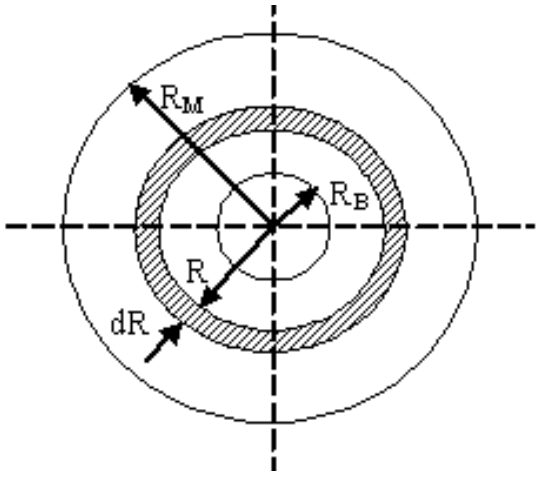

Fig. 3.8 Circular zone of influence of interface pressure

Hence, the total normal force at the interfaces under each connecting rivet is given by;

$$N = 2\pi \int_{R_B}^{R_M} pRdR$$

$$= 2\pi \int_{R_B}^{R_M} \left[C_1 \left(R/R_B \right)^{10} + C_2 \left(R/R_B \right)^8 + C_3 \left(R/R_B \right)^6 + C_4 \left(R/R_B \right)^4 + C_5 \left(R/R_B \right)^2 + C_6 \right]$$

$$\text{x} \left(\frac{P}{2.0625 R_B{}^2} \right) RdR$$

$$= \left(\frac{P}{2.0625} \right) \left[\begin{array}{l} (C_1/6)\left\{ \left(R_M/R_B \right)^{12} - 1 \right\} + (C_2/5)\left\{ \left(R_M/R_B \right)^{10} - 1 \right\} + (C_3/4)\left\{ \left(R_M/R_B \right)^8 - 1 \right\} \\ + (C_4/3)\left\{ \left(R_M/R_B \right)^6 - 1 \right\} + (C_5/2)\left\{ \left(R_M/R_B \right)^4 - 1 \right\} + C_6 \left\{ \left(R_M/R_B \right)^2 - 1 \right\} \end{array} \right] \quad (3.31)$$

where R_M is the limiting radius of the influencing zone under each connecting rivet. The initial tension "*P*" on the connecting rivet is the force with which the members are clamped together and is calculated from the relation $P = \sigma_0 \times A_0$, where σ_0 and A_0 are the initial stress on the rivet and cross-sectional area of the rivet, respectively. As per Maitra and Prasad [152], the initial stress (σ_0) in case of power driven rivets is $100 N/mm^2$.

Friction arises due to relative motion between two surfaces in contact and its presence in a vibrating system is responsible for energy dissipation. The magnitude of the normal force quantifies friction force and thereby the energy loss. Assuming that the Coulomb friction law is valid, the maximum frictional force at the interfaces is given by;

$$F_{rM} = \mu N \quad (3.32)$$

where μ is the kinematic coefficient of friction.

Energy dissipation in joints primarily occurs because of the presence of friction and micro-slip at the sliding interfaces. Assuming that the energy loss at the interfaces occurs within the area of influence of the interface pressure, the energy dissipation per cycle of vibration is determined from the area of the hysteresis loop as shown in Fig. 3.9 and is given in the integral form as;

$$E_f = \oint F_r du_r = 2 F_{rM} u_{rM} \quad (3.33)$$

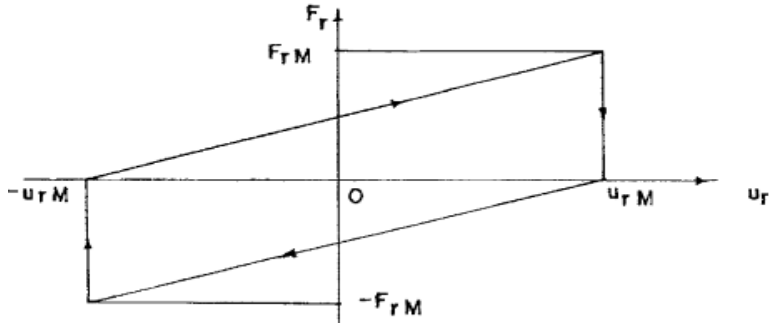

Fig. 3.9 Relationship between the friction force and relative dynamic slip during one cycle

3.7 Determination of Logarithmic Decrement

For a lightly damped linear system, the damping capacity of a jointed beam is usually determined from the logarithmic decrement method. Logarithmic decrement (δ), a measure of damping capacity, is defined as the natural logarithm of the ratio of two consecutive amplitudes in a given cycle. This approach is generally used to estimate the damping from the experiments in which the decaying amplitude is recorded from the time history plot. For the theoretical evaluation of damping, the energy approach is popular because the logarithmic decrement is fundamentally equal to the energy loss per cycle of vibration. Nishiwaki et al. [30] have presented that the logarithmic decrement depends on both the energy stored (E_n) and energy loss (E_{loss}) in a system during one cycle of vibration. Thus, the logarithmic decrement is expressed as;

$$\delta = \frac{1}{2}\left(E_{loss}/E_n\right) \tag{3.34}$$

The energy loss (E_{loss}) in a structural system usually consists of the sum of the energy loss (E_f) arising from friction at the joints and the energy loss (E_o) arising in material and at the support. Therefore, the logarithmic decrement (δ) of a jointed cantilever beam consists of δ_f caused by E_f and δ_o caused by E_o. Thus, the Eq. (3.34) is rewritten as;

$$\delta = \frac{1}{2}\left(\frac{E_f}{E_n}\right) + \frac{1}{2}\left(\frac{E_o}{E_n}\right) = \delta_f + \delta_o \tag{3.35}$$

The cause of energy loss may be due to different effects such as material, joint friction and support damping. However, it is assumed that all the energy dissipation is due to

the joint friction only. Therefore, the logarithmic decrement is theoretically evaluated from the energy loss arising from the friction only. Based on this assumption, the Eq. (3.35) is simplified as;

$$\delta \approx \frac{1}{2}\left(\frac{E_f}{E_n}\right) = \delta_f \tag{3.36}$$

The energy is stored within the system in the form of elastic bending strain energy when an initial excitation is given at the free end of the jointed cantilever beam. When the amplitude of excitation at the free end is $y(l.0)$, the amount of energy stored within the system per cycle of vibration (E_n) is given by;

$$E_n = \frac{1}{2} k\, y^2 (l,0) \tag{3.37}$$

where k is the static bending stiffness of the layered and jointed cantilever beam. The static stiffness of a jointed beam is always less than that of its equivalent solid one. The static stiffness of the jointed cantilever beam is calculated from the experiments to find out the energy stored in a vibrating system accurately.

Substituting the values of E_f and E_n as presented in Eq. (3.33) and (3.37), respectively; the Eq. (3.36) for logarithmic decrement is modified as;

$$\delta = \frac{\mu N \alpha (h_1 + h_2) X \lambda}{k\, y(l,0)} \tag{3.38}$$

This is the generalized expression for numerical evaluation of logarithmic decrement for two-layered beams of any thickness. When the thickness of each layer of the beam is equal, i.e., $2h_1 = 2h_2$ ($h_1 = h_2$), the expression (3.38) is modified to;

$$\delta = \frac{2\mu N \alpha h X \lambda}{k\, y(l,0)} \tag{3.39}$$

Moreover, this can be extended to cantilever beams having multi-number of layers of equal thickness. The use of more number of layers increases the number of interfaces and hence the energy losses, thereby increasing the logarithmic decrement of a multi-layered beam. If '*m*' number of layers are used to construct a jointed beam, the

number of interfacial layers is always (m-1) and therefore, the logarithmic decrement for such a multi-layered beam is found out modifying expression (3.39) as;

$$\delta = \frac{2(m-1)\mu N \alpha h X \lambda}{k\, y(l,0)} \tag{3.40}$$

However, the use of increased number of layers also affects the energy stored in the system (E_n) due to varying stiffness of the jointed beam.

The energy dissipation principally depends upon the kinematic coefficient of friction (μ) and dynamic slip ratio (α) at the interfaces. It is very difficult to assess the damping produced in the joints due to variations of the above two vital parameters under dynamic conditions. These two parameters are inter-dependent and inversely related, i.e., if one is increasing, the other is decreasing and vice versa. However, their product ($\alpha.\mu$) is found to be constant for a particular specimen irrespective of the surface condition. Thus, this product $\alpha.\mu$ is found out modifying Eq. (3.38) as;

$$\alpha.\mu = \frac{k\, y(l,0)\delta}{N(h_1 + h_2)X\lambda} \tag{3.41}$$

This product has been found out from the experimental results of logarithmic decrement for a particular rivet diameter using the Eq. (3.41) and subsequently used to find out the numerical values of the logarithmic decrement for other conditions of the beam using Eq. (3.38).

3.8 Chapter Summary

In this chapter, an exact solution is presented considering the distributed-parameter model for the beam structure. The governing equations of the transverse vibration have been derived on the assumption of the Euler-Bernoulli beam theory neglecting the effects of shear deformation and rotary inertia. Further, the total relative dynamic slip at the interfaces has been evaluated considering the expressions for the slope and deflection. It is found that the total slip is a function of the distance from the fixed end. The interface pressure distribution has been determined and is found to be nonlinear being maximum at the rivet and decreases monotonically and radially away from the rivet. Subsequently, the equations of logarithmic decrement for two as well as multi-layered beams jointed with rivets have been developed. Moreover, the

damping capacity of cantilever beams with different thickness ratio has been evaluated theoretically. It is established that the micro-slip, kinematic coefficient of friction and the nature of pressure distribution at the interfaces, diameter of the rivets, thickness, cantilever length and number of layers play major roles in quantifying the damping of such beam structures. Therefore, an extensive study on all the above vital parameters has been carried out in the present investigation.

CHAPTER 4

THEORETICAL ANALYSIS BY FINITE ELEMENT APPROACH

4.1 Introduction

In the Chapter 3, the analysis of a jointed cantilever beam has been dealt in detail considering the model as a distributed-parameter system. Although a distributed-parameter model accurately reflects the real situation thus giving an exact solution, but its application is restricted to relatively simple systems. In fact, many practical problems in engineering deal with complicated shapes with arbitrary boundary conditions whose analysis becomes extremely difficult and in a few cases almost impossible by the conventional methods. Therefore, various numerical solution techniques are available to solve all these engineering problems. One of such numerical techniques used is the *finite element method* based on the Galerkin's method of residual approach which presents an approximate solution by discretizing the continuous beam into finite number of elements of equal length. In contrast to the analytical solutions which show the exact behavior of a system at any point within the system, numerical solutions are approximate ones agreeing with the exact solutions at some discrete points.

There are two common classes of numerical methods: (1) finite difference methods and (2) finite element methods. In the finite difference methods, the differential equation is written for each node and the derivatives are replaced by difference equations. This approach results in a set of simultaneous linear equations. Although finite difference methods are easy to understand in simple problems, but their application becomes difficult to problems with complex geometries or complex boundary conditions.

Contrary to this, the finite element method uses integral formulations to create a system of algebraic equations. In this technique, all the complexities of the problems such as varying shape, boundary conditions and loads are maintained as usual and the solutions are obtained in an approximate manner. The finite character of the structural

connectivity makes it possible to obtain a solution by means of simultaneous algebraic equations. Because of its diversity and flexibility, it receives much attention in present day engineering problems. Over the years, this technique has been so well established that it is considered to be one of the best methods now for solving a wide variety of practical problems efficiently. Both the static and dynamic problems are effectively analyzed by this method.

4.2 Basic Concepts of Finite Element Method

The basic concept of the finite element method is that the actual continuum is represented as an assemblage of subdivisions called finite elements. Each element is free to deform and may have different material and geometrical properties. The proper choice of the element varies from one-dimensional axial element to three-dimensional solid element depending upon the nature of problem. The elements considered in the present investigation are one-dimensional beam elements representing the neutral axis of the beam. These elements are considered to be interconnected at specified joints called nodes. These nodes usually lie on the element boundaries where adjacent elements are considered to be connected.

The actual variation of the field variable (e.g., displacement) inside an element is not known. Instead, the field variable within an element is normally expressed in terms of nodal values. The variation of this field variable within a finite element is approximated by a simple function called shape function. The shape function dictates the size of these nodal contributions. Further, the element stiffness and mass matrices of the individual elements are evaluated. The governing equations for each element are derived and assembled to find out the system equations describing the behavior of the body. Thus, each individual element and its contributions are considered adequately in obtaining a global model of a structure.

Summarizing the above, the finite element analysis consists of the following steps:

• Discretization of the domain into a finite number of elements

• Selection of proper shape functions

• Development of the element stiffness and mass matrices

• Assembly of the element matrices to obtain the global matrix for the entire domain

• Imposition of the boundary conditions

• Solution of equations

4.3 Dynamic Equations of Motion

Most physical phenomena encountered in engineering applications are modeled by differential equations. The Euler-Bernoulli equation for bending of the beam undergoing free transverse vibration is given by the partial differential equation as;

$$\rho A\frac{\partial^2 v}{\partial t^2}+EI\frac{\partial^4 v}{\partial x^4}=0 \tag{4.1}$$

where ρ, A, $v(x,t)$, E and I are the mass density, cross-sectional area, transverse displacement, modulus of elasticity, and second moment of area of the beam, respectively.

In most problems, it is difficult to obtain an exact solution and hence, an approximate solution is used to solve such problems. Obviously, this solution is erroneous and therefore, various weighted residual techniques are used to minimize this error. In particular, the Galerkin's weighted residual approach is a powerful method of finding approximate solutions to differential equations and is most popular with respect to finite element technique. Applying the Galerkin's method, Eq. (4.1) is modified as;

$$\int_0^L\left(\rho A\frac{\partial^2 v}{\partial t^2}+EI\frac{\partial^4 v}{\partial x^4}\right)w dx=0 \tag{4.2}$$

where $w(x)$ is the Galerkin's weighting function and L is the length of the beam.

Discretizing the beam into "n" number of finite elements of length l as shown in Fig. 4.1, the weak form of the residual statement has been developed integrating second term of Eq. (4.2) twice such that the differentiation between the field variable and the weighting function are evenly distributed. The weak form of the above differential equation is given by;

$$\sum_{i=1}^{n}\left[\int_0^l \rho A\frac{\partial^2 v}{\partial t^2}w dx+\int_0^l EI\frac{\partial^2 v}{\partial x^2}\frac{\partial^2 w}{\partial x^2}dx\right]+\left[Vw-M\frac{\partial w}{\partial x}\right]_0^L=0 \tag{4.3}$$

where $V = EI\left(\partial^3 v/\partial x^3\right)$ and $M = EI\left(\partial^2 v/\partial x^2\right)$ are the shear force and bending moment of the beam, respectively. The last term in Eq. (4.3), i. e., $\left[Vw - M\dfrac{\partial w}{\partial x}\right]_0^L$ represents the boundary conditions of shear force and bending moment at the locations $x = 0$ and $x = L$ of the beam which vanishes for a cantilever beam. Accordingly, the Eq. (4.3) has been simplified as;

$$\sum_{i=1}^{n}\left(\int_0^l \rho A\frac{\partial^2 v}{\partial t^2}w\,dx + \int_0^l EI\frac{\partial^2 v}{\partial x^2}\frac{\partial^2 w}{\partial x^2}\,dx\right) = 0 \tag{4.4}$$

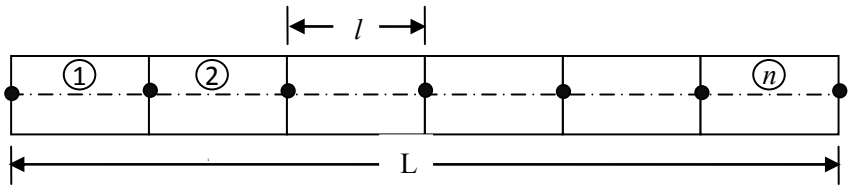

Fig. 4.1 Mess of *n* number of beam elements

The particular beam is divided into a number of elements equal to twice the number of rivets used in that specimen. Each element is considered as one-dimensional of equal length. A standard beam element is modeled using two nodes with two degrees of freedom per node (translation and rotation) as shown in Fig. 4.2. The contribution of each element depends on both the displacement and rotation at the nodes associated with the corresponding element. The four degrees of freedom for an element are indicated by v_1, θ_1, v_2 and θ_2. Since there are four nodal displacements, a cubic displacement model for *v(x,t)* has been assumed as;

$$v(x,t) = a_0 + a_1 x + a_2 x^2 + a_3 x^3 \tag{4.5}$$

Differentiating with respect to *x*, the slope is given by;

$$dv/dx = a_1 + 2a_2 x + 3a_3 x^2 \tag{4.6}$$

where the constants a_0, a_1, a_2, a_3 are evaluated using the following boundary conditions:

$$\begin{aligned} v(x) &= v_1 \quad and \quad \frac{dv}{dx}(x) = \theta_1 \quad at\ x = 0 \\ v(x) &= v_2 \quad and \quad \frac{dv}{dx}(x) = \theta_2 \quad at\ x = l \end{aligned} \tag{4.7}$$

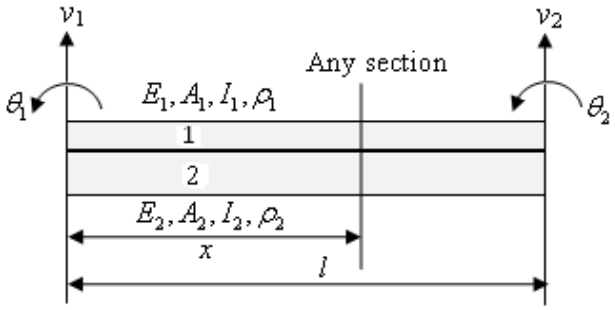

Fig. 4.2 A beam element along with its nodal displacements

The constants a_0, a_1, a_2, a_3 are found out in terms of nodal variables $v_1, \theta_1, v_2, \theta_2$. Substituting the above, the Eq. (4.5) is modified as;

$$v(x,t) = S_1(x)v_1(t) + S_2(x)\theta_1(t) + S_3(x)v_2(t) + S_4(x)\theta_2(t) \tag{4.8}$$

where

$$\begin{aligned} S_1(x) &= \left(2x^3 - 3lx^2 + l^3\right)/l^3 \\ S_2(x) &= \left(x^3 - 2lx^2 + l^2x\right)/l^3 \\ S_3(x) &= \left(-2x^3 + 3lx^2\right)/l^3 \\ S_4(x) &= \left(x^3 - lx^2\right)/l^3 \end{aligned} \tag{4.9}$$

Assuming that each layer has the same transverse displacement and rotation at any section, the deformation within the eth element *v(x,t)* of the Eq. (4.8) is expressed in the form of compact matrix as;

$$v(x,t) = \mathbf{S}(x)\boldsymbol{d}^e(t) \tag{4.10}$$

where the vector $\boldsymbol{d}^e(t) = \begin{bmatrix} v_1(t) & \theta_1(t) & v_2(t) & \theta_2(t) \end{bmatrix}^T$ contains the element nodal degrees of freedom and the matrix $\mathbf{S}(x) = \begin{bmatrix} S_1 & S_2 & S_3 & S_4 \end{bmatrix}$ defines the cubic shape functions.

As per Galerkin's method, both the weighting and shape functions are same and applying the cubic shape functions to the first term of the Eq. (4.4), i. e., $\int_0^l \rho A \frac{\partial^2 v}{\partial t^2} w dx$, the element mass matrix is found to be;

$$\int_0^l \rho A \frac{\partial^2 v}{\partial t^2} w dx = \int_0^l \rho A \frac{\partial^2}{\partial t^2}\left(\mathbf{S}\boldsymbol{d}^e\right)\mathbf{S} dx$$
$$= \int_0^l \rho A \mathbf{S}^{\mathbf{T}}\mathbf{S}\ddot{\boldsymbol{d}}^e dx$$

Since nodal accelerations ($\ddot{\boldsymbol{d}}^e$) remains constant within the element, these terms are taken out and the above equation is modified as;

$$\int_0^l \rho A \frac{\partial^2 v}{\partial t^2} w dx = \left(\int_0^l \rho A \mathbf{S}^{\mathbf{T}}\mathbf{S}\, dx\right)\ddot{\boldsymbol{d}}^e = \mathbf{m}^{\mathbf{e}}\ddot{\boldsymbol{d}}^e \tag{4.11}$$

where the superscript double dot denotes the second derivative of time and $\mathbf{m}^{\mathbf{e}} = \left(\int_0^l \rho A \mathbf{S}^{\mathbf{T}}\mathbf{S} dx\right)$ represents the consistent mass matrix of the element. Assuming that the quantity ρA is constant, the element mass matrix is given by;

$$\mathbf{m}^{\mathbf{e}} = \frac{\rho A l}{420}\begin{bmatrix} 156 & 22l & 54 & -13l \\ 22l & 4l^2 & 13l & -3l^2 \\ 54 & 13l & 156 & -22l \\ -13l & -3l^2 & -22l & 4l^2 \end{bmatrix} \tag{4.12}$$

where $\rho A = \rho_1 A_1 + \rho_2 A_2$

Again applying the Galerkin's method to the second term of the Eq. (4.4), i.e., $\int_0^l EI \frac{\partial^2 v}{\partial x^2}\frac{\partial^2 w}{\partial x^2} dx$, the element stiffness matrix is obtained as;

$$\int_0^l EI \frac{\partial^2 v}{\partial x^2}\frac{\partial^2 w}{\partial x^2} dx = \int_0^l EI \frac{\partial^2}{\partial x^2}\left(\mathbf{S}\boldsymbol{d}^e\right)\frac{\partial^2 \mathbf{S}}{\partial x^2} dx$$
$$= \int_0^l EI \frac{\partial^2 \mathbf{S}}{\partial x^2}\boldsymbol{d}^e \frac{\partial^2 \mathbf{S}}{\partial x^2} dx$$

Since nodal displacements ($\boldsymbol{d}^e$) are constant at the nodes, the above equation is modified as;

$$\int_0^l EI \frac{\partial^2 v}{\partial x^2}\frac{\partial^2 w}{\partial x^2} dx = \left(\int_0^l EI\, \mathbf{S}''^{\mathbf{T}}\mathbf{S}'' dx\right)\boldsymbol{d}^e = \mathbf{k}^{\mathbf{e}}\boldsymbol{d}^e \tag{4.13}$$

where the double prime denotes the second derivative of the function and $\mathbf{k}^{\mathbf{e}} = \left(\int_0^l EI\, \mathbf{S}''^{\mathbf{T}} \mathbf{S}'' dx \right)$ represents the element stiffness matrix. Assuming that the beam rigidity *EI* is constant within the element, the element stiffness matrix is simplified to;

$$\mathbf{k}^{\mathbf{e}} = \frac{EI}{l^3} \begin{bmatrix} 12 & 6l & -12 & 6l \\ 6l & 4l^2 & -6l & 2l^2 \\ -12 & -6l & 12 & -6l \\ 6l & 2l^2 & -6l & 4l^2 \end{bmatrix} \tag{4.14}$$

where $EI = E_1 I_1 + E_2 I_2$

The Eq. (4.4) is modified substituting Eqs. (4.11) and (4.13) as;

$$\sum_{i=1}^{n} \left(\mathbf{m}^{\mathbf{e}} \ddot{\boldsymbol{d}}^{e} + \mathbf{k}^{\mathbf{e}} \boldsymbol{d}^{e} \right) = \boldsymbol{0} \tag{4.15}$$

Considering the effect of all the elements, the above equation is further modified to;

$$\mathbf{M}\ddot{\boldsymbol{D}} + \mathbf{K}\boldsymbol{D} = \boldsymbol{0} \tag{4.16}$$

where $\boldsymbol{D}$ and $\ddot{\boldsymbol{D}}$ are the displacement and acceleration vectors of all the nodes of the entire structure; **K** and **M** are the global stiffness and mass matrices, respectively. The above equation represents the required dynamic equation for the free un-damped vibration of the cantilever beam.

The effect of damping has not been considered in the above derivation since the direct formation of damping matrix due to interfacial slip is very difficult in actual practice. Instead, an alternative approach has been used to account for damping in terms of logarithmic decrement. In this regard, the expressions for dynamic slip, input strain energy and energy loss in a jointed beam have been formulated using the same stiffness matrix, shape function and displacement vector. The detailed procedure for evaluating damping in a layered and jointed structure has been discussed in the subsequent section.

4.4 Natural Frequencies and Mode Shapes

The finite element method can be advantageously used to evaluate the natural frequencies and mode shapes of a dynamic system. If an elastic structure is excited, it

oscillates harmonically depending on the distribution of the mass and stiffness in the structure. The amplitude of oscillations will decay progressively in the presence of damping and if the magnitude of damping exceeds a certain critical value, the oscillatory character of the motion will cease altogether. On the other hand, if damping is absent, the oscillatory motion will continue indefinitely with the same initial amplitude of excitation. In all practical cases, the vibration always occurs at certain frequencies known as natural frequencies which follow the well defined deformation patterns known as mode shapes. The study of natural frequencies and mode shapes in a vibrating system is known as modal analysis.

For multiple degrees of freedom systems, the modes essentially describe the nature of motion and provide physical understanding of their dynamic behavior. The modes are characterized by the eigenvalues and eigenvectors representing the natural frequencies and mode shapes, respectively. The global mass and stiffness matrices are utilized to determine the natural frequencies of vibration and mode shapes. Depending on the damping, the eigenvalues and eigenvectors can be real or complex. However, the effect of damping is generally neglected in the determination of natural frequencies and mode shapes of a lightly vibrating system. Therefore, real eigenvalues and eigenvectors are derived from the assumed undamped equation of motion. This assumption fairly holds good in most of the practical cases where damping is less pronounced.

4.4.1 Determination of Natural Frequencies

The natural frequency is an important parameter in the dynamic analysis of structures. If such a system is excited by an external force and both the exciting and natural frequencies are very close to each other, the resonant condition will prevail, thereby resulting violent vibration of the structure. This condition often leads to the catastrophic failure of the system. Therefore, it becomes imperative to design the dynamic system for its safe operation. The structure generally possesses as many natural frequencies as its degrees of freedom (also modes of vibration). In fact, it is not necessary to calculate all the natural frequencies since many of the frequencies do not get excited in actual practice.

Generally, the micro-slip at the interfaces due to initial excitation of the jointed beam is more at lower modes than the higher ones as established by Nishiwaki et al. [30]. Moreover, Clough and Penzien [153] have shown that the mathematical idealization of any structural system is more reliable at lower modes of vibration. Considering all these, the higher modes are usually ignored in the dynamic analysis of structures. Therefore, the first mode of vibration has been taken into account in the present investigation neglecting the effect of higher modes.

The equation of motion for free vibration as given in Eq. (4.16) represents a generalized linear eigenvalue problem and its solution is given by;

$$\boldsymbol{D} = \boldsymbol{\phi} e^{i\omega t} \tag{4.17}$$

where $\boldsymbol{\phi}$ and ω are the mode shapes (eigenvector) and natural frequency (eigenvalue) of vibration, respectively.

Substituting Eq. (4.17) in Eq. (4.16) results;

$$\left[\mathbf{K} - \omega^2 \mathbf{M}\right] \boldsymbol{\phi} = \boldsymbol{0} \tag{4.18}$$

In order to obtain a non-trivial solution, the coefficient matrix must be singular, which means its determinant must be equal to zero, i.e.,

$$\left|\mathbf{K} - \omega^2 \mathbf{M}\right| = \boldsymbol{0} \tag{4.19}$$

An algebraic polynomial equation is obtained in ω^2 after expanding the above determinant. The roots of this equation give the eigenvalues representing natural frequencies of the system. The solution for ω produces pairs of positive and negative values of equal magnitude. The negative values of ω are usually ignored. The positive values of ω must be ordered so that the first lowest frequency is the fundamental frequency.

4.4.2 Determination of Mode Shapes

The structures usually vibrate in a definite way depending upon its natural frequency so that the characteristic shape or mode of vibration is established distinctly. Therefore, the information regarding the deflection pattern associated with each natural frequency is to be known for accurate dynamic analysis.

The mode shapes in the form of eigenvectors are found out from Eq. (4.18) as;

$$\left[\mathbf{K} - \omega_i^2 \mathbf{M}\right] \boldsymbol{\phi}_i = \mathbf{0} \tag{4.20}$$

where ω_i and $\boldsymbol{\phi}_i$ are the eigenvalues and eigenvectors representing the natural frequencies and mode shapes of the vibrating system at i^{th} mode, respectively.

Since the system of equations represented in Eq. (4.20) is homogeneous, the mode shape is not unique. The first mode shape along with its natural frequency of a particular cantilever beam specimen is shown in Fig. 4.3.

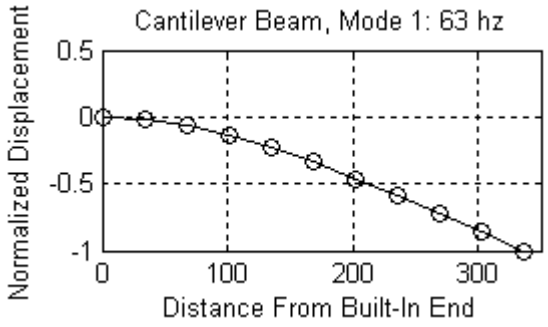

Fig. 4.3 Mode shapes for single degree of freedom

4.5 Determination of Logarithmic Decrement

The nature of the interface pressure profile across the beam layer and its magnitude depends on the thickness ratio of the connecting members as discussed in the previous chapter. Minakuchi et al. [32] have established that the pressure distribution at the interfaces is parabolic with a circular influence zone circumscribing the rivet with diameter equal to 4.125, 5.0 and 5.6 times the diameter of the connecting rivet for thickness ratios 1.0, 1.5 and 2.0, respectively. The interface pressure under each rivet in a non-dimensional polynomial has been given in Eq. (3.29) which is expressed as;

$$\frac{p}{\sigma_S} = C_1\left(\frac{R}{R_B}\right)^{10} + C_2\left(\frac{R}{R_B}\right)^{8} + C_3\left(\frac{R}{R_B}\right)^{6} + C_4\left(\frac{R}{R_B}\right)^{4} + C_5\left(\frac{R}{R_B}\right)^{2} + C_6 \tag{4.21}$$

The constants of the polynomial C_1 to C_6 have been evaluated from the numerical data of Minakuchi et al. [32] using the curve fitting with MATLAB software and are presented in Table 3.1. The profile and magnitude of the pressure distribution at the interfaces of a layered and jointed cantilever beam are shown in Fig. 3.7. It is

established that the beam thickness ratio has an effect on the interface pressure distribution.

The maximum frictional force has been found out previously as given by Eq. (3.32) which is given as;

$$F_{rM} = \mu N \tag{4.22}$$

where N is the total normal force under each connecting rivet which is evaluated using the Eq. (3.31).

When the beam is excited at the free end, relative motion takes place at the mating surfaces as shown in Fig. 3.2 to produce the required damping effects. The relative dynamic slip under a connecting rivet is given by;

$$u_r(x,t) = \alpha\left(h_1 + h_2\right)\frac{\partial v(x,t)}{\partial x} = \alpha\left(h_1 + h_2\right)\left[\frac{d\mathbf{S}}{dx}\right]\left\{\boldsymbol{d}^e\right\} \tag{4.23}$$

where α is the dynamic slip ratio.

As discussed, the amount of slip under one rivet differs from another because of different placement of rivets from the fixed end. Considering the influence of "q" number of equi-spaced rivets, the overall maximum relative dynamic slip of a jointed cantilever beam is found to be;

$$u_{rM} = \alpha\left(h_1 + h_2\right)Y \tag{4.24}$$

where $Y = \sum_{i=1}^{q}\frac{d\mathbf{S}}{dx}\left\{\boldsymbol{d}^e\right\}$

The energy dissipated per cycle of vibration is of paramount importance in computing the damping of the jointed structures. The energy is dissipated through frictional effects associated with relative shear displacements of the structural members and is a function of micro-slip as well as friction at the interfaces. The energy loss per cycle of vibration as given by Eq. (3.33) has been modified as;

$$E_f = 2\alpha\,\mu\,N\left(h_1 + h_2\right)Y \tag{4.25}$$

The beam will deflect in the transverse direction on excitation at the free end. The strain energy stored per cycle of vibration is given by;

$$E_n = \frac{1}{2}\boldsymbol{D}^T\mathbf{K}\boldsymbol{D} \tag{4.26}$$

The damping capacity in terms of logarithmic decrement has been evaluated as given in Eq. (3.36) which is written as;

$$\delta = \frac{E_f}{2E_n} \tag{4.27}$$

The logarithmic damping decrement is found out combining the Eqs. (4.25) and (4.26) with Eq. (4.27) as;

$$\delta = \frac{2\alpha\,\mu N\left(h_1 + h_2\right)Y}{\boldsymbol{D}^T\mathbf{K}\boldsymbol{D}} \tag{4.28}$$

This equation presents the generalized expression for logarithmic decrement for two-layered beams of unequal thickness. When the thickness of each layer of the beam remains the same ($2h$), the expression (4.28) is modified to;

$$\delta = \frac{4\alpha\,\mu N\,hY}{\boldsymbol{D}^T\mathbf{K}\boldsymbol{D}} \tag{4.29}$$

More often multi-layered beams are used in engineering applications where higher damping is required. The above formulation can also be extended for such cases with multi-number of layers of equal thickness. If 'm' number of layers are used to construct a jointed beam, the logarithmic decrement for such a beam is found out modifying the expression (4.29) as;

$$\delta = \frac{4\left(m-1\right)\alpha\,\mu N\,hY}{\boldsymbol{D}^T\mathbf{K}\boldsymbol{D}} \tag{4.30}$$

4.6 Chapter Summary

In gist of the present chapter, the formulation of the finite element equations has been presented from the weak form of the Galerkin weighted residual statement. An approximate solution is obtained considering the beam model as a discrete system. The basic concept of this method is that a body is considered to consist of an assemblage of individual elements interconnected at finite number of nodal points. In the present problem, a given beam is discretized into finite number of one-dimensional elements of equal length. The number of elements is taken as twice the

number of rivets used in a particular specimen. In principle, rapid convergence to the exact solution occurs with an increasing number of finite elements. However, no significant improvement in convergence is observed with further increase in the number of elements thus establishing the optimality condition. Further, each element consists of two nodes with each node having two degrees of freedom, i.e. transverse displacement and rotation. Cubic shape functions are considered for the transverse vibration of the beam in terms of nodal variables. In the derivation of vibration equation, the Euler-Bernoulli beam theory is assumed along with other assumptions discussed in the introduction chapter.

The damping has been defined in terms of logarithmic decrement because they can be determined experimentally or computed numerically with adequate precision. The formulation of damping matrix in case of slip damping has not yet been available in the literature and this study is another piece of work for future researchers. For this reason, it is generally more convenient and physically reasonable to assess the damping effect due to micro-slip using an alternative energy approach rather than by means of an explicit damping matrix. In this regard, the dynamic slip, input strain energy and energy loss in a jointed beam have been formulated using the same stiffness matrix, mass matrix, shape function and displacement vector. The consistent-mass matrix has been used for greater accuracy in the present formulation with the inclusion of all rotational and translational degrees of freedom.

CHAPTER 5

EXPERIMENTAL ANALYSIS

5.1 Introduction

In the last two chapters, the classical and finite element methods for measuring the damping in layered and jointed cantilever beams of the present problem have been discussed at length. In practice, the experimental study of damping becomes necessary as the theoretically computed results of a machine or structure may be different from that of the actual values due to the various assumptions made in the analysis. Unlike mass and stiffness properties, damping is purely a dynamic characteristic of a system which needs to be measured by conducting the dynamic tests on a structure. Therefore, the purpose of this chapter is to verify the theories developed in Chapters 3 and 4 by conducting experiments and to assess the accuracy of the analysis. A number of experiments have been conducted using mild steel and aluminium beam specimens to find out the natural frequencies and logarithmic decrements undergoing free vibration. The details of the experimental set-up, specimens used and the procedures adopted along with the results are enumerated in the succeeding sections.

5.2 Preparation of Specimens

The test specimens of different sizes are prepared from the same stock of commercial mild steel and aluminium flats as presented in Tables 5.1 to 5.4. Equi-spaced rivets of 4, 5, 6, 8, 10 and 12 mm diameter are used to fabricate two-layered specimens with a constant clamping force. Moreover, multi-layered specimens made up of mild steel and aluminium is fabricated from 10 mm diameter connecting rivets. For all these specimens, the distance between the consecutive rivets is so arranged that their influence zone just touches each other at the point of separation. The width and length of the specimens are also taken from the rivet diameter and beam thickness ratio as per the zone of influence. For example, the centre distance between two consecutive rivets and width of specimens are kept as 4.125, 5.0 and 5.6 times the diameter of the rivet for beam thickness ratios of 1.0, 1.5 and 2.0, respectively. This is in accordance

with the zone of influence as developed in the theory. The length of the specimens has also been varied accordingly in order to accommodate different number of rivets. This variation in cantilever length and width for a particular specimen affects the static bending stiffness as well as natural frequency of vibration of the layered and jointed cantilever specimens. The photographs of a few specimens used in the experiments are presented in Fig. 5.1.

(a)

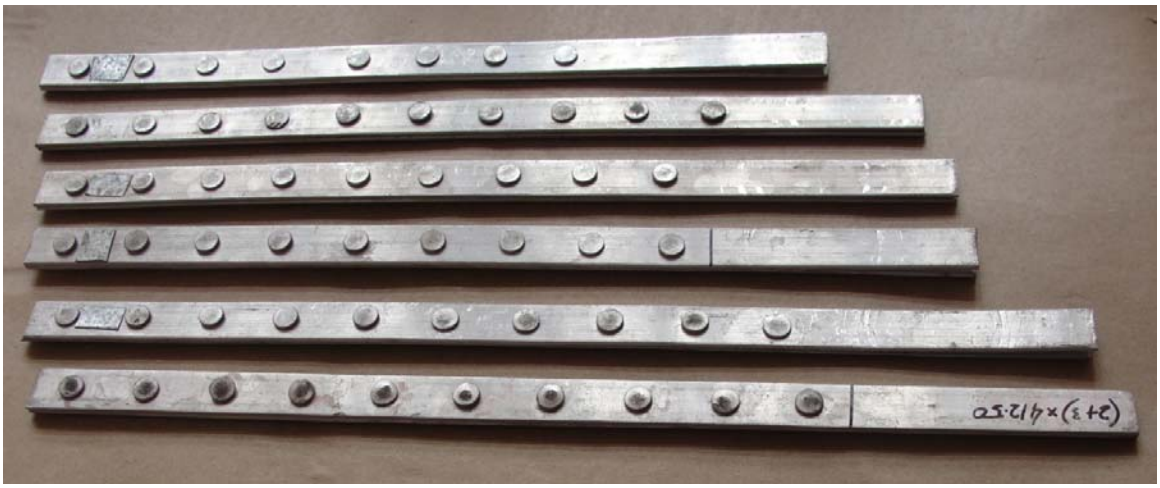

(b)

Fig. 5.1 Photographs of test specimens of (a) mild steel and (b) aluminium

Before clamping the specimens with rivets, the interfaces of the contacting members are cleaned properly to obtain perfect contact at the mating surfaces. The usual rivet consists of a solid cylindrical shank with a head at one end. Generally, there are six

types of rivet heads used in practice as shown in Fig. 5.2. The button head with power riveting technique has been used in the present investigation to clamp the beams. The hot rivet is inserted into the hole and a head is formed on the blunt end with a pneumatic pressure with the help of a die. The shank of the rivet is compressed causing it to expand and fill the hole almost completely. The rivet shrinks on cooling, thereby creates a clamping force between the connecting parts.

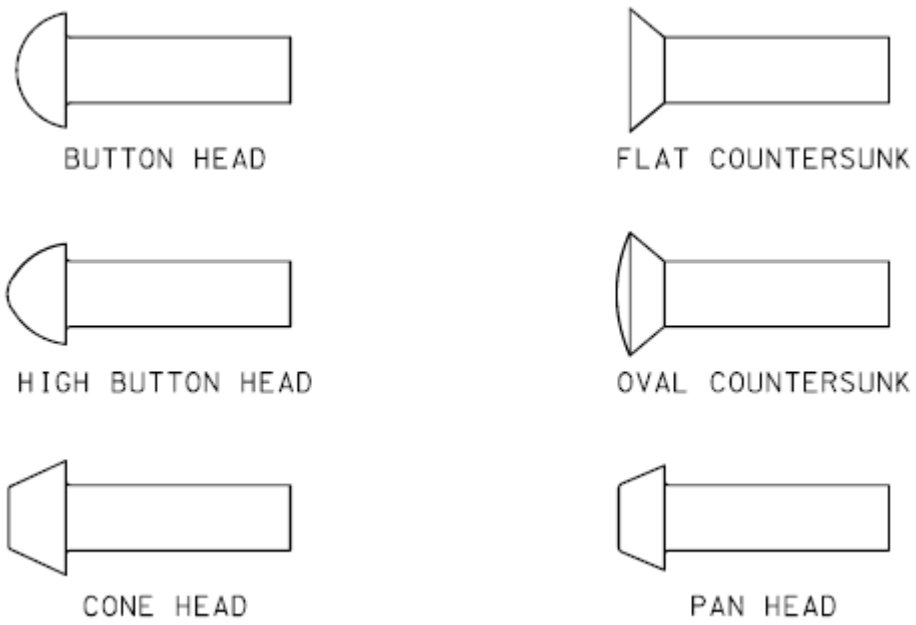

Fig. 5.2 Types of rivet head

Table 5.1 Details of mild steel specimens used in the experiment for the thickness ratio 1.0

Thickness x Width (mm x mm)	Number of layers	Type of specimen	Diameter of rivet (mm)	Number of rivets used	Cantilever length (mm)
(3+3)x41.25	2	Jointed	10	8	330.00
(4+4)x41.25	2			9	371.25
(6+6)x41.25	2			10	412.50
(4+4+4)x41.25	3			11	453.75
(3+3+3+3)x41.25	4				
				10	330.00
(3+3)x33.00				11	363.00
(4+4)x33.00	2	Jointed	8	12	396.00
(6+6)x33.00				13	429.00
				14	346.50
(3+3)x24.75				15	371.25
(4+4)x24.75	2	Jointed	6	16	396.00
(6+6)x24.75				17	420.75
				17	350.625
(3+3)x20.625	2	Jointed	5	18	371.25
(4+4)x20.625				19	391.875
(6+6)x20.625				20	412.50
					330.00
6x41.25					371.25
8x41.25	-	Solid	10	-	412.50
12x41.25					453.75

Table 5.2 Details of mild steel specimens used in the experiment for the thickness ratio 1.5

Thickness x Width (mm x mm)	Type of specimen	Diameter of rivet (mm)	Number of rivets used	Cantilever length (mm)
(2+3)x50.00 (2.4+3.6)x50.00 (4+6)x50.00	Jointed	10	6 7 8 9	300.00 350.00 400.00 450.00
(2+3)x40.00 (2.4+3.6)x40.00 (4+6)x40.00	Jointed	8	8 9 10 11	320.00 360.00 400.00 440.00
(2+3)x40.00 (2.4+3.6)x30.00 (4+6)x40.00	Jointed	6	12 13 14 15	360.00 390.00 420.00 450.00
(2+3)x25.00 (2.4+3.6)x25.00 (4+6)x25.00	Jointed	5	15 16 17 18	375.00 400.00 425.00 450.00
6.0x50.00	Solid	10	-	300.00 350.00 400.00 450.00

Table 5.3 Details of mild steel specimens used in the experiment for the thickness ratio 2.0

Thickness x Width (mm x mm)	Type of specimen	Diameter of rivet (mm)	Number of rivets used	Cantilever length (mm)
(2+4)x67.20 (3+6)x67.20	Jointed	12	4 5 6 7	268.80 336.00 403.20 470.40
(2+4)x56.00 (3+6)x56.00	Jointed	10	5 6 7 8	280.00 336.00 392.00 448.00
(2+4)x44.80 (3+6)x44.80	Jointed	8	7 8 9 10	313.60 358.40 403.20 448.00
(2+4)x33.60 (3+6)x33.60	Jointed	6	10 11 12 13	336.00 369.60 403.20 436.80
(2+4)x28.00 (3+6)x28.00	Jointed	5	13 14 15 16	364.00 392.00 420.00 448.00
(2+4)x22.40 (3+6)x22.40	Jointed	4	15 16 17 18	336.00 358.40 380.80 403.20
6x56.00	Solid	10	-	280.00 336.00 392.00 448.00

Table 5.4 Details of aluminium specimens used in the experiment

Thickness x width (mm x mm)	Number of layers	Type of specimen	Thickness ratio	Diameter of rivet (mm)	Number of rivets used	Cantilever length (mm)
(2+2)x 41.25 (3+3)x41.25	2	Jointed	1.0	10	8 9 10 11	330.00 371.25 412.50 453.75
(2+2)x33.00 (3+3)x33.00	2	Jointed	1.0	8	10 11 12 13	330.00 363.00 396.00 429.00
(2+2)x24.75 (3+3)x24.75	2	Jointed	1.0	6	15 16 17 18	371.25 396.00 420.75 445.50
(2+2)x20.625 (3+3)x20.625	2	Jointed	1.0	5	19 20 21 22	371.875 412.50 433.125 453.75
(2.4+3.6)x50.00	2	Jointed	1.5	10	6 7 8 9	300.00 350.00 400.00 450.00

Table 5.4 (Continued)

(2+4)x56.00	2	Jointed	2.0	10	5 6 7 8	280.00 336.00 392.00 448.00
(6+6)x41.25 (4+4+4)x41.25 (3+3+3+3)x41.25	2 3 4	Jointed	1.0	10	8 9 10 11	330.00 371.25 412.50 453.75
6.0x41.25 6.0x50.00 6.0x56.00	-	Solid	1.0 1.5 2.0	10	-	450.00

5.3 Description of the Experimental Set-up

The schematic diagram of the experimental set-up with the instrumentation and photographic views are shown in Fig. 5.3 and 5.4, respectively. The set-up consists of a frame work fabricated from steel channel sections by welding. The frame is grouted to a heavy and rigid concrete base by means of foundation bolts and it has the provision of slotted guide ways to accommodate the beams of different lengths. The frame has the provision to hold the fixed end of the cantilever beam specimens tightly and rigidly in order to ensure perfect cantilever condition. This clamping is achieved using a mechanical vice. The vice working on the screw-jack principle consists of a base plate and a spindle with internal and external threading, respectively. An arm is attached to this spindle at the upper end. On rotating the arm, it moves axially downward and imparts the necessary clamping force to the base plate thereby holding the specimen to achieve a perfect cantilever condition. The base plate prevents the rotation of the specimens while applying the fixed end load. A spring loaded exciter is used to initiate vibration at the free end of the specimens with predetermined amplitudes. The use of spring in the exciter ensures zero initial velocity of the specimen at the time of excitation. It is provided with a dial gauge which is calibrated

to read the initial amplitudes of excitation. The dial gauge is mounted to a vertical stand with a magnetic base.

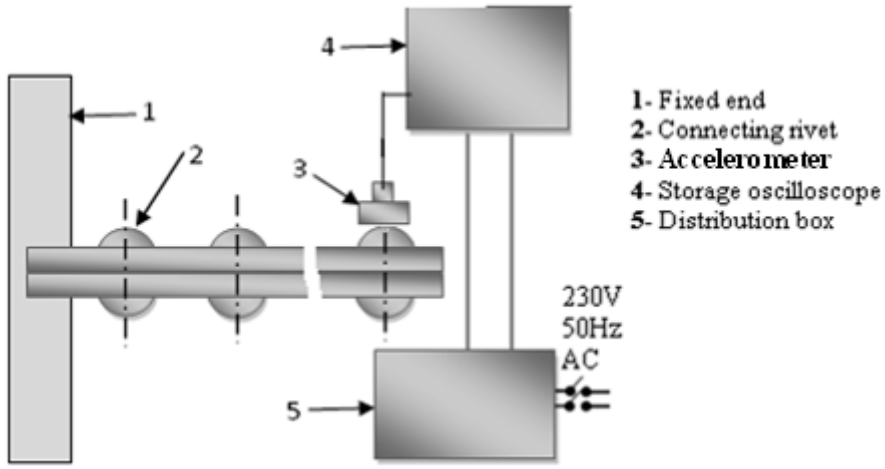

Fig. 5.3 Schematic diagram of the experimental set-up

The test rig includes the following instruments.

1. Digital storage oscilloscope
2. Accelerometer/Vibration pick-up (contacting type magnetic probe)
3. Dial gauge
4. Distribution box

A brief functional description of each instrument listed above along with their specifications is presented below in detail.

A digital storage oscilloscope as shown in Fig. 5.5 is widely used for the processing and display of vibration signals and has a display screen, numerous input connectors, control knobs and buttons on the front panel. The signal to be measured is fed to one of the connectors. It plots a two dimensional graph of the time history curve.

Specifications:

DPO 4000 series Oscilloscope

Input Voltage: 100 V to 240 V ± 10%

Input Power Frequency: 47 Hz to 66 Hz (100 V to 240 V)
400 Hz (100 V to 132 V)

Power Consumption: 250 W maximum

Weight: 5 kg (11 lbs), standalone instrument

Clearance: 51 mm (2 in)

Operating Temperature: 0 to 50 ^{0}C

High Operating Humidity: 40 to 50 ^{0}C, 10 to 60% RH

Low Operating Humidity: 0 to 40 ^{0}C, 10 to 90% RH

Operating Altitude: 3000 m (about 10,000 ft)

Operating Random Vibration: 0.31 G_{RMS}, 5 – 500 Hz, 10 minutes per axis, 3 axes (30 minutes total)

Pollution Degree: 2, Indoor use only

The accelerometer is a device that transforms changes in mechanical quantities (such as displacement, velocity or acceleration) into changes in electrical quantities (such as voltage or current). One end of the accelerometer is held magnetically to the vibrating surface and the other end is connected to one of the connectors of the storage oscilloscope. The accelerometer used in the experiments is of contacting-type as shown in Fig. 5.6.

Specifications:

Type: MV-2000

Make: NAL, Bangalore, India

Optional gap: 2 mm

Coil resistance: 1000 ohms

Operating temperature: 10 to 40 degree centigrade

Dynamic frequency range: 2 c/s to 1000c/s

Vibration amplitude: ± 1.5 mm maximum

Weight: 130 gm

A high precision dial gauge mounted on a stand with magnetic base is used to record the amplitude of vibration given at the tip of the specimen. The dial gauge as shown in Fig. 5.7 is shock proof and can measure the amplitude of excitation in the range of 0.01 to 10 mm.

A distribution box supplies the AC power to the storage oscilloscope at a voltage and frequency of 230V and 50Hz, respectively.

Power supply: 200-240 V, 50 Hz

Moreover, the Surtronic 3+ surface measuring instrument as shown in Fig. 5.8 is used for measuring the interface roughness of various mild steel and aluminium specimens.

Specification:

Make: Taylor Hobson Limited, England

Battery: Alkaline non-rechargeable battery with minimum 600 measurements of 4 mm measurement length

NiCad rechargeable battery with minimum 200 measurements of 4 mm measurement length

110/240V, 50/60 Hz

Traverse speed: 1 mm/sec

Measurement units: Metric/Inch

Cut-off values: 0.25mm, 0.80mm and 2.50mm (0.01in, 0.03in and 0.1in)

Filter: Digital Gauss filter or 2CR filter

Parameters: Ra, Rq, Rz(DIN), Ry and Sm

Calculation time: Less than reversal time or 2 sec whichever is the longer

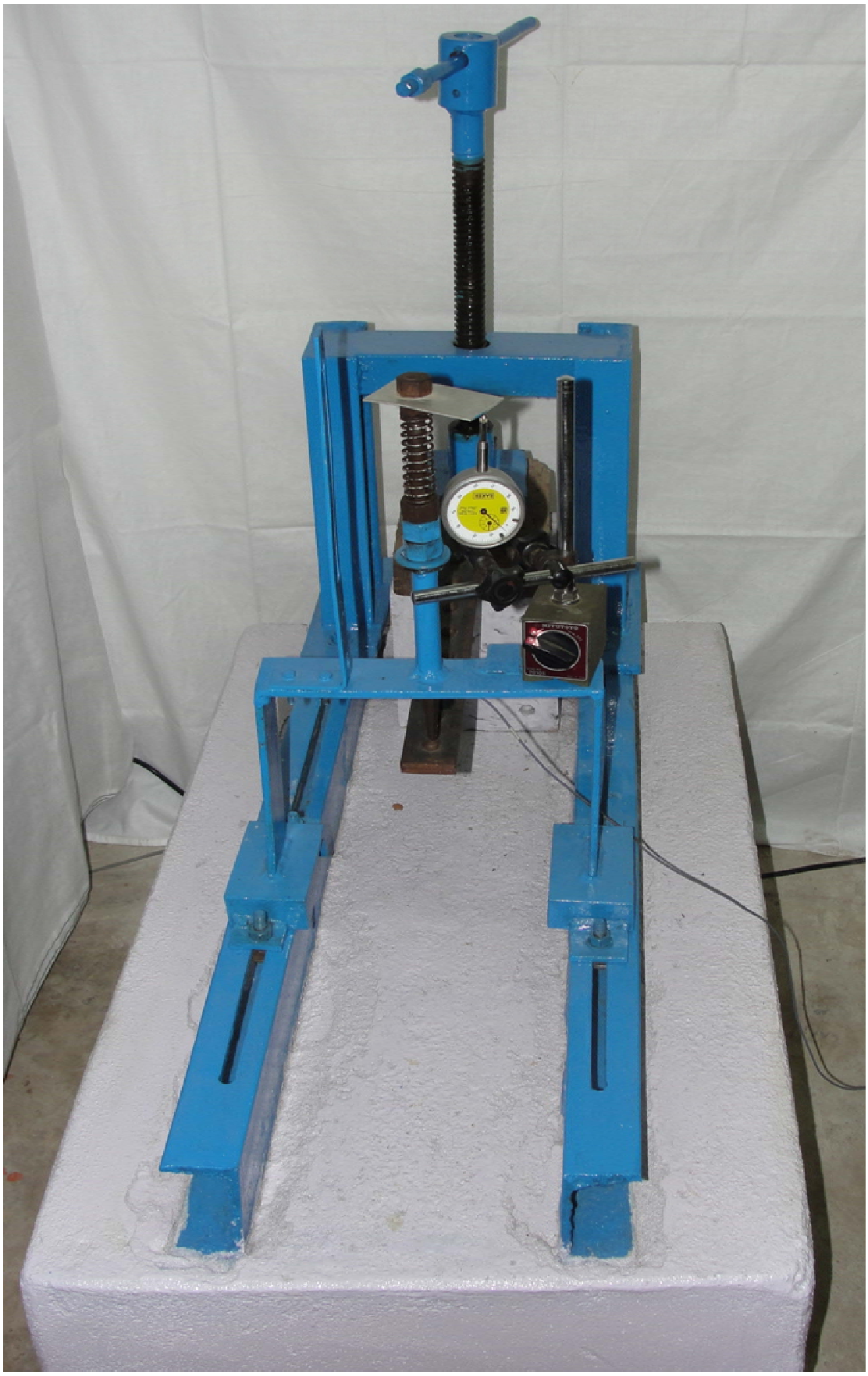

(a) Front view of the experimental set-up

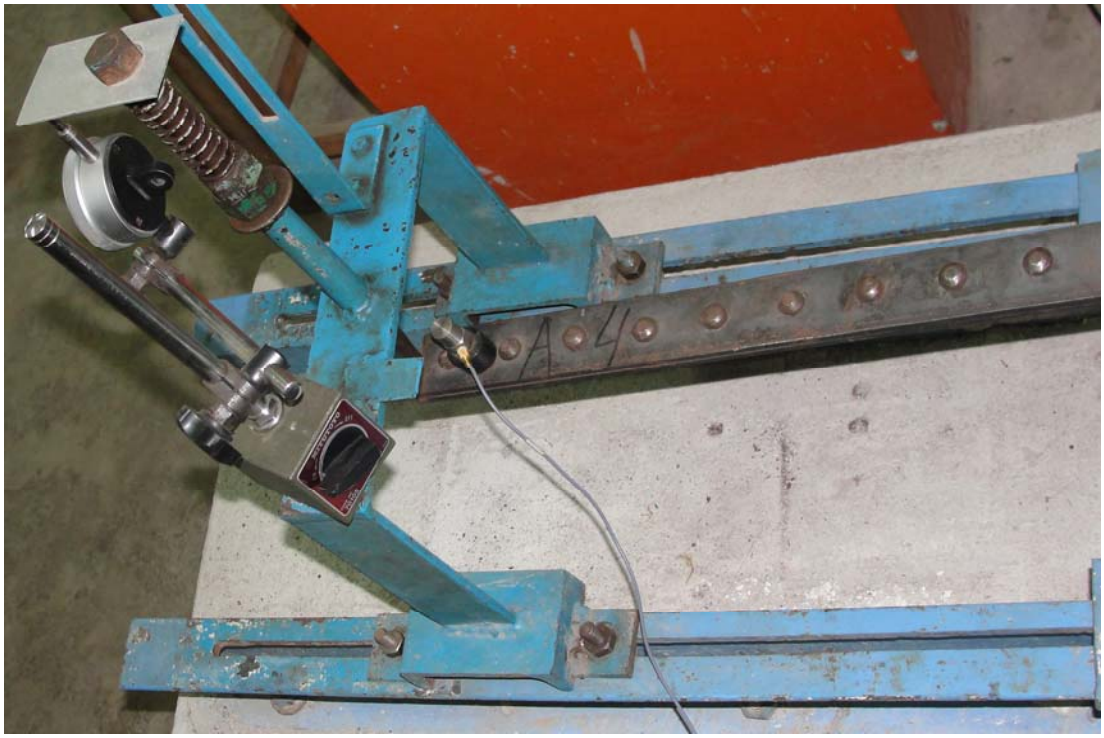

(b) Top view of the experimental set-up

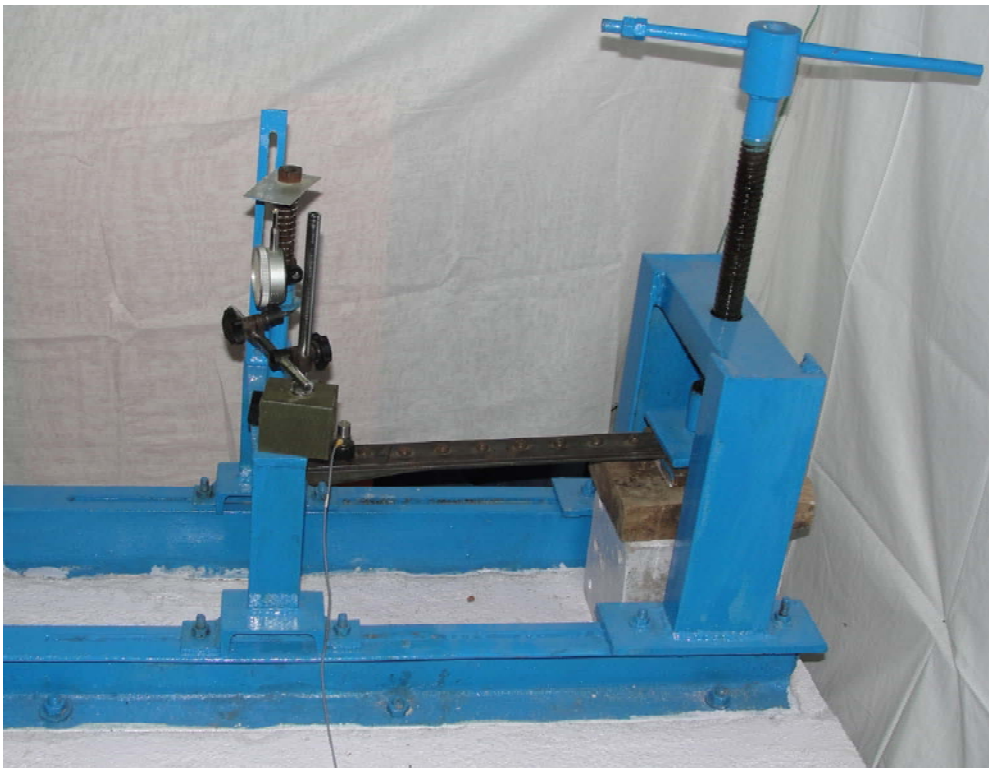

(c) Side view of the experimental set-up

(d) Complete view of the experimental set-up with the storage oscilloscope

Fig. 5.4 Different views of the experimental set-up

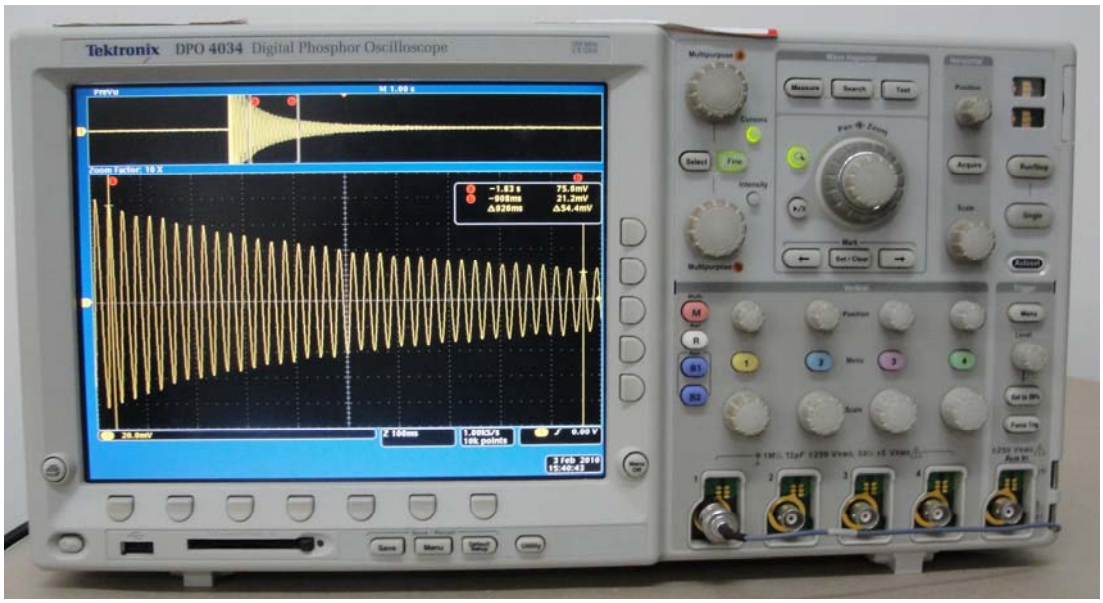

Fig. 5.5 Digital storage oscilloscope

Fig. 5.6 Accelerometer (Contacting type magnetic probe)

Fig. 5.7 Dial gauge mounted on a stand with magnetic base

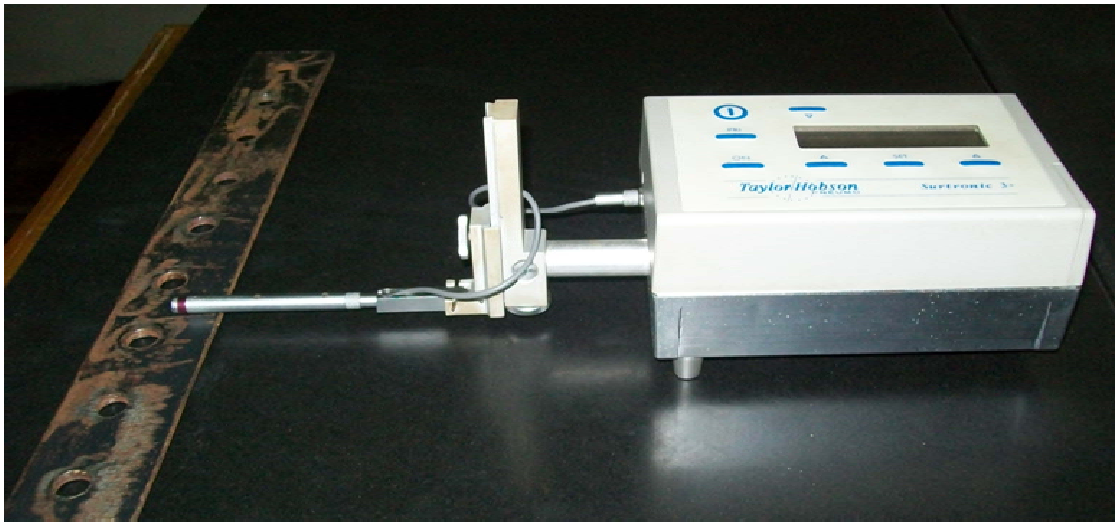

Fig. 5.8 Roughness test for specimens

5.4 Testing Procedure

The tests are performed in the prevailing laboratory environment. In order to perform the experiments, the specimens are rigidly mounted to the support as discussed earlier. At first, the Young's modulus of elasticity and static bending stiffness are measured by carrying out static deflection tests. These measured values are subsequently used for the theoretical evaluation of logarithmic decrement of all the specimens. Later, the experimental logarithmic decrement is calculated from the time history curve of decaying signals. The detailed procedure to find out the above quantities is discussed in the succeeding sections.

5.4.1 Measurement of Young's Modulus of Elasticity (*E*)

As mentioned in the preceding paragraph, the Young's modulus of elasticity (E) of the specimen material is found out by conducting static deflection tests. For this purpose, few samples of solid beams are selected from the same stock of mild steel and aluminium flats. These specimens are mounted on the same experimental set-up rigidly so as to ensure perfect fixed boundary conditions as mentioned earlier. Static loads (W) are applied at the free end and the corresponding deflections (Δ) are recorded. The Young's modulus for the specimen material is then determined using the expression $E = WL^3/3I\Delta$, where L and I are the free length and moment of inertia of the cantilever specimen. The average of five readings is recorded from the tests from which the average value of Young's modulus for different material is evaluated as presented in Table 5.5.

Table 5.5 Young's modulus of specimen materials

Material	Average E (GPa)
Mild steel	196.0
Aluminium	67.6

5.4.2 Measurement of Static Bending Stiffness (*k*)

It is a well known fact that the stiffness of a jointed beam is always less compared to an equivalent solid one. It means that the incorporation of joints to assemble layers of

beams is accompanied by a decrease in the stiffness. The amount of reduction in the stiffness is quantified by a factor called stiffness ratio which is defined as the ratio of the stiffness of a jointed beam (k) to that of an identical solid one (k'). The stiffness ratio is inversely related to the number of layers used in the jointed specimen. Its exact assessment carries much significance in the theoretical evaluation of logarithmic decrement. The same static deflection tests as used in case of Young's modulus are performed to measure the actual stiffness (k) of a jointed specimen using the relation $k = W / \Delta$. However, the stiffness of an identical solid cantilever beam is theoretically calculated from the expression $k' = 3EI/L^3$. The average values of the stiffness ratios for two layered cantilever beams jointed with rivets has been calculated and presented in Tables 5.6 and 5.7 as samples for mild steel and aluminium materials, respectively. It is seen that there is marginal variation in the stiffness ratio for the group of specimens considered in the above mentioned table.

Further, the stiffness ratio of multi-layered jointed beams has been calculated in the similar manner as in case of two layered ones. The corresponding values of average stiffness ratios for jointed beams consisting of varying number of layers for a constant overall thickness are given in Table 5.8 and 5.9 for mild steel and aluminium specimens, respectively. It is observed that the stiffness ratio decreases with the number of layers in the jointed construction. These calculated stiffness ratios are utilized in determining the actual stiffness of jointed beams and further used for the theoretical evaluation of logarithmic decrement.

Table 5.6 Average stiffness ratio for two layered mild steel beams jointed with rivets

Thickness x Width (mm x mm)	Cantilever length (mm)	Static bending stiffness (N/mm)		Stiffness ratio (k/k')	Average stiffness ratio
		Experimental (k)	Theoretical (k')		
(3+3)x41.25	371.25	7.2467	8.5325	0.8493	0.8503
	412.50	5.2666	6.2202	0.8467	
	453.75	3.9882	4.6733	0.8534	
(4+4)x41.25	371.25	17.0862	20.2251	0.8448	
	412.50	12.6018	14.7441	0.8547	
	453.75	9.4391	11.0775	0.8521	
(6+6)x41.25	371.25	57.9934	68.2597	0.8496	
	412.50	42.05825	49.7613	0.8452	
	453.75	32.0439	37.3864	0.8571	
(2.4+3.6)x50.00	350.00	10.4742	12.3429	0.8486	
	400.00	7.0103	8.2688	0.8478	
	450.00	4.9589	5.8074	0.8539	
(2+4)x56.00	336.00	13.3469	15.6250	0.8542	
	392.00	8.3372	9.8397	0.8473	
	448.00	5.5991	6.5918	0.8494	

Table 5.7 Average stiffness ratio for two layered aluminium beams jointed with rivets

Thickness x Width (mm x mm)	Cantilever length (mm)	Static bending stiffness (N/mm)		Stiffness ratio (k/k')	Average stiffness ratio
		Experimental (k)	Theoretical (k')		
(3+3)x41.25	371.25	2.5726	2.9428	0.8742	0.8714
	412.50	1.8651	2.1453	0.8694	
	453.75	1.3995	1.6118	0.8683	
(2.4+3.6)x50.00	350.00	3.6925	4.2570	0.8674	
	400.00	2.4988	2.8519	0.8762	
	450.00	1.7504	2.0030	0.8739	
(2+4)x56.00	336.00	4.6868	5.3890	0.8697	
	392.00	2.9444	3.3937	0.8676	
	448.00	1.9918	2.2735	0.8761	

Table 5.8 Average stiffness ratio for mild steel jointed beams with more number of layers

Number of layers used		
2 layers	3 layers	4 layers
0.8503	0.8231	0.7943

Table 5.9 Average stiffness ratio for aluminium jointed beams with more number of layers

Number of layers used		
2 layers	3 layers	4 layers
0.8714	0.8493	0.8106

5.4.3 Measurement of Damping (δ)

After finding out the Young's modulus and static bending stiffness of the specimen materials, the tests are further conducted on the same set of specimens for evaluating the logarithmic decrement. The test specimens are first rigidly mounted on the set-up one after another. The test procedure is essentially the same for all the cases. A spring loaded exciter is used to excite the specimens at the free ends. The excitation is imparted for a range of beam-tip amplitudes varying from 0.1 to 0.5 mm in steps of 0.1 mm. For a particular test specimen, the beam is deflected and released to oscillate at its first mode of free vibration. The beam response is sensed by a contacting-type accelerometer attached to the tip of the beam. In view of non-magnetic property of aluminium specimen, the beam-tip is glued with a square size strip of some magnetic material for sensing of the signal. One end of the accelerometer is held magnetically to the vibrating surface of the specimen and the other is connected to one of the connectors of the storage oscilloscope. The output from the accelerometer is proportional to the frequency and amplitude of vibration. This output signal is fed to a digital storage oscilloscope for processing and display. The data is then analyzed to determine the natural frequency and damping characteristics of the beam structure. Figure 5.9 shows the block diagram of the basic vibration measurement scheme used in the present study. The decaying signal is recorded on the screen of the storage oscilloscope indicating that the energy dissipation is taking place. The cause of energy dissipation may be due to different effects such as material, joint friction and support damping. However, it is assumed that all the energy dissipation is due to the joint friction only.

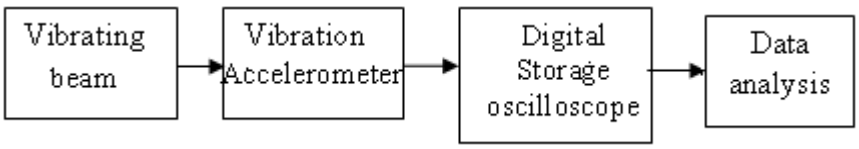

Fig. 5.9 Basic scheme of vibration measurement

Several techniques are used to quantify the level of damping in a structure as discussed in the literature review. Out of them, the logarithmic decrement technique is the most popular time-response method used for measuring the damping. The logarithmic decrement represents the rate at which the amplitude of a free damped

vibration decreases. As the structure is considered to vibrate with small excitation level in the low and moderate frequency range, this method produces fairly good results for lightly damped linear systems. In this method, the structure is set into free vibration with the fundamental mode dominating the response since all the higher modes are damped out quite quickly. The vibration response of the specimen is picked up by the accelerometer and a time history curve showing the decay of amplitude is displayed on the digital storage oscilloscope. This decay can be further used to estimate the damping in jointed specimens using the expression $\delta = \ln\left(x_1 / x_{z+1}\right)/z$, where x_1, x_{z+1} and z are the recorded values of the amplitudes of the first cycle, last cycle and the number of cycles, respectively. Each test during experiments is repeated at least for five times and the average value is taken for accuracy.

The damped frequency of vibration (ω_d) is read directly from the data recorded on the oscilloscope. The natural frequency of vibration (ω_n) is calculated from this damped one using the expression $\omega_n = \omega_d / \sqrt{1-\xi^2}$, where ξ is the damping ratio. As the value of ξ is very small for lightly damped structures, the natural frequency of vibration is fairly same as the damped frequency of vibration, i.e., $\omega_n \approx \omega_d$. It is observed that the natural frequency of transverse vibration vary only with the physical dimensions of the layered and jointed beam specimens. However, it is independent of the amplitudes of excitation.

Design of experimental set-up for measurement of damping requires some primary consideration. It is assumed that the energy losses due to support friction, air drag, connecting wires, accelerometer mountings etc., are neglected. Secondly, proper care has been taken while preparing the specimens, assembling the test rig and conducting the experiments. The connecting members of any test specimen should be flat with perfect contact at the interfaces. This will ensure identical pressure distribution under each connecting rivet along the interfaces so that proper energy dissipation takes place. While mounting the specimen in the test rig, sufficient clamping has to be provided in order to achieve a perfect cantilever condition which will greatly reduce the errors due to support damping. Further, some errors may build up while giving the initial excitation which may not be instantaneous. This may not ensure perfect

sinusoidal waveforms thus containing some harmonic contents. All these factors should be considered during experimentation in order to minimize the errors.

5.5 Experimental Evaluation of $\alpha.\mu$

The energy dissipation at the interfaces of jointed structures primarily depends upon the kinematic coefficient of friction (μ) and dynamic slip ratio (α). These two vital parameters are to be correctly assessed for accurate evaluation of the logarithmic decrement. It is generally known that the dynamic slip at the interfaces increases with a decrease in coefficient of friction and vice versa. They are inter-dependent with each other and inversely related. Further, they exhibit complex behavior under dynamic condition making it difficult to assess the exact value of the individual parameters at a particular condition of excitation. In view of the above factors, it is convenient to evaluate the product $\alpha.\mu$ as a single parameter from the experimental results and use it for theoretical calculations for other conditions of the beam. However, their product ($\alpha.\mu$) is found to be constant for a particular specimen under a particular condition of vibration irrespective of surface roughness.

In view of the discussions in the preceding paragraph, the product $\alpha.\mu$ has been determined from the experimental results of logarithmic decrement for two layered and jointed cantilever beam specimens of mild steel and aluminium with 10 mm diameter connecting rivets using Eq. (3.41). Since this product is frequency and amplitude dependent, plots displaying its variation with the above two parameters are shown in Figs. 5.10 to 5.12 and 5.13 to 5.15 for mild steel and aluminium specimens, respectively. These plots are further used for the numerical evaluation of logarithmic decrements of layered and jointed beams with respect to other diameters and conditions of excitation using Eq. (3.38) and (4.28) for classical and finite element methods, respectively. It is observed from the above plots that this product increases with an increase in both the natural frequency and amplitude of excitation.

However, the product ($\alpha.\mu$) is established to be constant for a particular specimen irrespective of any surface condition at the mating surfaces. In order to authenticate this, experiments are conducted with a few layered and jointed beams made up of mild steel and aluminium connected with 10 mm diameter rivets and excited at 0.1 mm. The roughness values at the interfaces of the specimens have been varied. These

values are measured with the help of a Surtronic 3 + surface texture measuring instrument and found to be 0.8, 1.2 and 1.6 micron for mild steel and 02, 0.3, and 0.4 micron for aluminium specimens. The results of the effect of surface roughness on the damping capacity of the jointed structures have been presented in Table 5.10. It is observed that the logarithmic decrement remains almost constant irrespective of condition of roughness at the interfaces since the maximum deviation is found to be 0.2%.

The presence of joints to assemble the layered and jointed structures damp out the vibrations and reduces the stiffness. This reduction in the stiffness brings about a slight decrease in the natural frequency. It is thus observed that the jointed beam has lower frequencies compared to its equivalent solid one. This difference in frequency is fairly close at lower modes of vibration. Further, the reduction in the frequency of vibration results a change in the product of "$\alpha.\mu$" under various conditions of the beam. This reduction of a jointed beam in relation to an identical solid one is shown in Figs. 5.16 and 5.17 for mild steel and aluminium specimen, respectively, for a particular specification of the beam with thickness ratio 1.0, overall beam thickness 6 mm, cantilever length 453.75 mm and diameter of rivet 10 mm.

Moreover, in order to compare the damping capacity of jointed beams with their equivalent solid ones, few experiments are conducted on geometrically identical specimens of mild steel and aluminium materials excited at 0.5 mm. The diameter of the connecting rivets for jointed beams is taken as 10 mm. The experimental results of logarithmic decrement as well as static bending stiffness for few sample specimens are presented in Table 5.11. It is observed from the results that the damping capacity of a jointed beam increases with a decrease in stiffness. Due to the incorporation of joints, it is estimated that the damping capacity increases approximately by 150 and 130% for mild steel and aluminium specimens, respectively, whereas their stiffness decreases by 15 and 13% only.

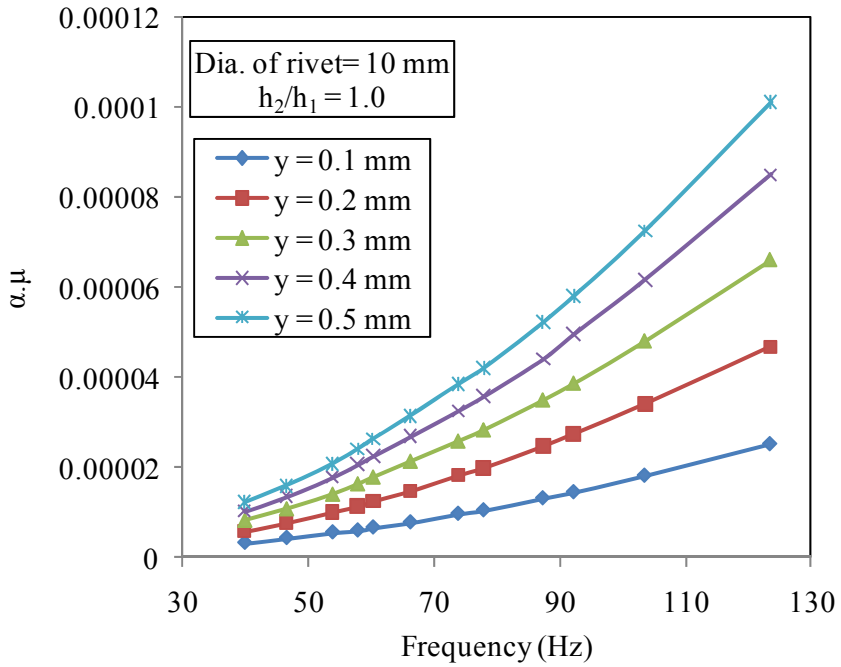

Fig. 5.10 Variation of $\alpha.\mu$ with frequency of vibration for mild steel specimens with beam thickness ratio 1.0 at different initial amplitudes of excitation (y)

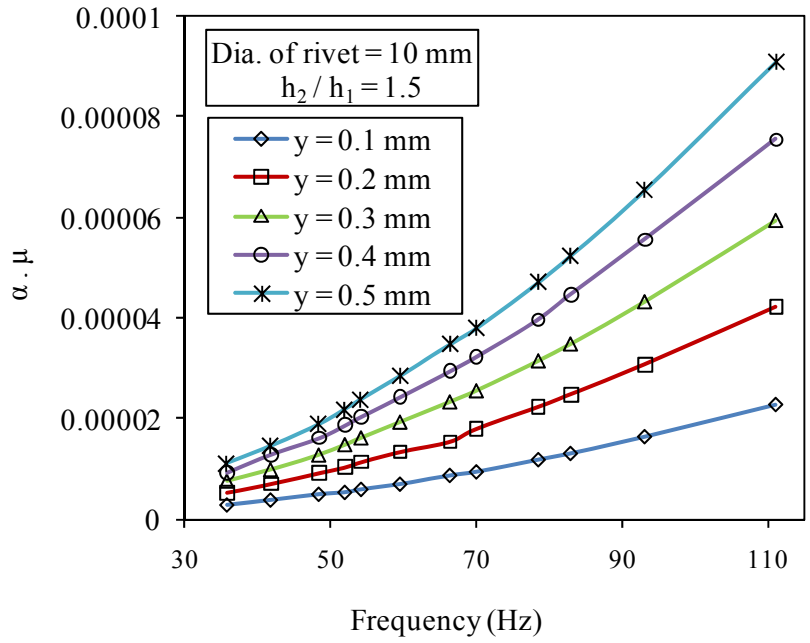

Fig. 5.11 Variation of $\alpha.\mu$ with frequency of vibration for mild steel specimens with beam thickness ratio 1.5 at different initial amplitudes of excitation (y)

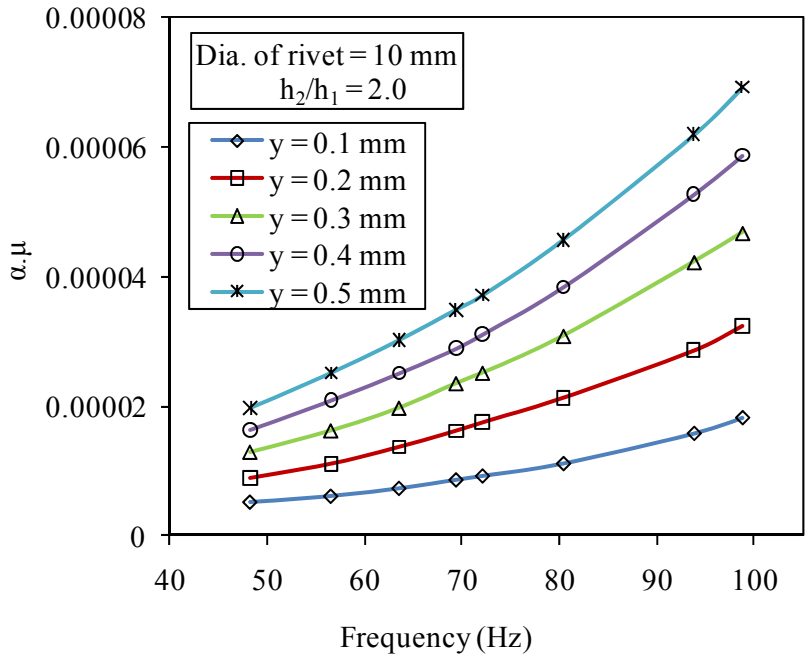

Fig. 5.12 Variation of $\alpha.\mu$ with frequency of vibration for mild steel specimens with beam thickness ratio 2.0 at different initial amplitudes of excitation (y)

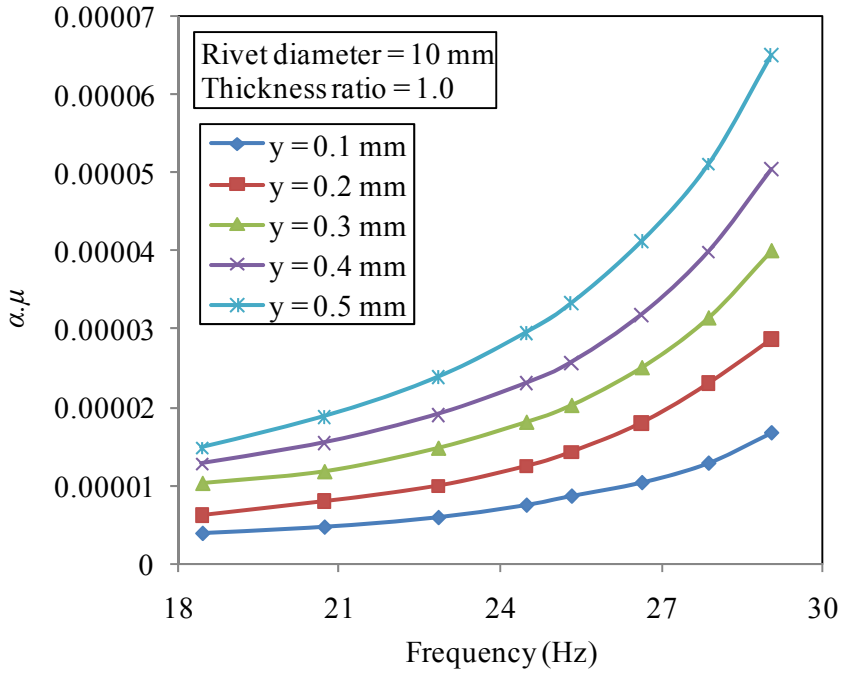

Fig. 5.13 Variation of $\alpha.\mu$ with frequency of vibration for aluminium specimens with beam thickness ratio 1.0 at different initial amplitudes of excitation (y)

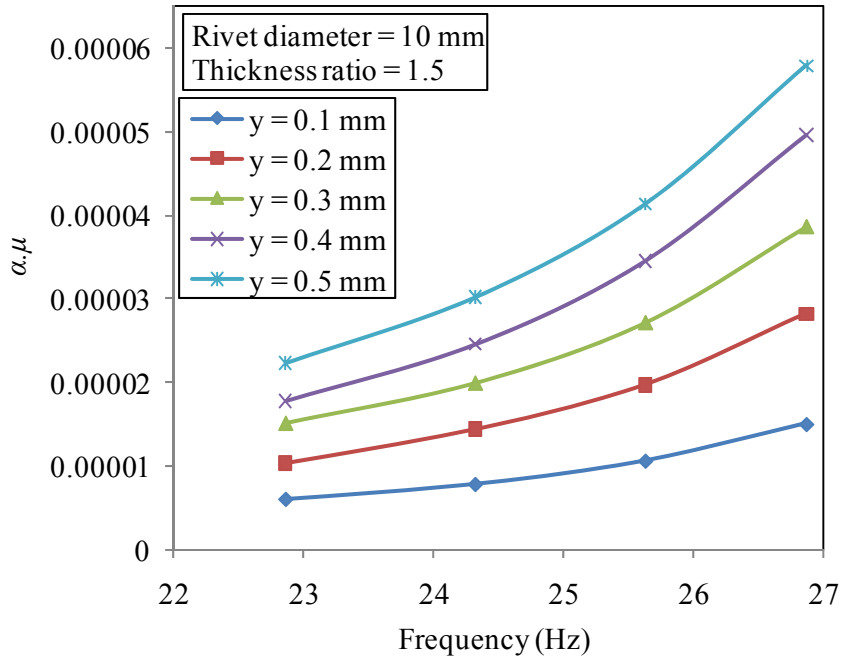

Fig. 5.14 Variation of $\alpha.\mu$ with frequency of vibration for aluminium specimens with beam thickness ratio 1.5 at different initial amplitudes of excitation (y)

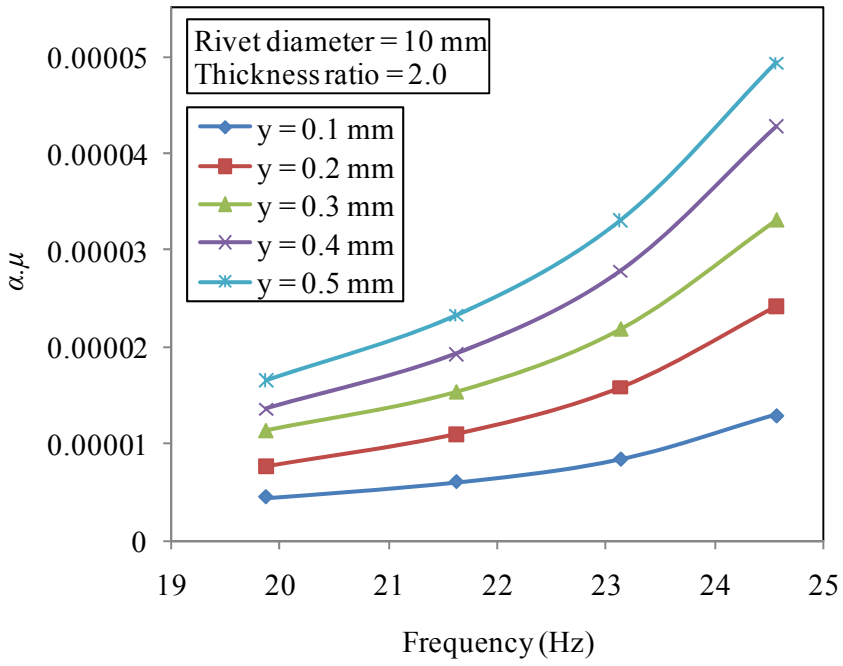

Fig. 5.15 Variation of $\alpha.\mu$ with frequency of vibration for aluminium specimens with beam thickness ratio 2.0 at different initial amplitudes of excitation (y)

Table 5.10 Experimental logarithmic decrement of mild steel and aluminium jointed beams with different surface roughness

Material	Length x thickness x width (mm x mm x mm)	Thickness ratio	Roughness (micron)	Logarithmic decrement
Mild Steel	453.75 x (3+3) x 41.25	1.0	0.8	0.00887
			1.2	0.00890
			1.6	0.00892
	450 x (2.4+3.6) x 50	1.5	0.8	0.00778
			1.2	0.00781
			1.6	0.00784
	448 x (2+4) x 56	2.0	0.8	0.00707
			1.2	0.00710
			1.6	0.00712
Aluminium	453.75 x (3+3) x 41.25	1.0	0.2	0.02218
			0.3	0.02220
			0.4	0.02221
	450 x (2.4+3.6) x 50	1.5	0.2	0.01945
			0.3	0.01947
			0.4	0.01948
	448 x (2+4) x 56	2.0	0.2	0.01816
			0.3	0.01818
			0.4	0.01819

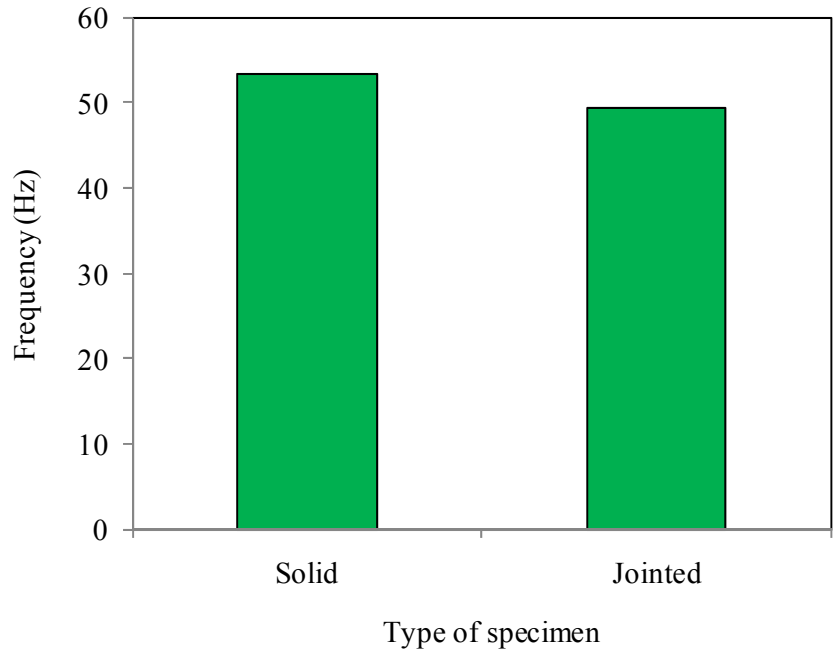

Fig. 5.16 Comparison of frequency between two identical mild steel beams

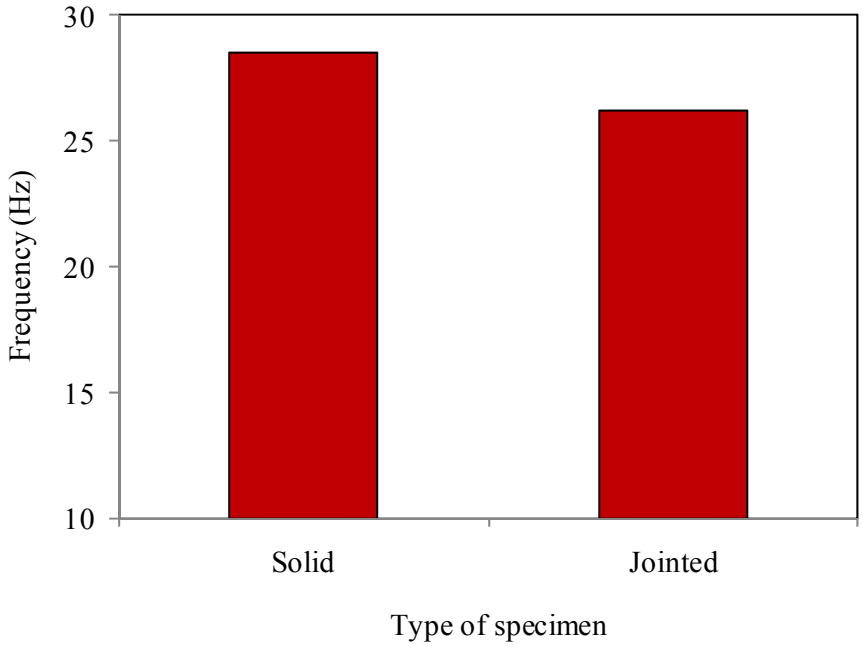

Fig. 5.17 Comparison of frequency between two identical aluminium beams

Table 5.11 Comparison of experimental logarithmic decrement and stiffness of identical solid and jointed beams (with 10 mm connecting rivets being excited at 0.5 mm)

Material	Length x width x thickness (mm x mm x mm)	Type of Specimen	Stiffness (k) (N/mm)	Damping (δ)	% decrease in k	% increase in δ
Mild steel	453.75x(3+3)x41.25	Jointed	3.9882	0.00652	14.66	150.77
	453.75x6x41.25	Solid	4.6733	0.00260		
	450x(2.4+3.6)x50	Jointed	4.9589	0.00572	14.61	148.26
	450x6x50	Solid	5.8074	0.00230		
	448x(2+4)x56	Jointed	5.5991	0.00520	15.06	146.45
	448x6x56	Solid	6.5918	0.00211		
Aluminium	453.75x(3+3)x41.25	Jointed	1.3995	0.01630	13.17	130.88
	453.75x6x41.25	Solid	1.6118	0.00706		
	450x(2.4+3.6)x50	Jointed	1.7504	0.01431	12.61	128.23
	450x6x50	Solid	2.0030	0.00627		
	448x(2+4)x56	Jointed	1.9918	0.01301	12.39	126.65
	448x6x56	Solid	2.2735	0.00574		

5.6 Comparison of Experimental and Numerical Results

As already discussed in the introduction chapter, the experimental measurement becomes necessary as the theoretically computed vibration of a machine or structure may be different from the actual values due to the assumptions made in the theoretical analyses. In view of this discrepancy in results, experiments are conducted for different set of mild steel and aluminium specimens under different vibrating conditions. The details of the specimens used in the experiments have been presented in Tables 5.1 to 5.4 in the earlier section of this chapter. These experimental results have been compared with the corresponding numerical ones obtained in chapters 3 and 4 for establishing the authenticity of the theory developed. These comparative results are presented in graphical forms from Figs. 5.18 to 5.75. In all these plots, the

numerical results obtained either by classical or finite element method is shown by solid lines (——) and the corresponding experimental ones by dashed lines (-------). In presenting the results, the variation of logarithmic decrement with respect to different influencing parameters such as; beam length, beam thickness ratio, amplitude of excitation, diameter of connecting rivets and number of layers have been shown. For the purpose of systematic presentation of results, this section has been conveniently divided into four succeeding subsections.

5.6.1 Comparison of Experimental and Classical Results for Mild Steel Specimens

A classical method has been discussed in Chapter 3 for the study and evaluation of damping of two as well as multi-layered beams. First, this method is used to formulate the equations (3.40) and (3.41) for evaluating the logarithmic decrement and product $\alpha.\mu$, respectively. The logarithmic decrement of various specimens connected with different size rivets are found out from Eq. (3.40) using the product $\alpha.\mu$ determined from Figs. 5.10 to 5.12 at different frequencies and amplitudes of vibration. Next, experiments are performed on all test specimens as discussed in the previous section. In this section, the comparison of the results by the classical approach and experiments has been shown in Figs. 5.18 to 5.42 for mild steel specimens. The variation of logarithmic decrement with different influencing parameters for specimens of equal and unequal thickness is presented in Figs. 5.18 to 5.27 and 5.28 to 5.42, respectively. Further, comparison of results of multi layered beams of 12 mm overall thickness and connected with 10 mm diameter rivets is presented in Figs. 5.21 to 5.24. It is observed from the above results that both the curves are close to each other with maximum variation of 2.68%.

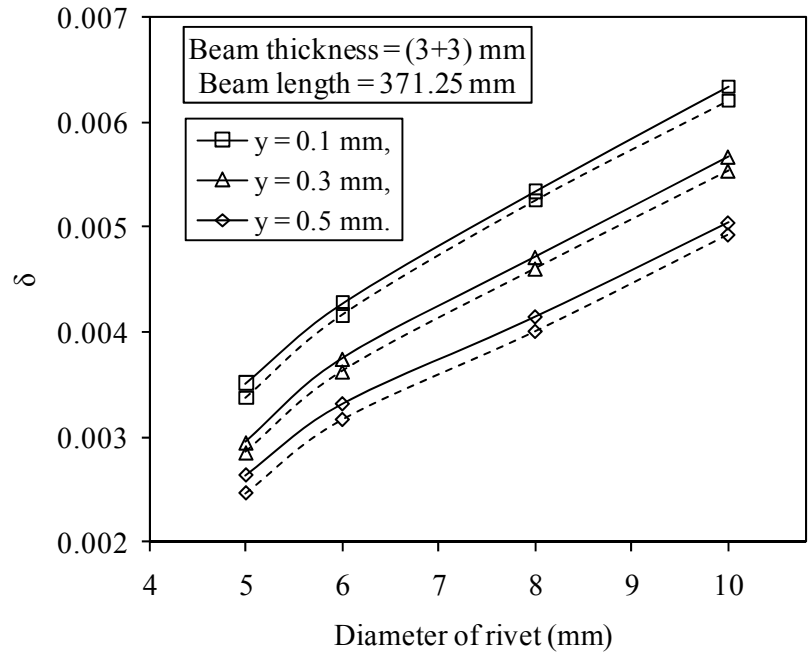

Fig. 5.18 Variation of logarithmic decrement with the diameter of rivet for mild steel specimens with beam length 371.25 mm and thickness (3+3) mm at different amplitudes of excitation (y). The theoretical and experimental values are shown by solid and dashed lines, respectively

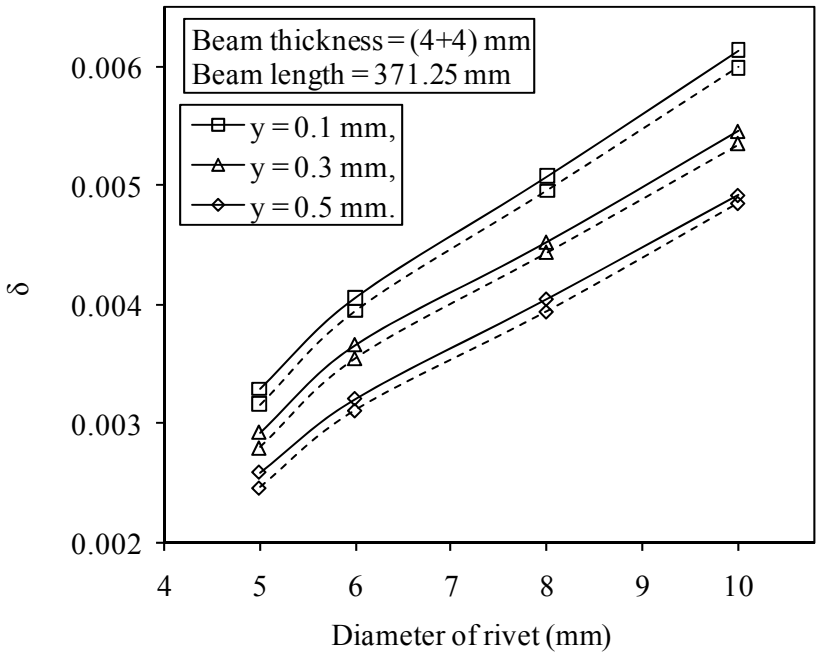

Fig. 5.19 Variation of logarithmic decrement with the diameter of rivet for mild steel specimens with beam length 371.25 mm and thickness (4+4) mm at different amplitudes of excitation (y). The theoretical and experimental values are shown by solid and dashed lines, respectively

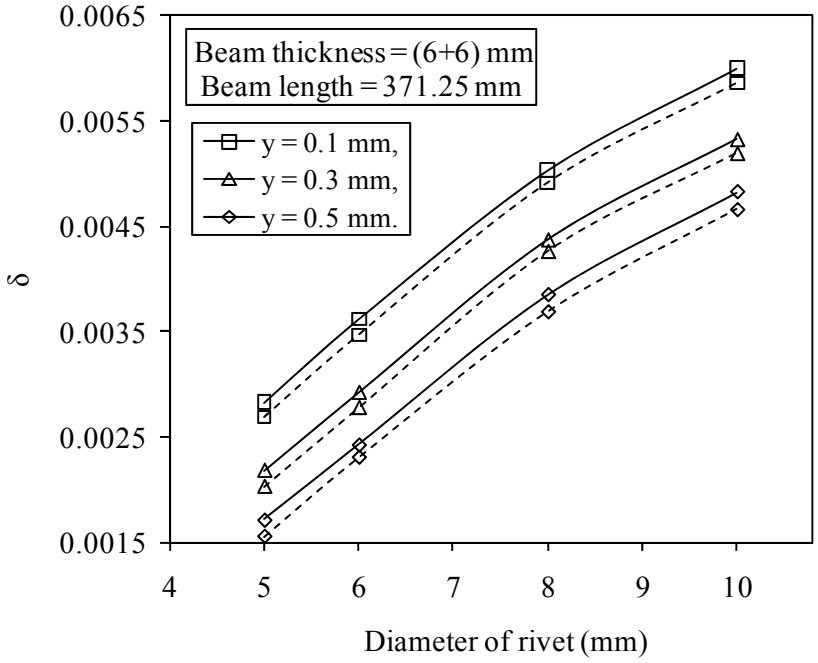

Fig. 5.20 Variation of logarithmic decrement with the diameter of rivet for mild steel specimens with beam length 371.25 mm and thickness (6+6) mm at different amplitudes of excitation (y). The theoretical and experimental values are shown by solid and dashed lines, respectively

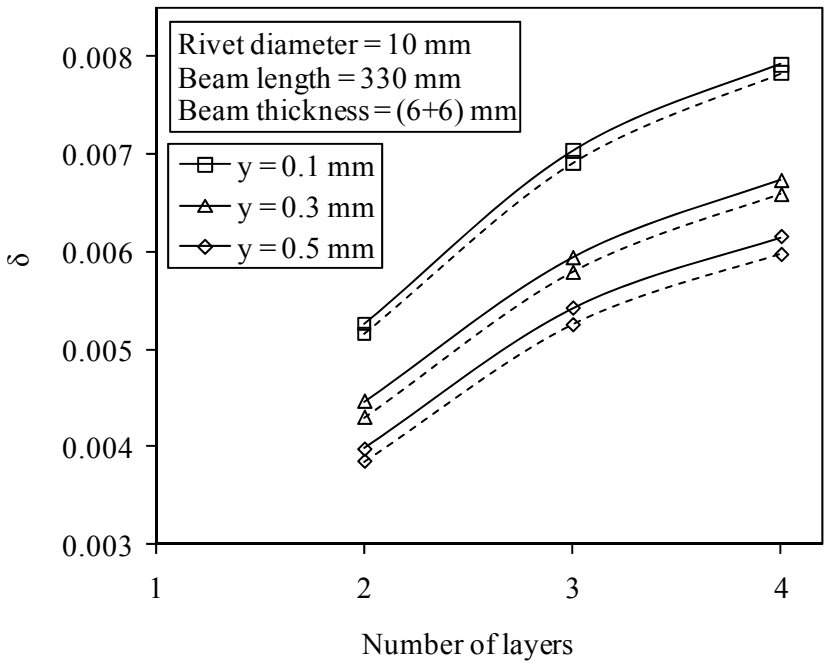

Fig. 5.21 Variation of logarithmic decrement with the number of layers for mild steel specimens with beam length 330 mm, thickness (6+6) mm and rivet diameter 10 mm at different amplitudes of excitation (y). The theoretical and experimental values are shown by solid and dashed lines, respectively

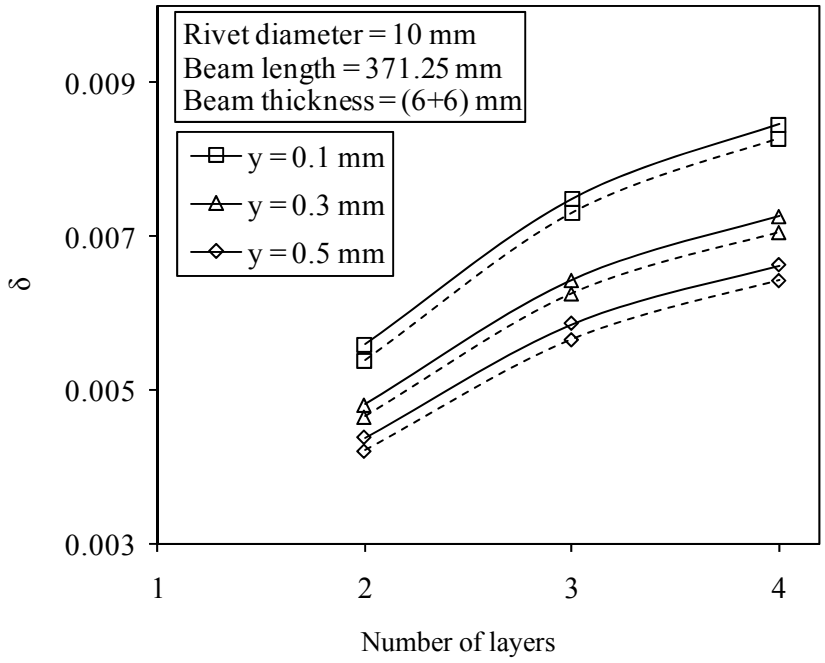

Fig. 5.22 Variation of logarithmic decrement with the number of layers for mild steel specimens with beam length 371.25 mm, thickness (6+6) mm and rivet diameter 10 mm at different amplitudes of excitation (y). The theoretical and experimental values are shown by solid and dashed lines, respectively

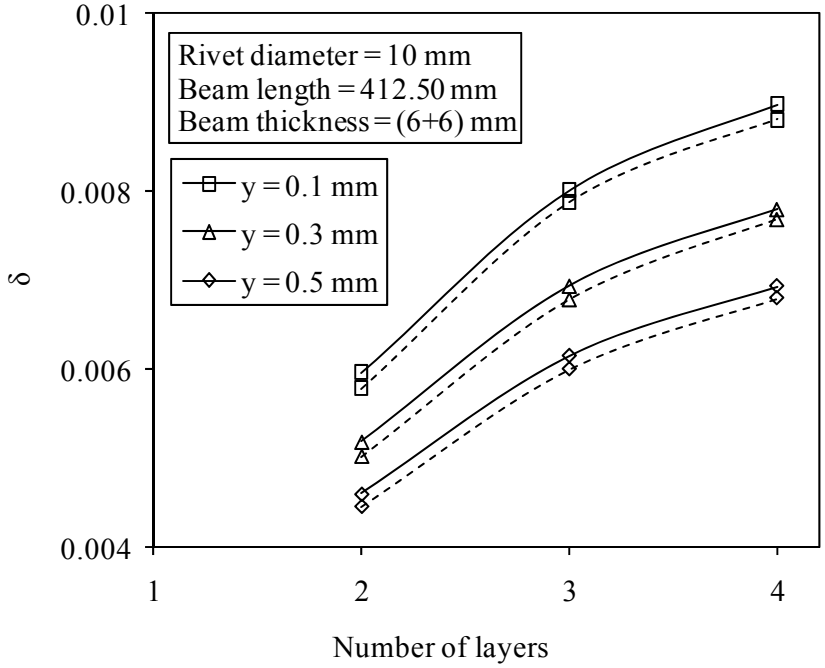

Fig. 5.23 Variation of logarithmic decrement with the number of layers for mild steel specimens with beam length 412.50 mm, thickness (6+6) mm and rivet diameter 10 mm at different amplitudes of excitation (y). The theoretical and experimental values are shown by solid and dashed lines, respectively

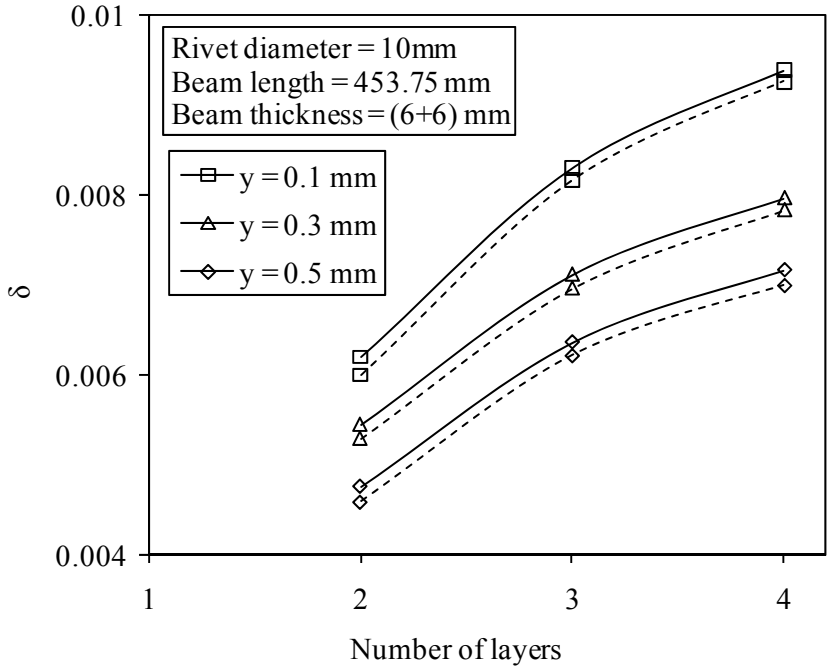

Fig. 5.24 Variation of logarithmic decrement with the number of layers for mild steel specimens with beam length 453.75 mm, thickness (6+6) mm and rivet diameter 10 mm at different amplitudes of excitation (y). The theoretical and experimental values are shown by solid and dashed lines, respectively

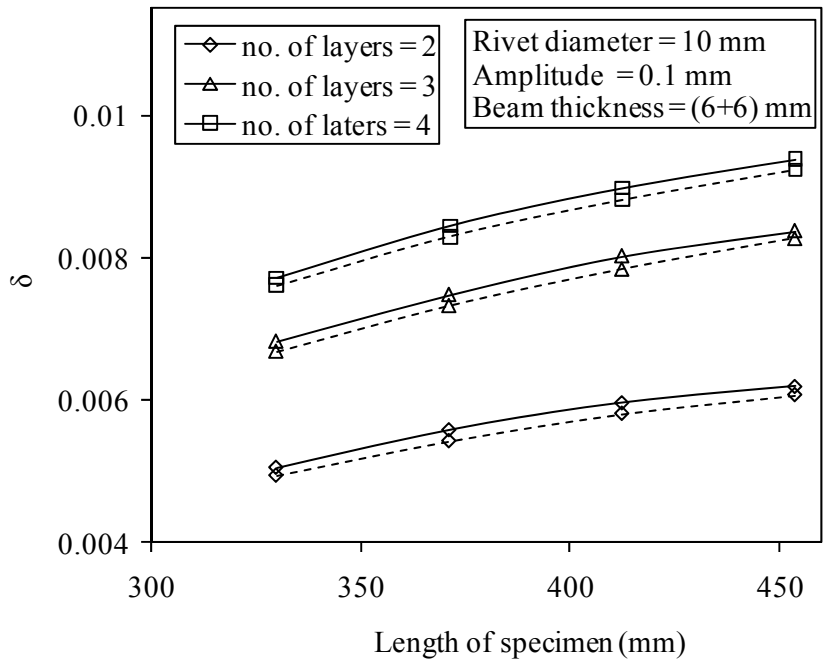

Fig. 5.25 Variation of logarithmic decrement with the length of specimen of mild steel with thickness (6+6) mm, amplitude of excitation 0.1 mm and rivet diameter 10 mm using different number of layers. The theoretical and experimental values are shown by solid and dashed lines, respectively

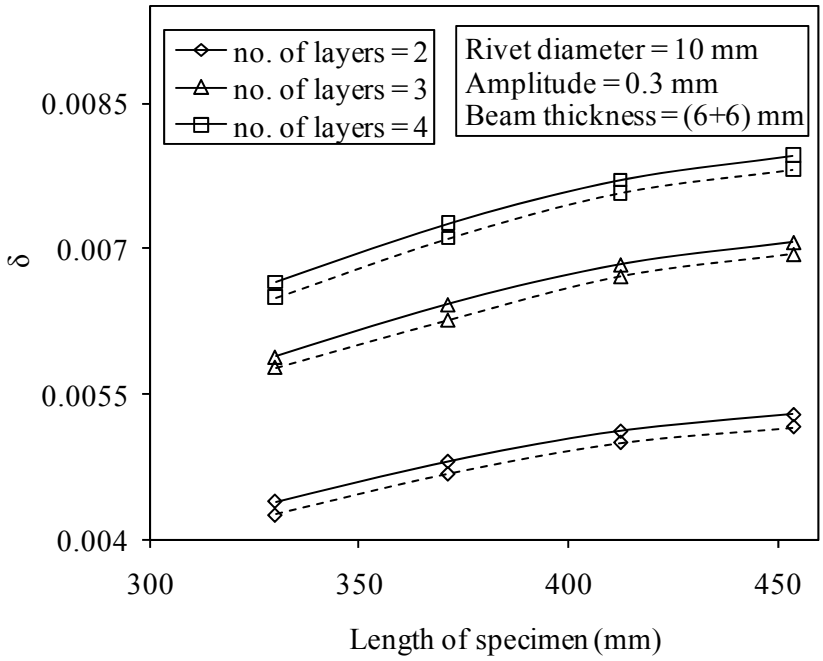

Fig. 5.26 Variation of logarithmic decrement with the length of specimen of mild steel with thickness (6+6) mm, amplitude of excitation 0.3 mm and rivet diameter 10 mm using different number of layers. The theoretical and experimental values are shown by solid and dashed lines, respectively

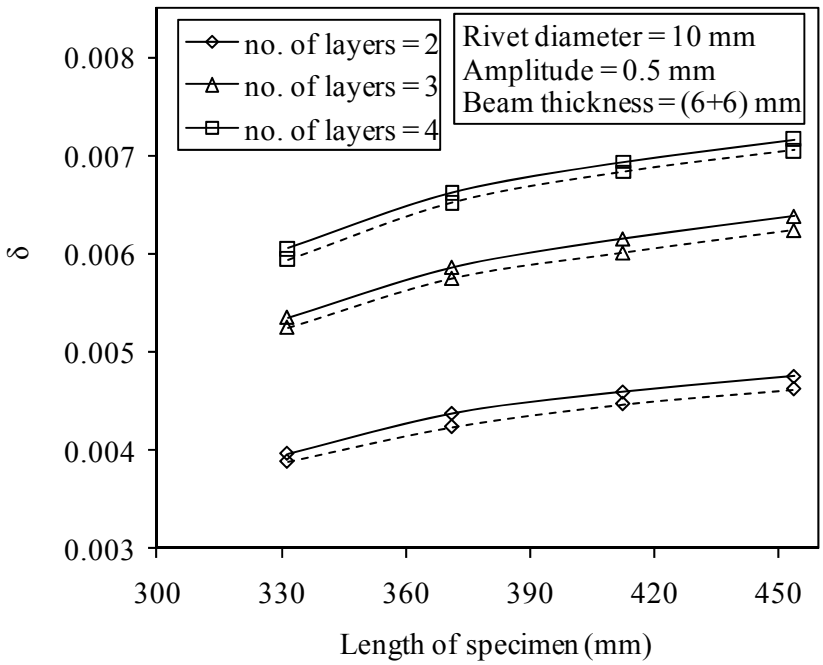

Fig. 5.27 Variation of logarithmic decrement with the length of specimen of mild steel with thickness (6+6) mm, amplitude of excitation 0.5 mm and rivet diameter 10 mm using different number of layers. The theoretical and experimental values are shown by solid and dashed lines, respectively

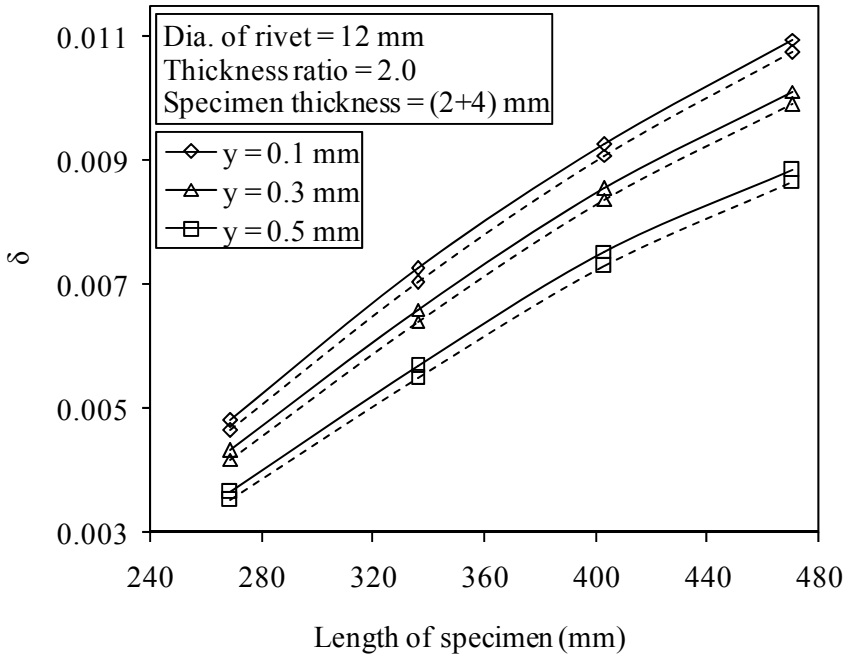

Fig. 5.28 Variation of logarithmic decrement with the length of specimen of mild steel with beam thickness (2+4) mm and rivet diameter 12 mm at different amplitudes of excitation (y). The theoretical and experimental values are shown by solid and dashed lines, respectively

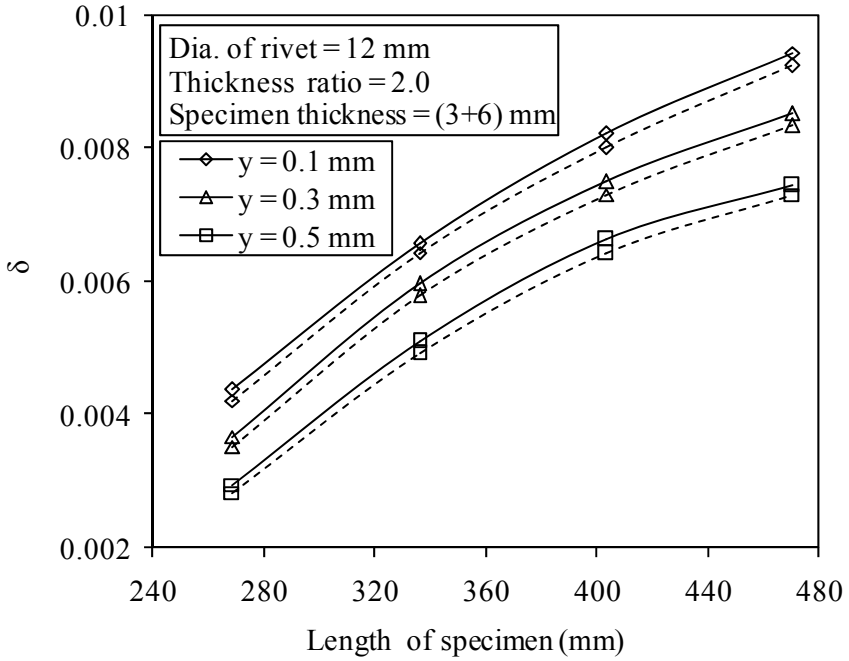

Fig. 5.29 Variation of logarithmic decrement with the length of specimen of mild steel with beam thickness (3+6) mm and rivet diameter 12 mm at different amplitudes of excitation (y). The theoretical and experimental values are shown by solid and dashed lines, respectively

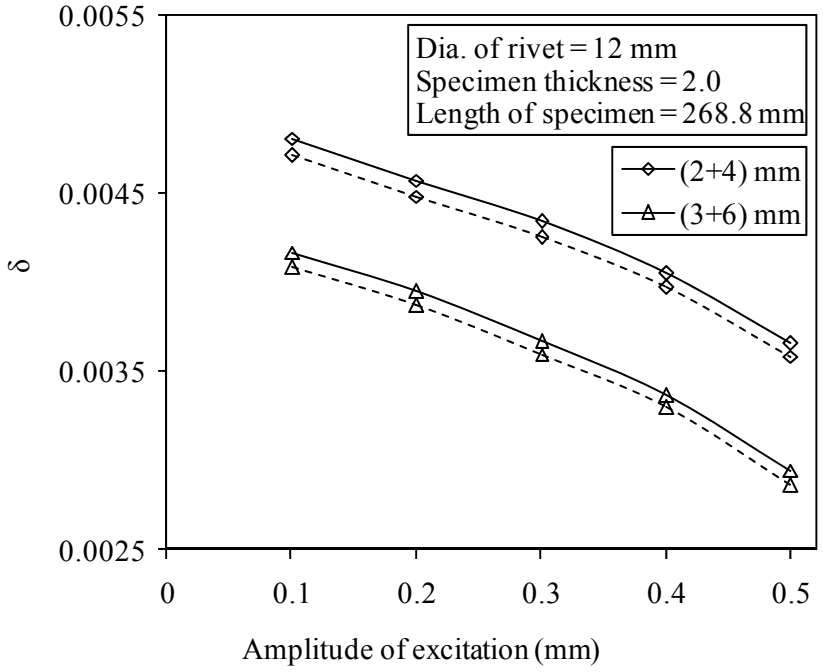

Fig. 5.30 Variation of logarithmic decrement with the amplitude of excitation for mild steel specimens with beam length 268.80 mm and rivet diameter 12 mm having different beam thickness. The theoretical and experimental values are shown by solid and dashed lines, respectively

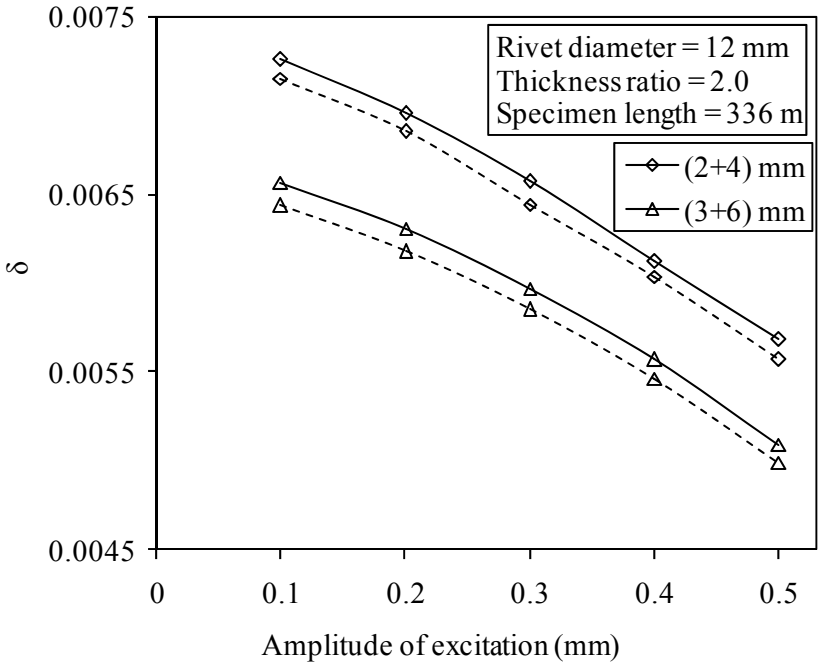

Fig. 5.31 Variation of logarithmic decrement with the amplitude of excitation for mild steel specimens with beam length 336 mm and rivet diameter 12 mm having different beam thickness. The theoretical and experimental values are shown by solid and dashed lines, respectively

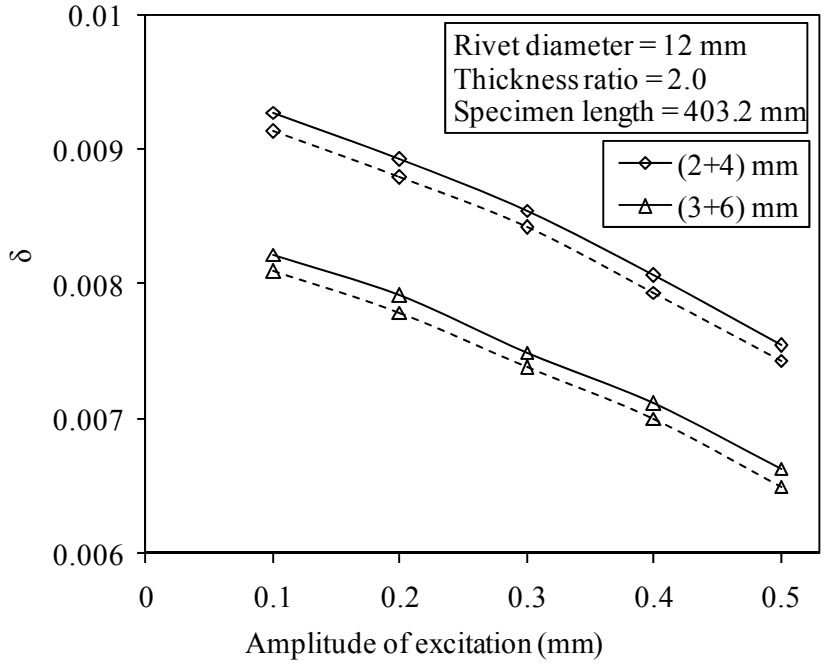

Fig. 5.32 Variation of logarithmic decrement with the amplitude of excitation for mild steel specimens with beam length 403.20 mm and rivet diameter 12 mm having different beam thickness. The theoretical and experimental values are shown by solid and dashed lines, respectively

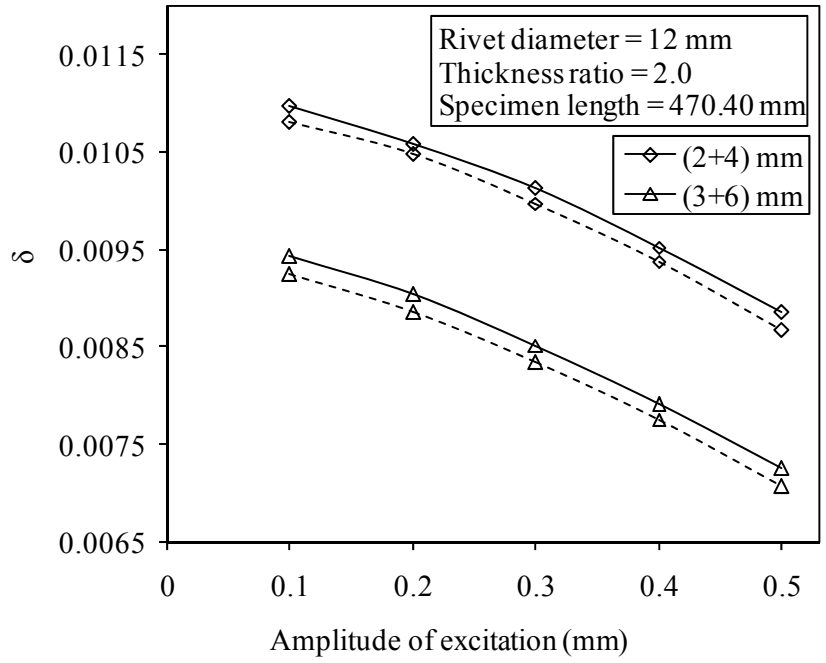

Fig. 5.33 Variation of logarithmic decrement with the amplitude of excitation for mild steel specimens with beam length 470.40 mm and rivet diameter 12 mm having different beam thickness. The theoretical and experimental values are shown by solid and dashed lines, respectively

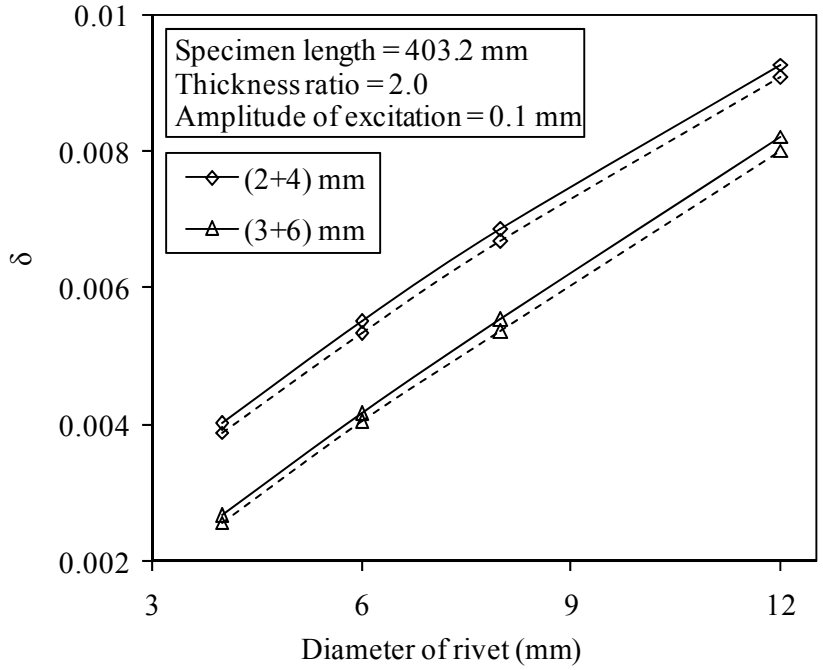

Fig. 5.34 Variation of logarithmic decrement with the diameter of rivet for mild steel specimens with beam length 403.20 mm and initial amplitude of excitation of 0.1 mm having different beam thickness. The theoretical and experimental values are shown by solid and dashed lines, respectively

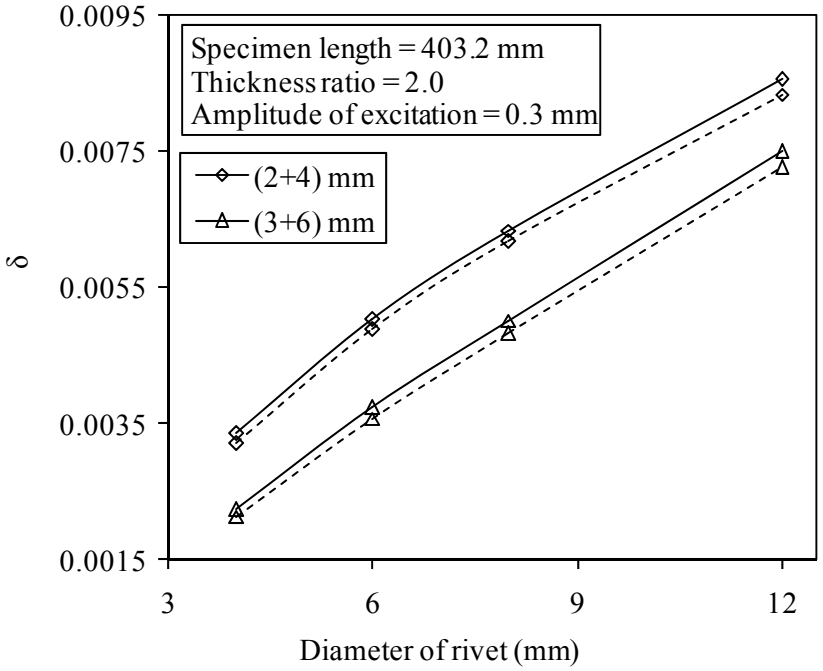

Fig. 5.35 Variation of logarithmic decrement with the diameter of rivet for mild steel specimens with beam length 403.20 mm and initial amplitude of excitation of 0.3 mm having different beam thickness. The theoretical and experimental values are shown by solid and dashed lines, respectively

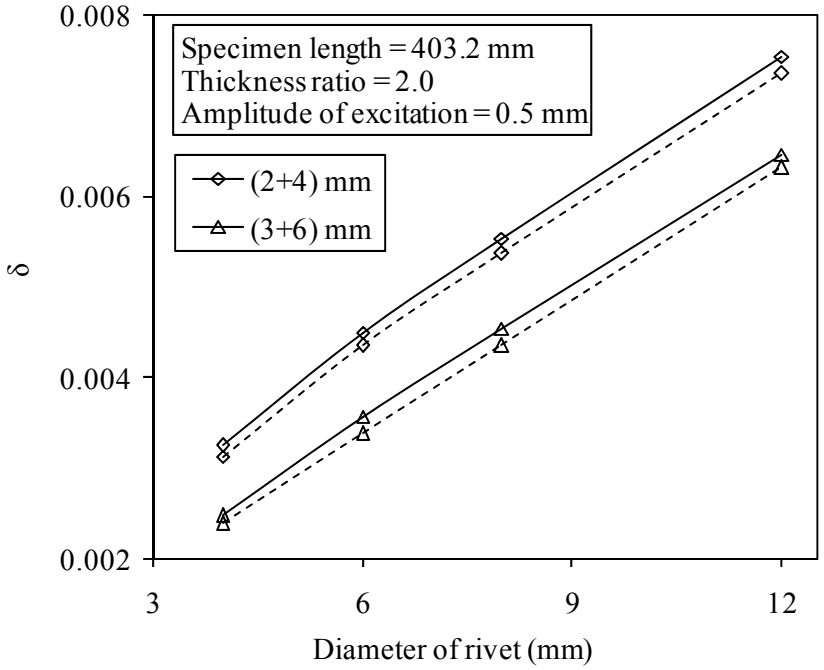

Fig. 5.36 Variation of logarithmic decrement with the diameter of rivet for mild steel specimens with beam length 403.20 mm and initial amplitude of excitation of 0.5 mm having different beam thickness. The theoretical and experimental values are shown by solid and dashed lines, respectively

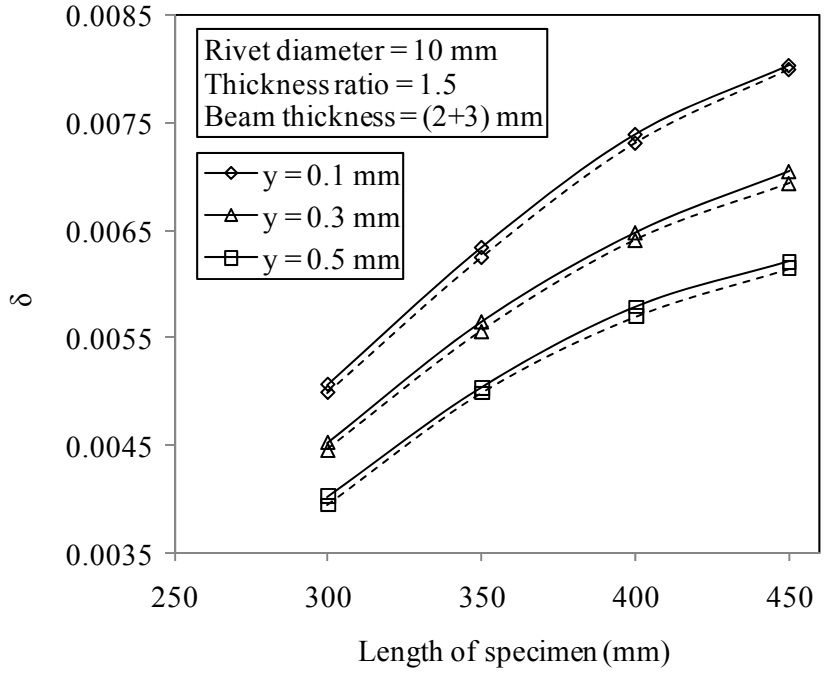

Fig. 5.37 Variation of logarithmic decrement with the length of specimen of mild steel with beam thickness (2+3) mm and rivet diameter 10 mm at different amplitudes of excitation (y). The theoretical and experimental values are shown by solid and dashed lines, respectively

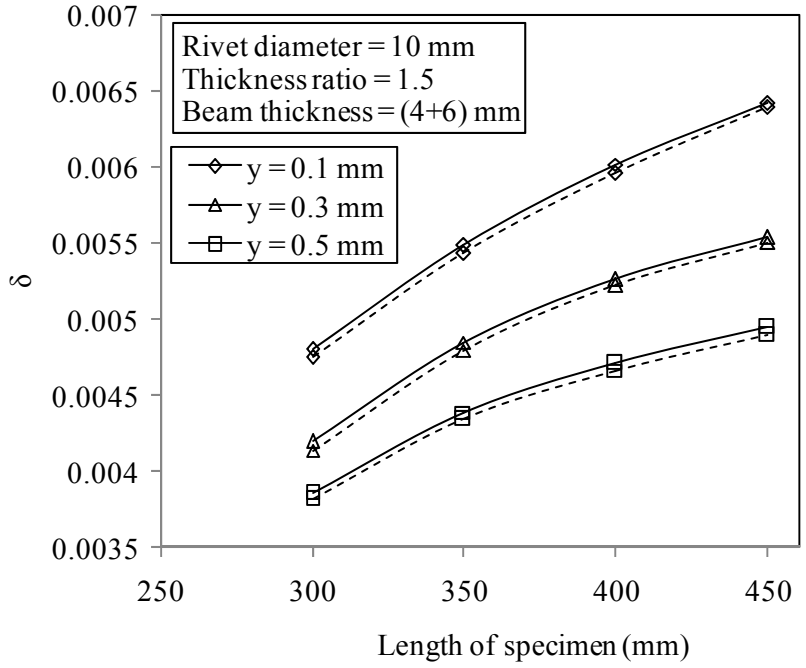

Fig. 5.38 Variation of logarithmic decrement with the length of specimen of mild steel with beam thickness (4+6) mm and rivet diameter 10 mm at different amplitudes of excitation (y). The theoretical and experimental values are shown by solid and dashed lines, respectively

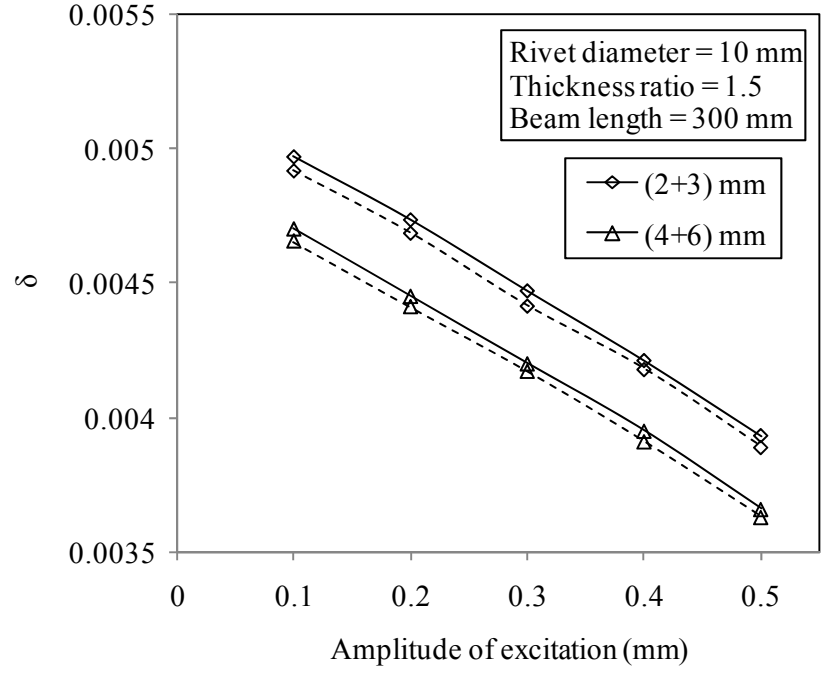

Fig. 5.39 Variation of logarithmic decrement with the amplitude of excitation for mild steel specimens with 300 mm beam length and rivet diameter 10 mm having different beam thickness. The theoretical and experimental values are shown by solid and dashed lines, respectively

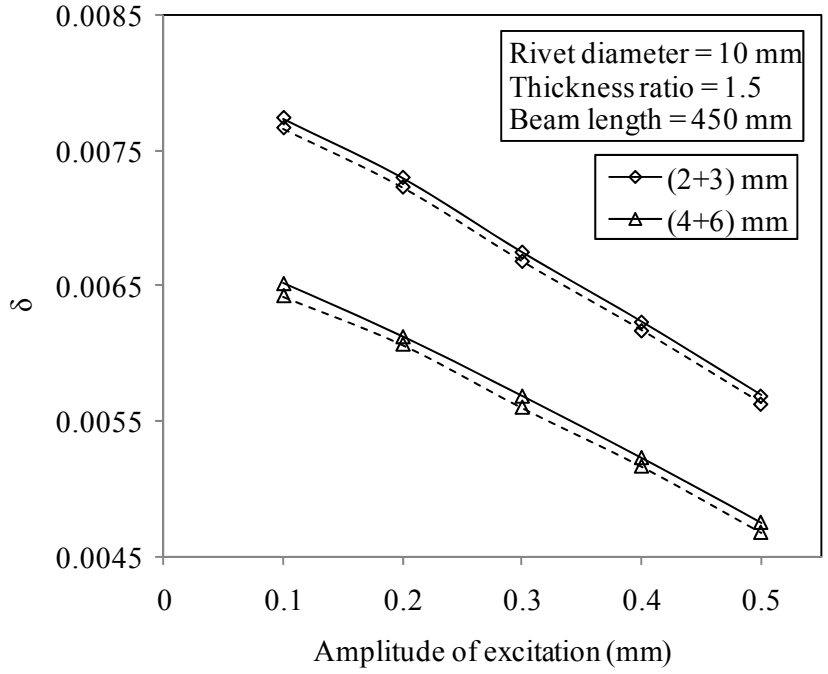

Fig. 5.40 Variation of logarithmic decrement with the amplitude of excitation for mild steel specimens with 450 mm beam length and rivet diameter 10 mm having different beam thickness. The theoretical and experimental values are shown by solid and dashed lines, respectively

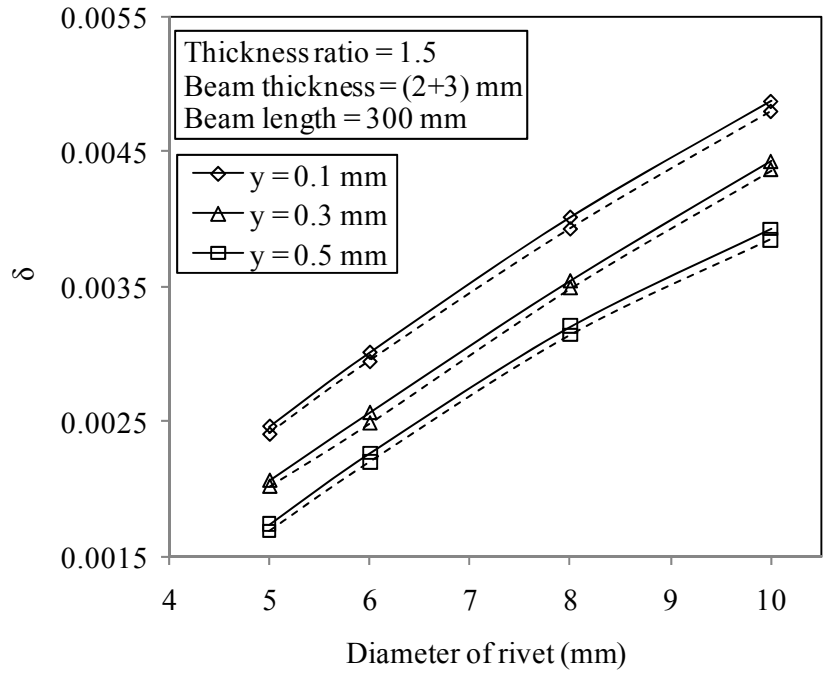

Fig. 5.41 Variation of logarithmic decrement with the diameter of rivet for mild steel specimens with beam length 300 mm and thickness (2+3) mm at different amplitudes of excitation (y). The theoretical and experimental values are shown by solid and dashed lines, respectively

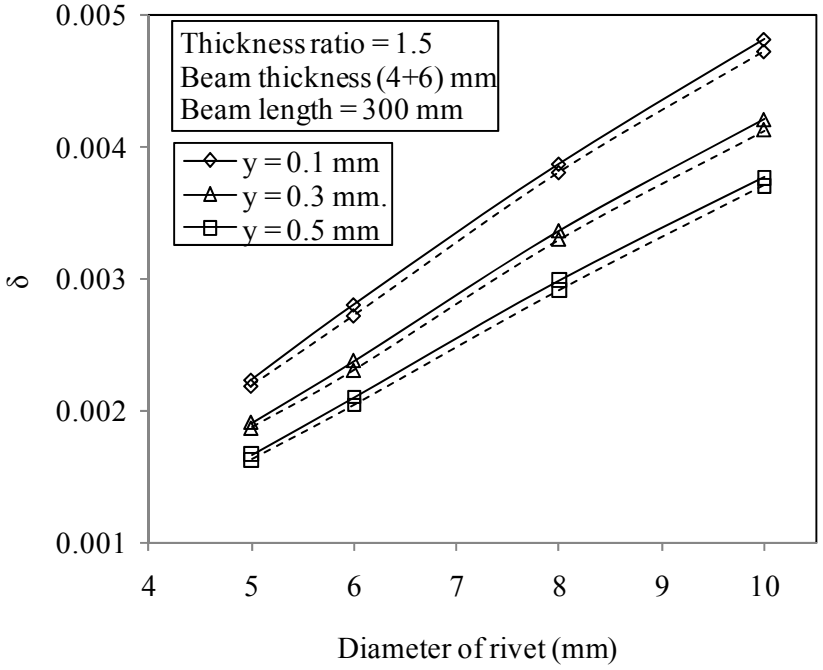

Fig. 5.42 Variation of logarithmic decrement with the diameter of rivet for mild steel specimens with beam length 300 mm and thickness (4+6) mm at different amplitudes of excitation (y). The theoretical and experimental values are shown by solid and dashed lines, respectively

5.6.2 Comparison of Experimental and Finite Element Results for Mild Steel Specimens

The study of damping in layered and jointed beams has been presented in Chapter 4 by finite element method. The stiffness and mass matrices have been derived considering that the hole in the specimen is completely occupied by the rivet. The necessary formulation for the logarithmic decrement has been presented in Eq. (4.30). The numerical results obtained by this method in conjunction with the corresponding experimental ones have been shown in Figs. 5.43 to 5.60 for comparison. The above plots show the variation of logarithmic decrement with respect to several influencing parameters mentioned earlier for different beam thickness ratios. It is observed from the above results that both the curves are close to each other with maximum variation of 1.46%.

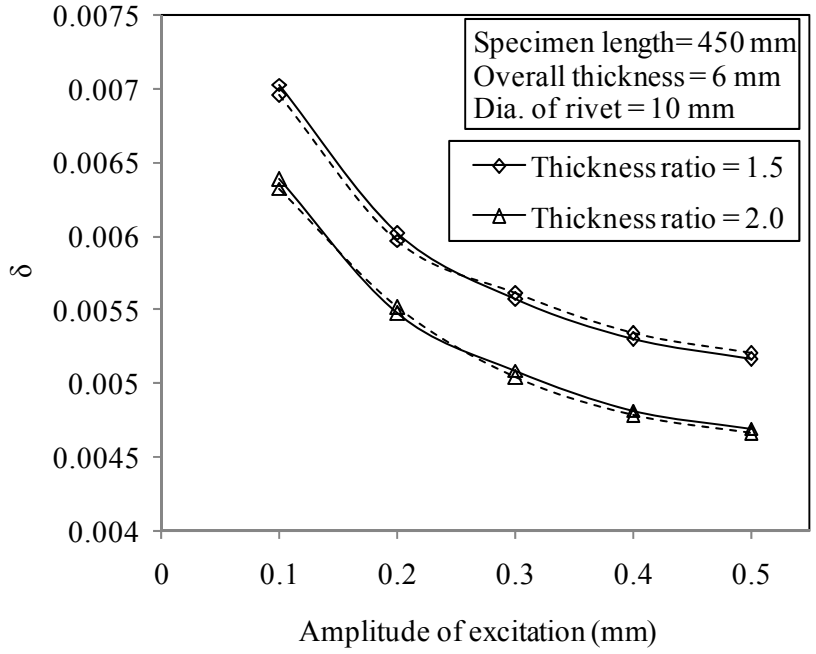

Fig. 5.43 Variation of logarithmic decrement with the amplitude of excitation for mild steel specimens with beam length 450 mm, overall thickness 6 mm and rivet diameter 10 mm having different beam thickness ratio. The theoretical and experimental values are shown by solid and dashed lines, respectively

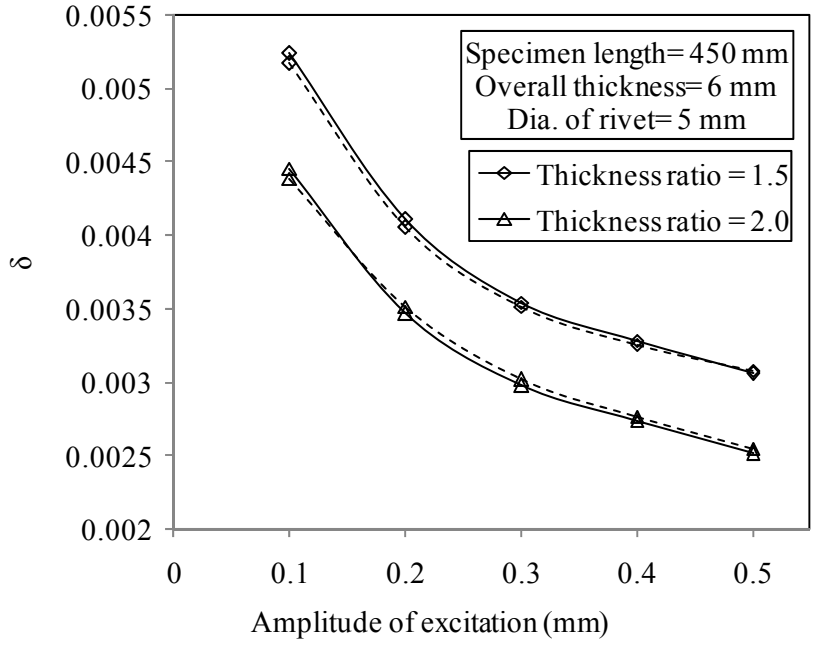

Fig. 5.44 Variation of logarithmic decrement with the amplitude of excitation for mild steel specimens with beam length 450 mm, overall thickness 6 mm and rivet diameter 5 mm having different beam thickness ratio. The theoretical and experimental values are shown by solid and dashed lines, respectively

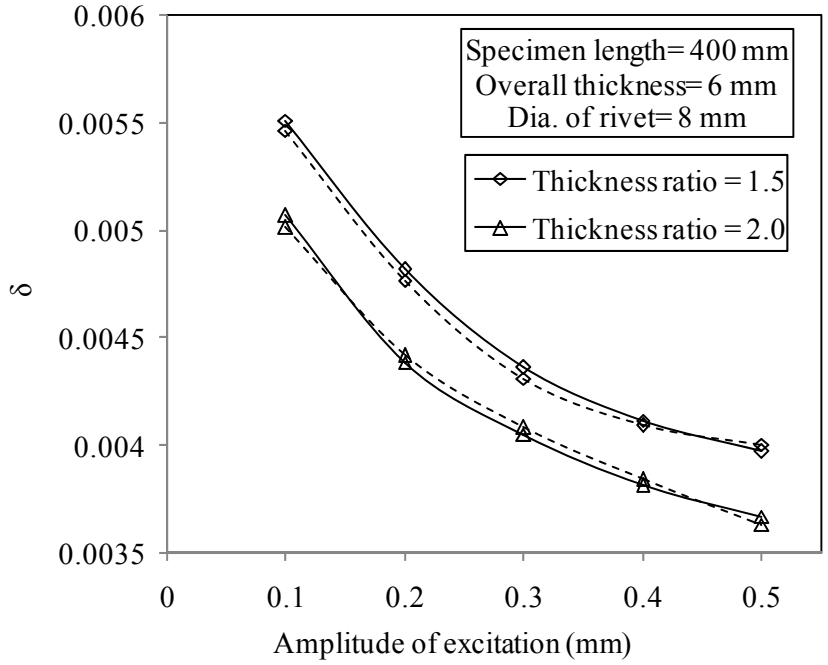

Fig. 5.45 Variation of logarithmic decrement with the amplitude of excitation for mild steel specimens with beam length 400 mm, overall thickness 6 mm and rivet diameter 8 mm having different beam thickness ratio. The theoretical and experimental values are shown by solid and dashed lines, respectively

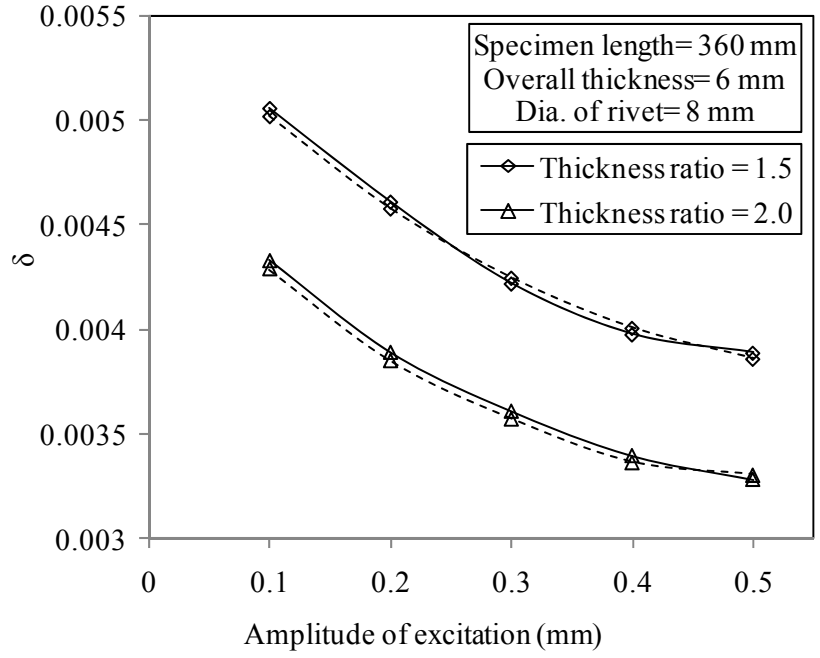

Fig. 5.46 Variation of logarithmic decrement with the amplitude of excitation for mild steel specimens with beam length 360 mm, overall thickness 6 mm and rivet diameter 8 mm having different beam thickness ratio. The theoretical and experimental values are shown by solid and dashed lines, respectively

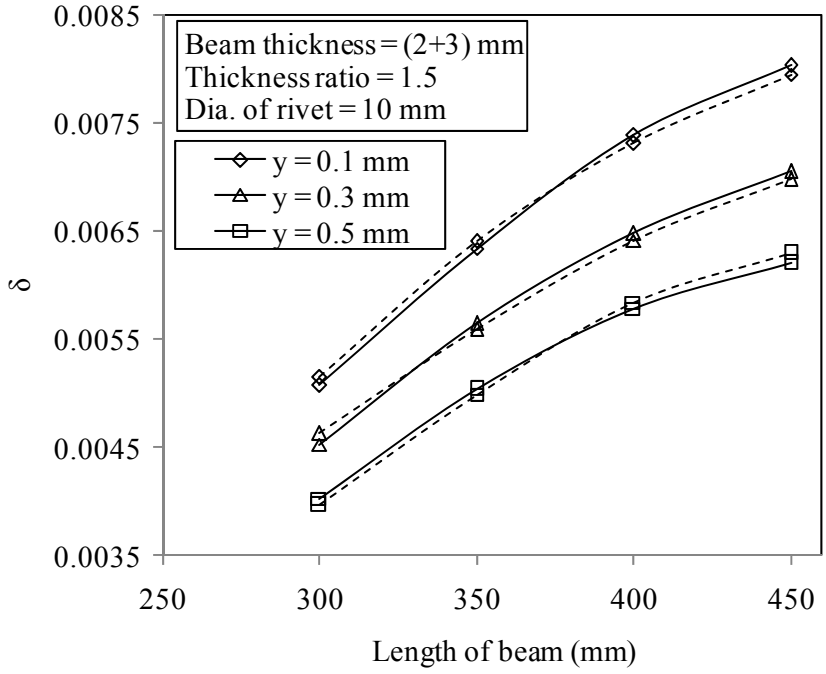

Fig. 5.47 Variation of logarithmic decrement with the length of specimen of mild steel with beam thickness (2+3) mm and rivet diameter 10 mm at different amplitudes of excitation (y). The theoretical and experimental values are shown by solid and dashed lines, respectively

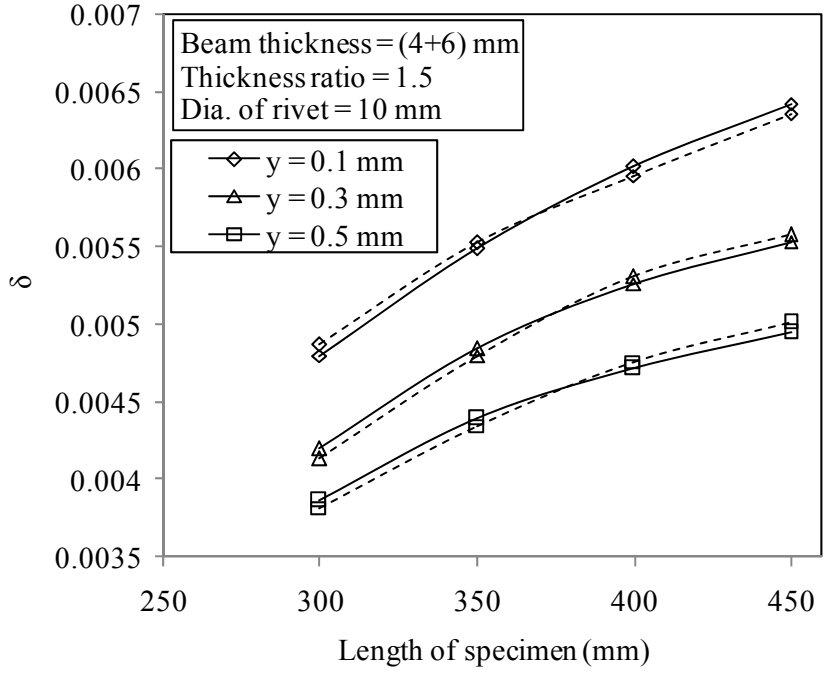

Fig. 5.48 Variation of logarithmic decrement with the length of specimen of mild steel with beam thickness (4+6) mm and rivet diameter 10 mm at different amplitudes of excitation (y). The theoretical and experimental values are shown by solid and dashed lines, respectively

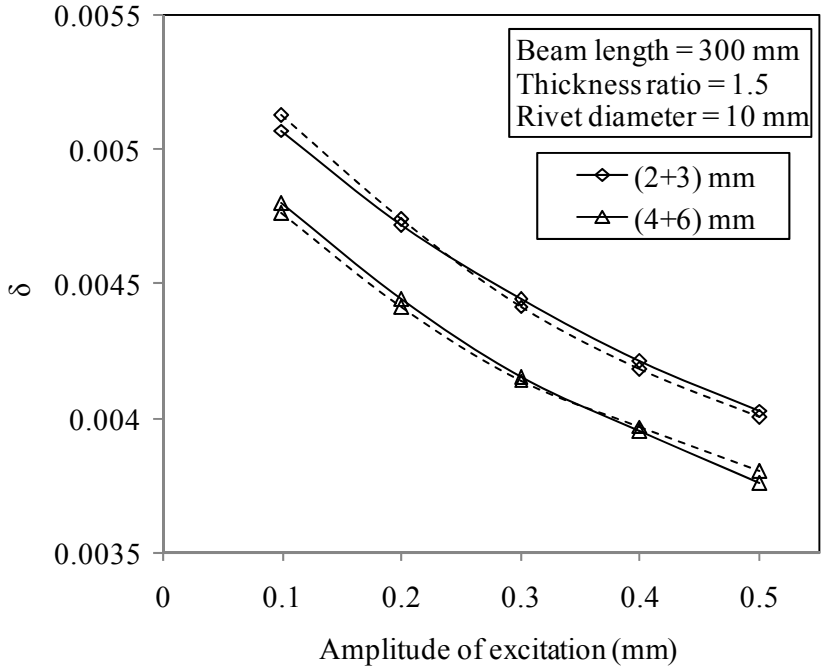

Fig, 5.49 Variation of logarithmic decrement with the amplitude of excitation for mild steel specimens with beam length 300 mm and rivet diameter 10 mm having different beam thickness. The theoretical and experimental values are shown by solid and dashed lines, respectively

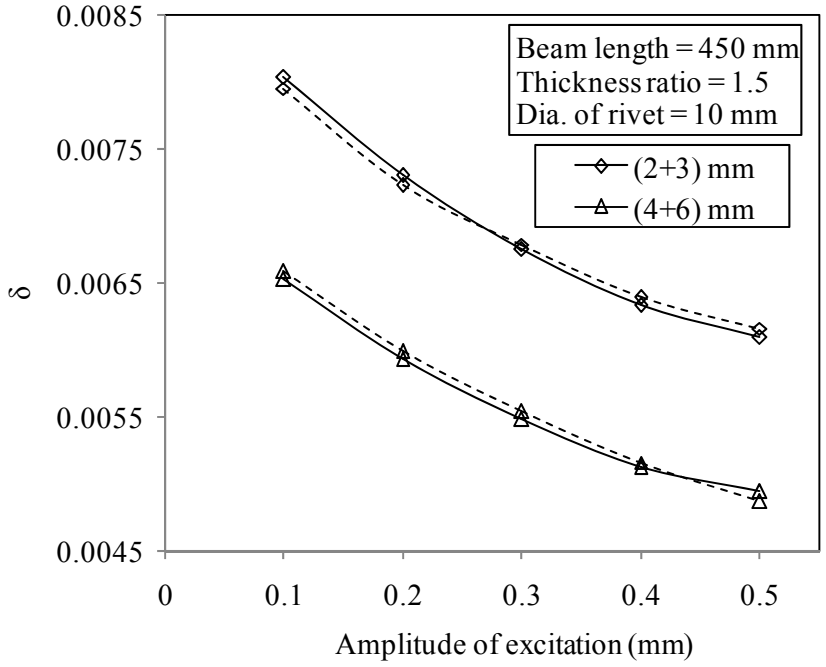

Fig, 5.50 Variation of logarithmic decrement with the amplitude of excitation for mild steel specimens with beam length 450 mm and rivet diameter 10 mm having different beam thickness. The theoretical and experimental values are shown by solid and dashed lines, respectively

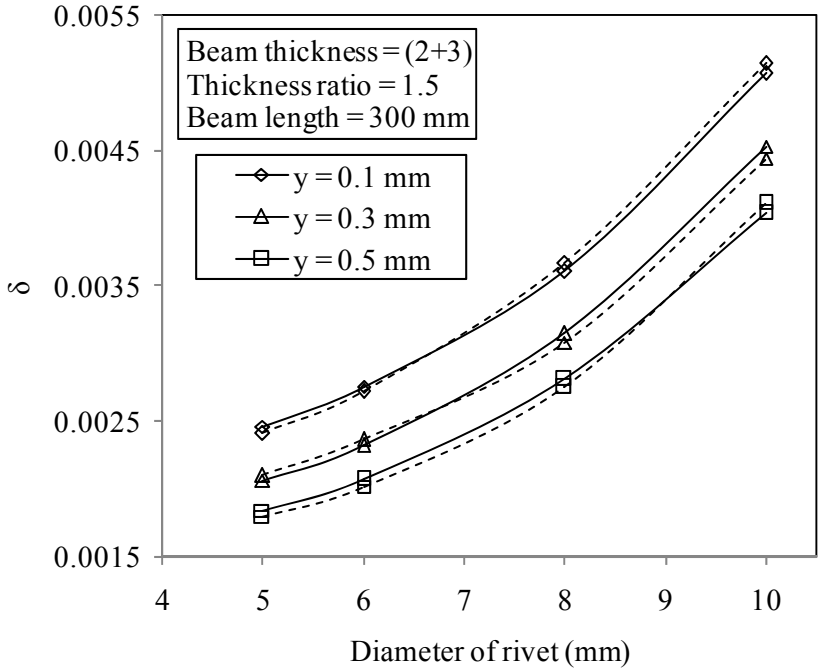

Fig. 5.51 Variation of logarithmic decrement with the diameter of rivet for mild steel specimens with beam length 300 mm and thickness (2+3) mm at different amplitudes of excitation (y). The theoretical and experimental values are shown by solid and dashed lines, respectively

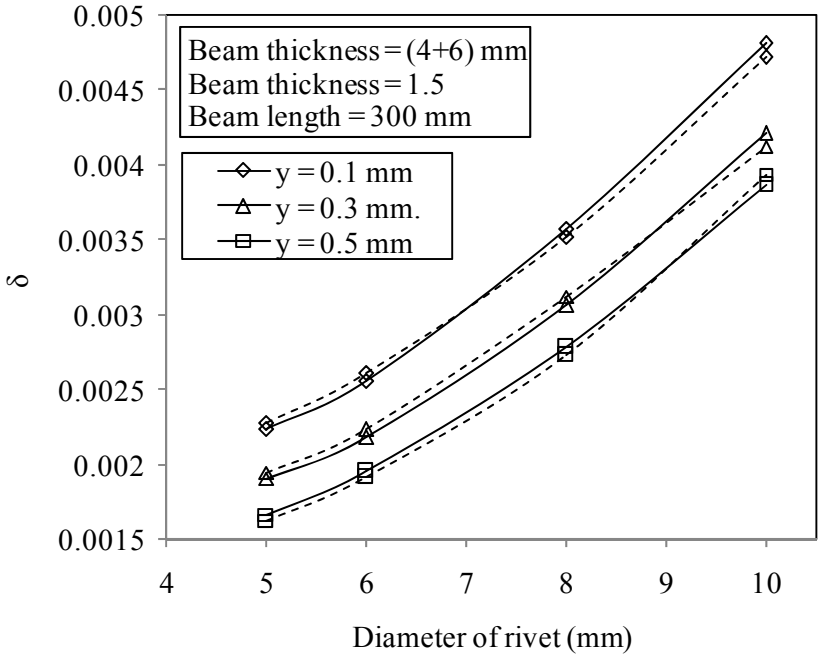

Fig. 5.52 Variation of logarithmic decrement with the diameter of rivet for mild steel specimens for beam length 300 mm and thickness (4+6) mm at different amplitudes of excitation (y). The theoretical and experimental values are shown by solid and dashed lines, respectively

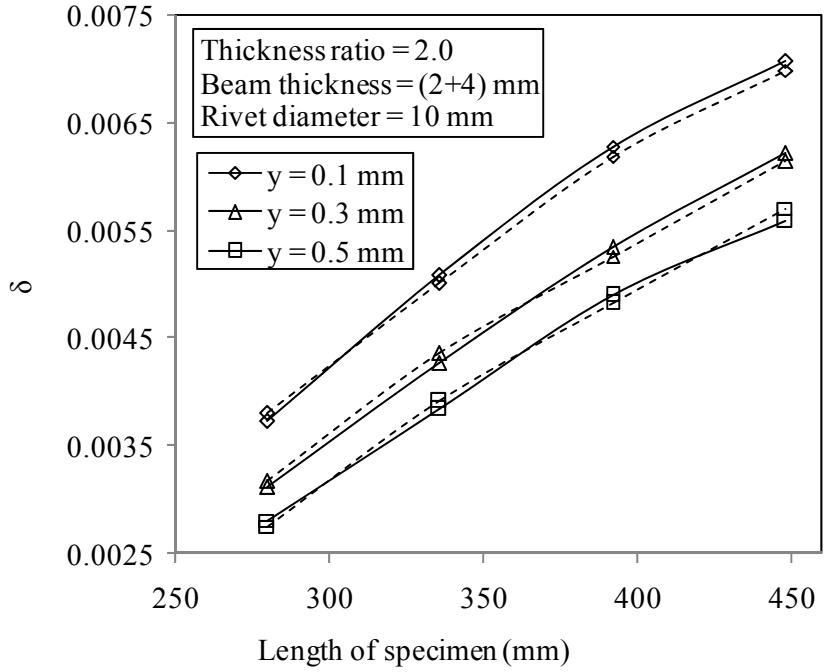

Fig. 5.53 Variation of logarithmic decrement with the length of specimen of mild steel with beam thickness (2+4) mm and rivet diameter 10 mm at different amplitudes of excitation (y). The theoretical and experimental values are shown by solid and dashed lines, respectively

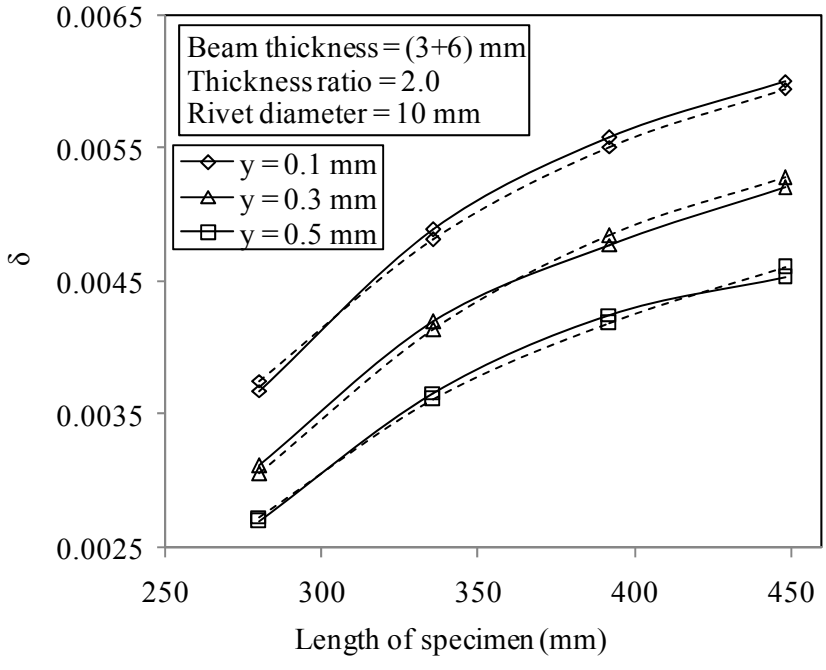

Fig. 5.54 Variation of logarithmic decrement with the length of specimen of mild steel with beam thickness (3+6) mm and rivet diameter 10 mm at different amplitudes of excitation (y). The theoretical and experimental values are shown by solid and dashed lines, respectively

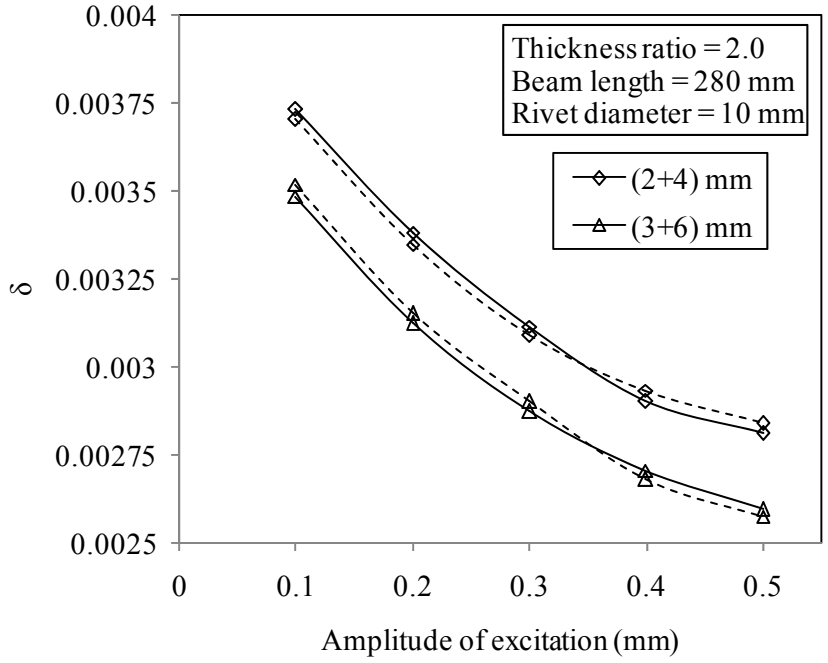

Fig. 5.55 Variation of logarithmic decrement with the amplitude of excitation for mild steel specimens with beam length 280 mm and rivet diameter 10 mm having different beam thickness. The theoretical and experimental values are shown by solid and dashed lines, respectively

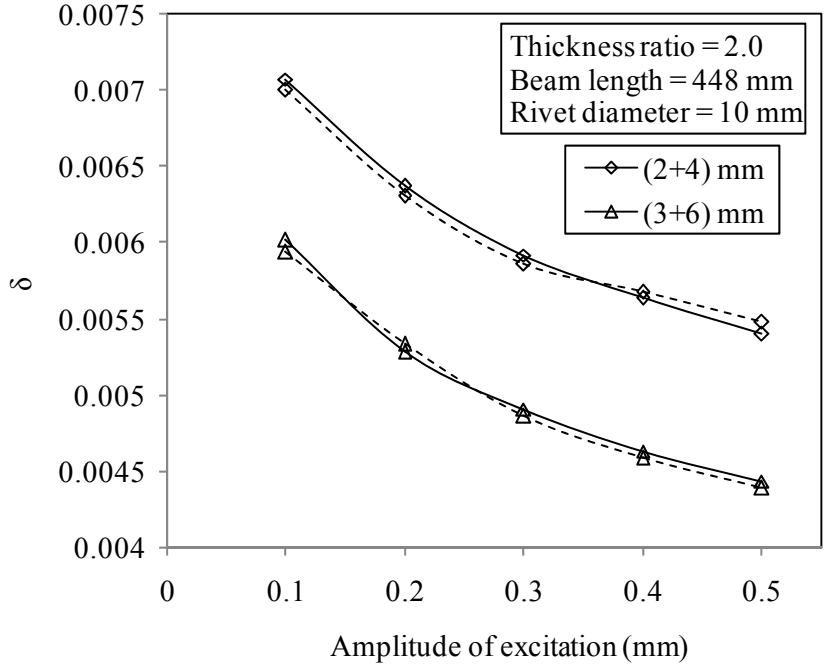

Fig. 5.56 Variation of logarithmic decrement with the amplitude of excitation for mild steel specimens with beam length 448 mm and rivet diameter 10 mm having different beam thickness. The theoretical and experimental values are shown by solid and dashed lines, respectively

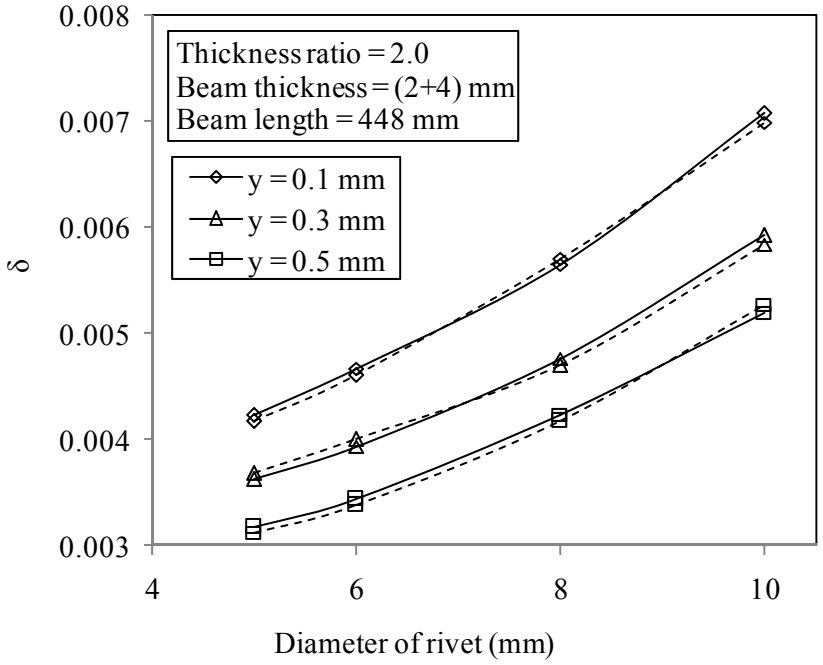

Fig. 5.57 Variation of logarithmic decrement with the diameter of rivet for mild steel specimens with beam length 448 mm and thickness (2+4) mm at different amplitudes of excitation (y). The theoretical and experimental values are shown by solid and dashed lines, respectively

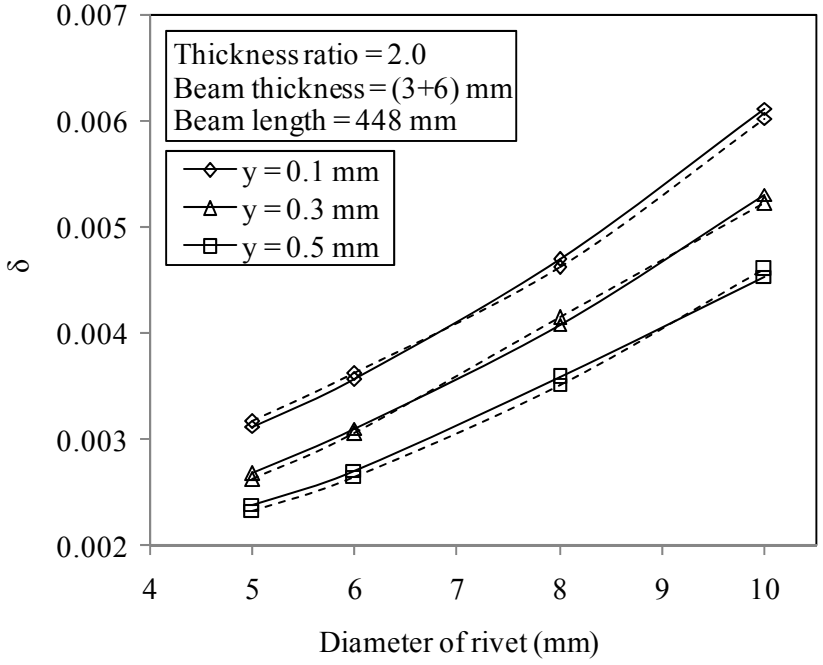

Fig. 5.58 Variation of logarithmic decrement with the diameter of rivet for mild steel specimens with beam length 448 mm and thickness (3+6) mm at different amplitudes of excitation (y). The theoretical and experimental values are shown by solid and dashed lines, respectively

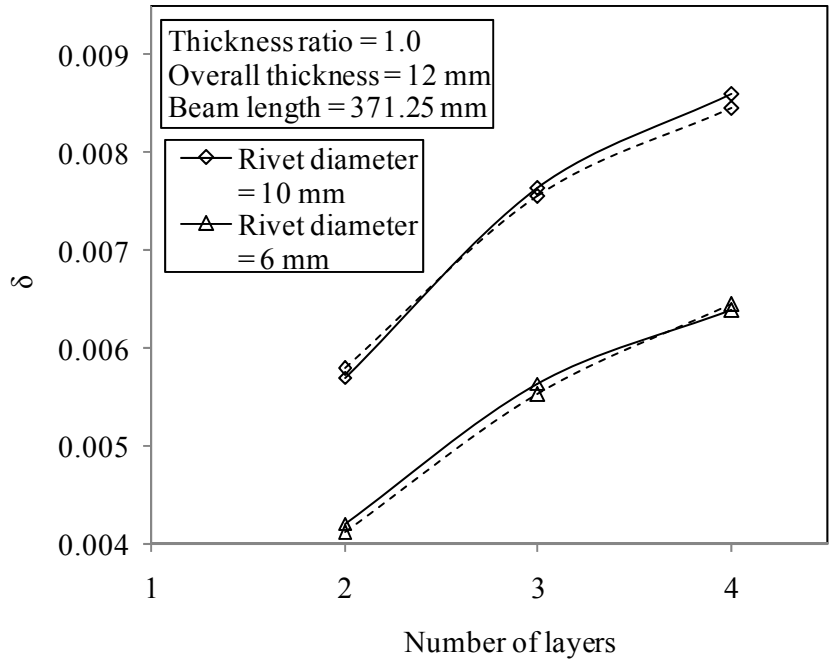

Fig. 5.59 Variation of logarithmic decrement with the number of layers for mild steel specimens with beam length 371.25 mm, overall thickness 12 mm and amplitude of excitation 0.1 mm using different rivet diameter. The theoretical and experimental values are shown by solid and dashed lines, respectively

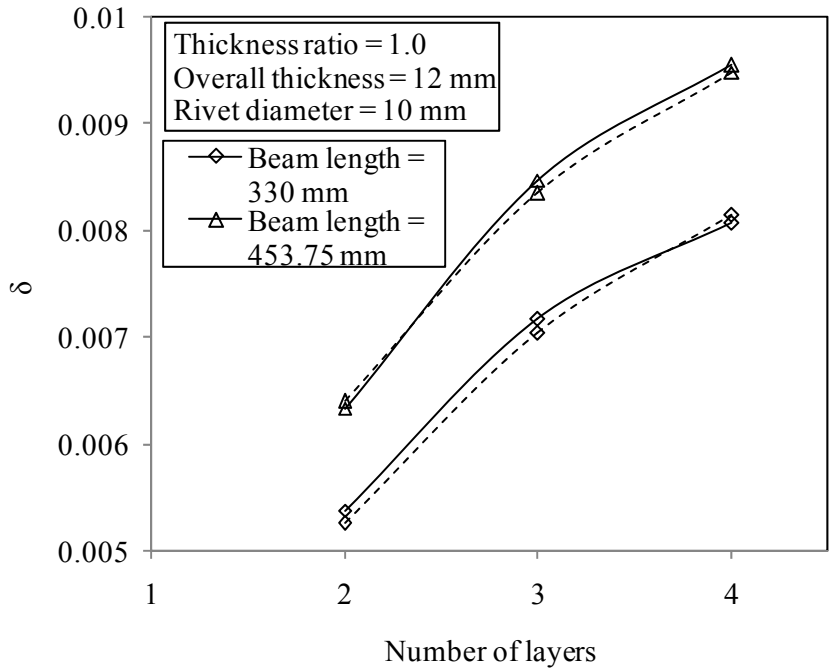

Fig. 5.60 Variation of logarithmic decrement with the number of layers for mild steel specimens with overall thickness 12 mm, amplitude of excitation 0.1 mm and rivet diameter 10 mm using different beam length. The theoretical and experimental values are shown by solid and dashed lines, respectively

5.6.3 Comparison of Experimental and Classical Results for Aluminium Specimens

The numerical results obtained by classical approach in conjunction with the corresponding experimental ones have been shown in Figs. 5.61 to 5.70 for comparison. It is observed from the above results that both the curves are close to each other with maximum variation of 3.62%.

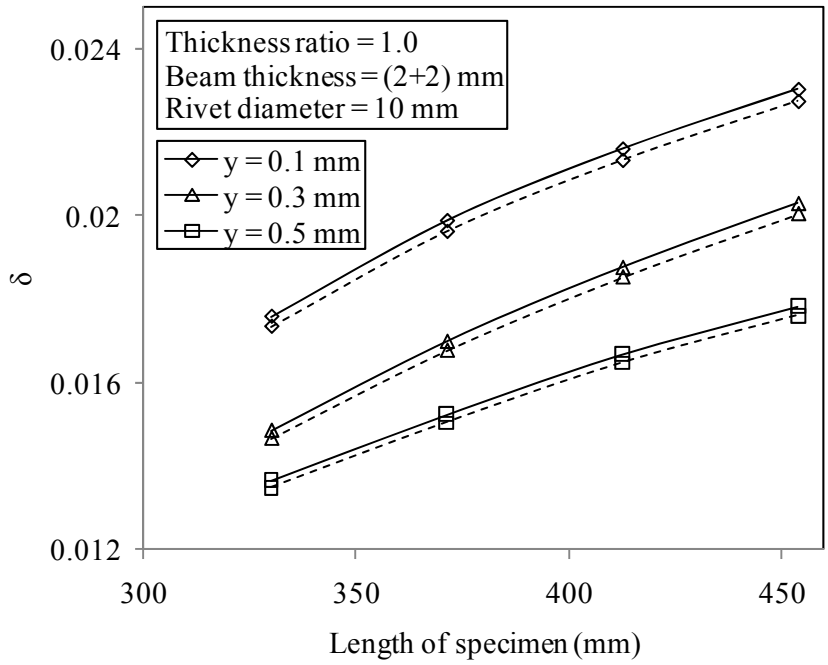

Fig. 5.61 Variation of logarithmic decrement with the length of specimen of aluminium with beam thickness (2+2) mm and rivet diameter 10 mm at different amplitudes of excitation (y). The theoretical and experimental values are shown by solid and dashed lines, respectively

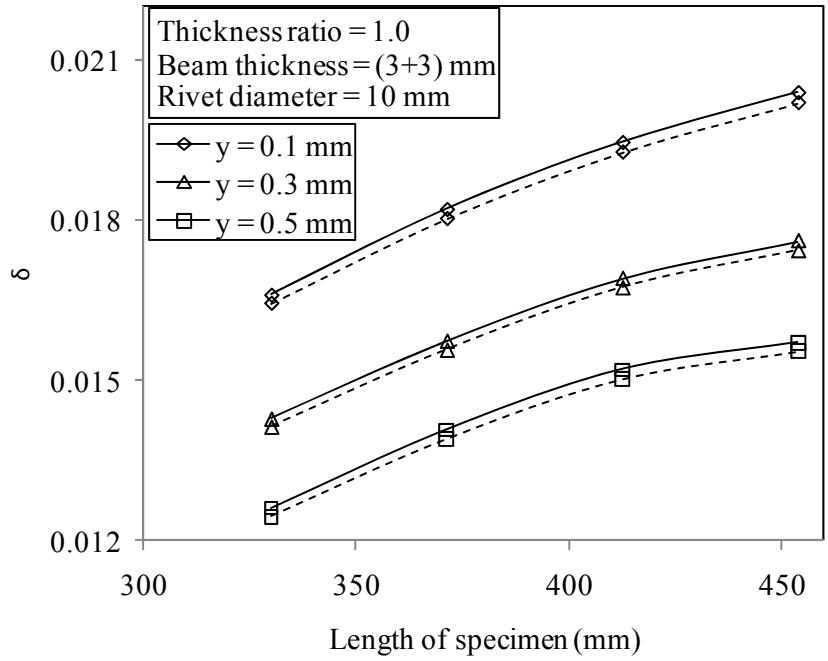

Fig. 5.62 Variation of logarithmic decrement with the length of specimen of aluminium with beam thickness (3+3) mm and rivet diameter 10 mm at different amplitudes of excitation (y). The theoretical and experimental values are shown by solid and dashed lines, respectively

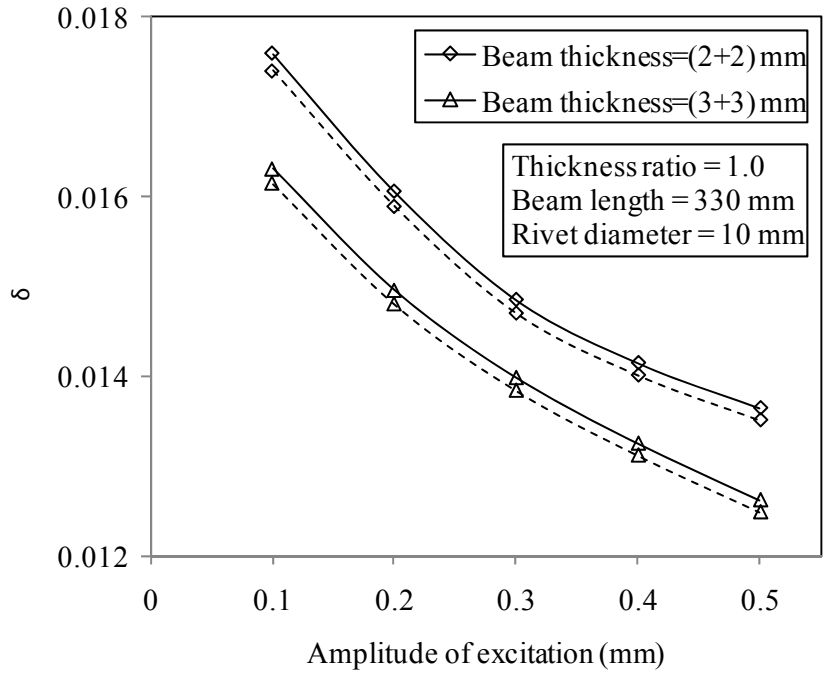

Fig. 5.63 Variation of logarithmic decrement with the amplitude of excitation for aluminium specimens with beam length 330 mm and rivet diameter 10 mm having different beam thickness. The theoretical and experimental values are shown by solid and dashed lines, respectively

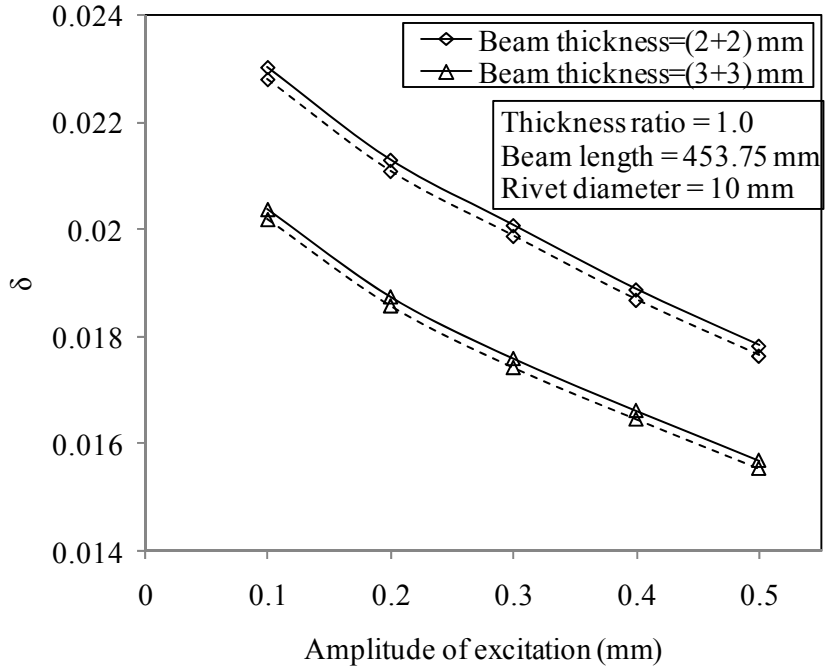

Fig. 5.64 Variation of logarithmic decrement with the amplitude of excitation for aluminium specimens with beam length 453.75 mm and rivet diameter 10 mm having different beam thickness. The theoretical and experimental values are shown by solid and dashed lines, respectively

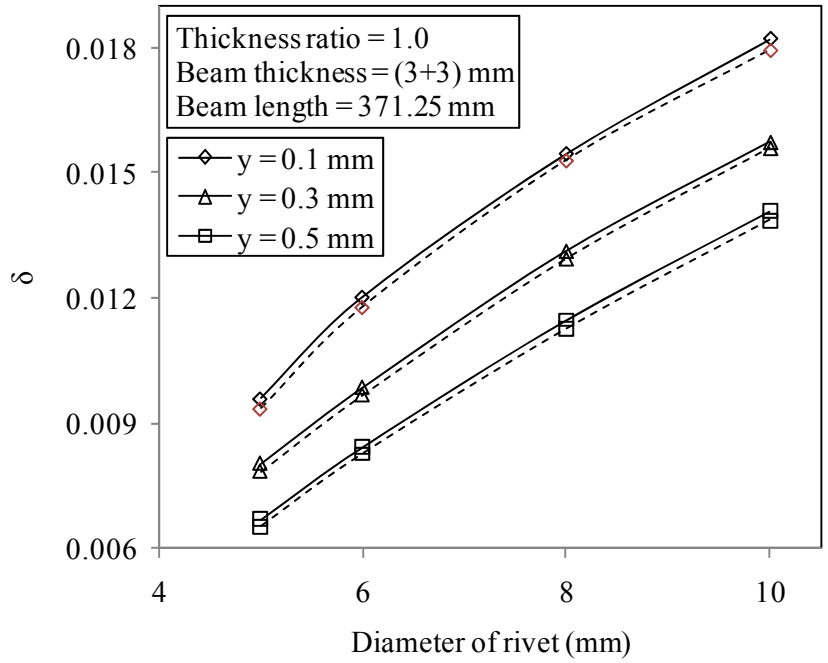

Fig. 5.65 Variation of logarithmic decrement with the diameter of rivet for aluminium specimens with beam length 371.25 mm and thickness (3+3) mm at different amplitudes of excitation (y). The theoretical and experimental values are shown by solid and dashed lines, respectively

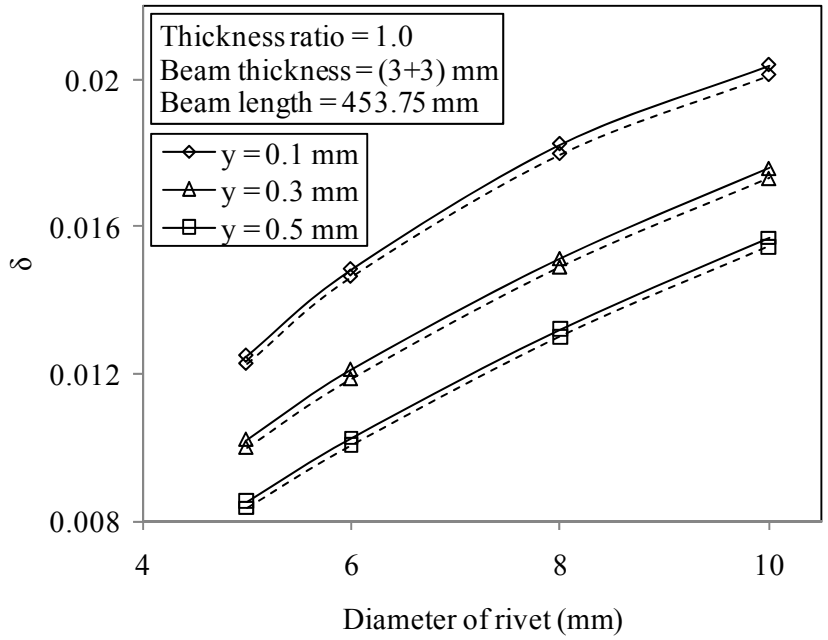

Fig. 5.66 Variation of logarithmic decrement with the diameter of rivet for aluminium specimens with beam length 453.75 mm and thickness (3+3) mm at different amplitudes of excitation (y). The theoretical and experimental values are shown by solid and dashed lines, respectively

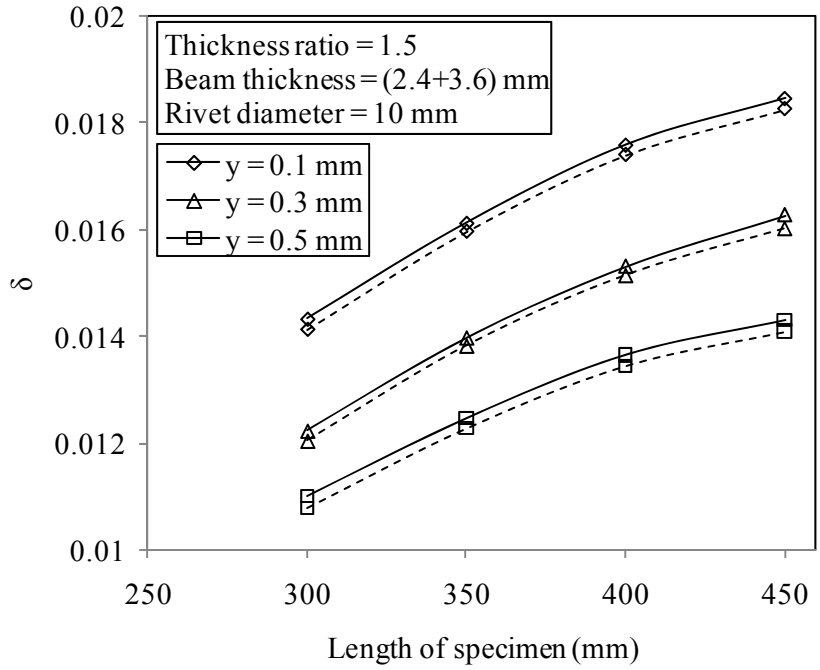

Fig. 5.67 Variation of logarithmic decrement with the length of specimen of aluminium with beam thickness (2.4+3.6) mm and rivet diameter 10 mm at different amplitudes of excitation (y). The theoretical and experimental values are shown by solid and dashed lines, respectively

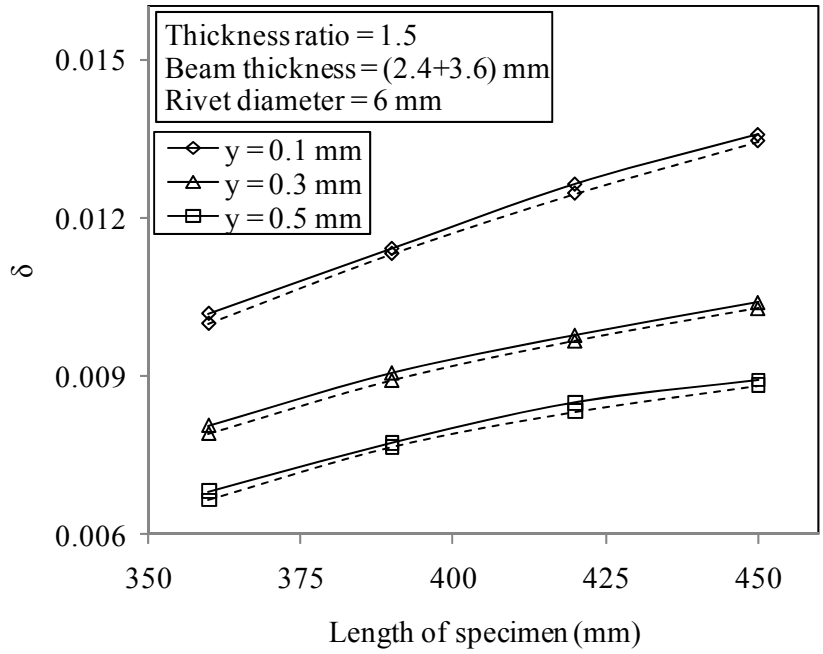

Fig. 5.68 Variation of logarithmic decrement with the length of specimen of aluminium with beam thickness (2.4+3.6) mm and rivet diameter 6 mm at different amplitudes of excitation (y). The theoretical and experimental values are shown by solid and dashed lines, respectively

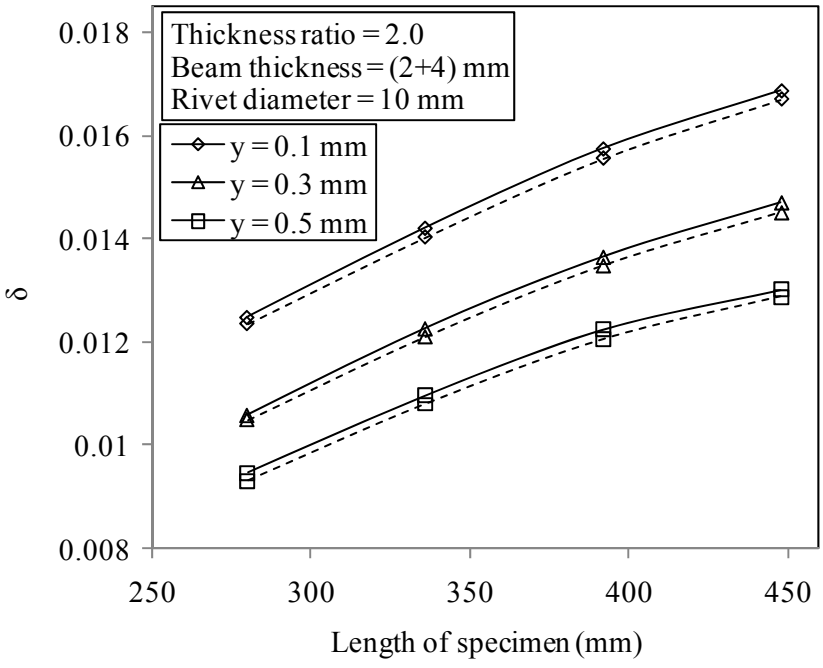

Fig. 5.69 Variation of logarithmic decrement with the length of specimen of aluminium with beam thickness (2+4) mm and rivet diameter 10 mm at different amplitudes of excitation (y). The theoretical and experimental values are shown by solid and dashed lines, respectively

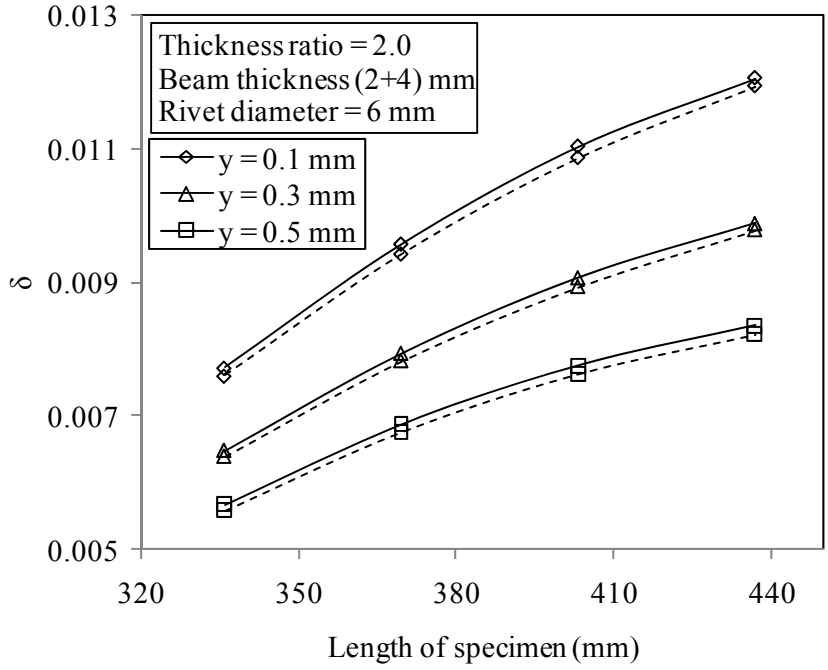

Fig. 5.70 Variation of logarithmic decrement with the length for specimen of aluminium beam thickness (2+4) mm and rivet diameter 6 mm at different amplitudes of excitation (y). The theoretical and experimental values are shown by solid and dashed lines, respectively

5.6.4 Comparison of Experimental and Finite Element Results for Aluminium Specimens

The numerical results obtained by finite element method along with the corresponding experimental ones are presented in Figs. 5.71 to 5.75 for comparison. It is observed from the above results that both the curves are close to each other with maximum variation of 2.54%.

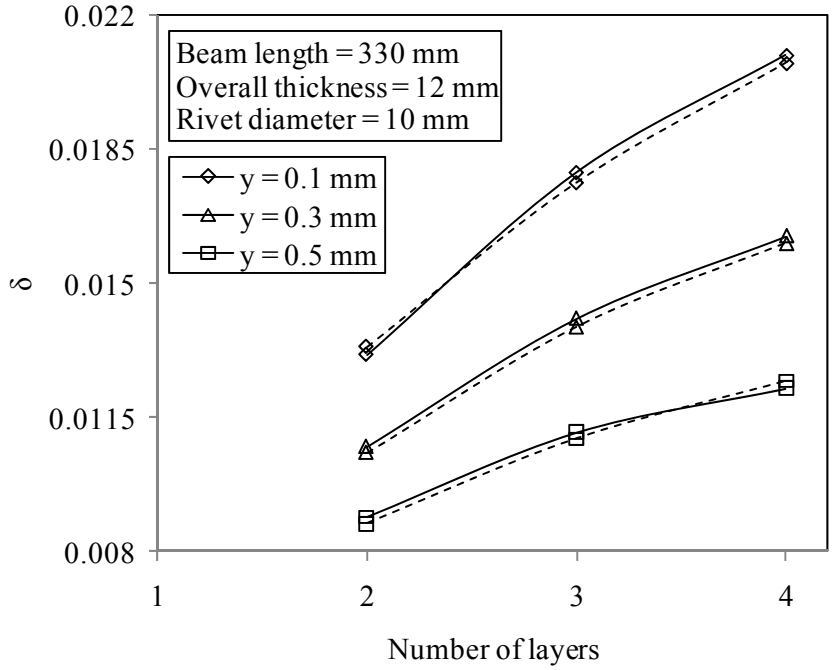

Fig. 5.71 Variation of logarithmic decrement with the number of layers for aluminium specimens with beam length 330 mm, overall thickness 12 mm and rivet diameter 10 mm at different amplitudes of excitation (y). The theoretical and experimental values are shown by solid and dashed lines, respectively

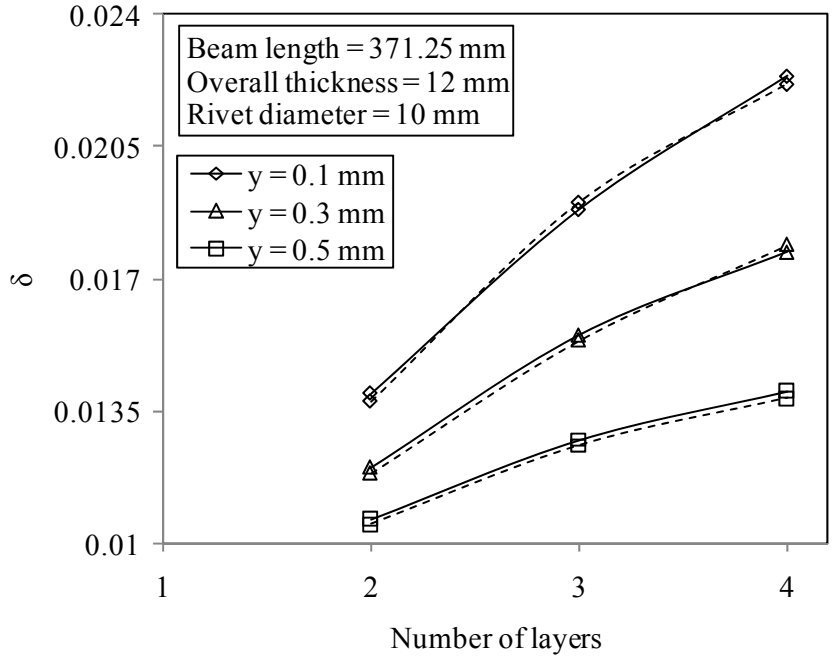

Fig. 5.72 Variation of logarithmic decrement with the number of layers for aluminium specimens with beam length 371.25 mm, overall thickness 12 mm and rivet diameter 10 mm at different amplitudes of excitation (y). The theoretical and experimental values are shown by solid and dashed lines, respectively

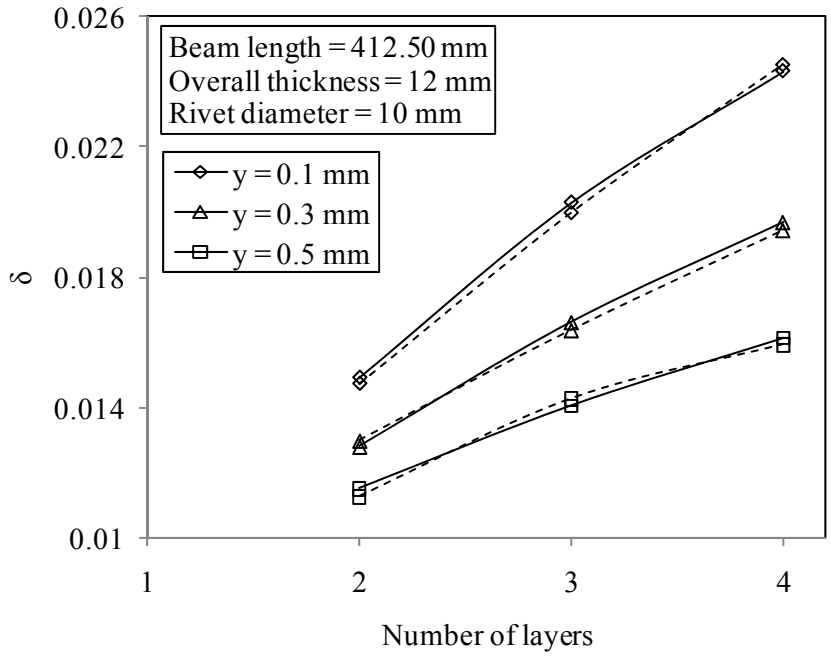

Fig. 5.73 Variation of logarithmic decrement with the number of layers for aluminium specimens with beam length 412.50 mm, overall thickness 12 mm and rivet diameter 10 mm at different amplitudes of excitation (y). The theoretical and experimental values are shown by solid and dashed lines, respectively

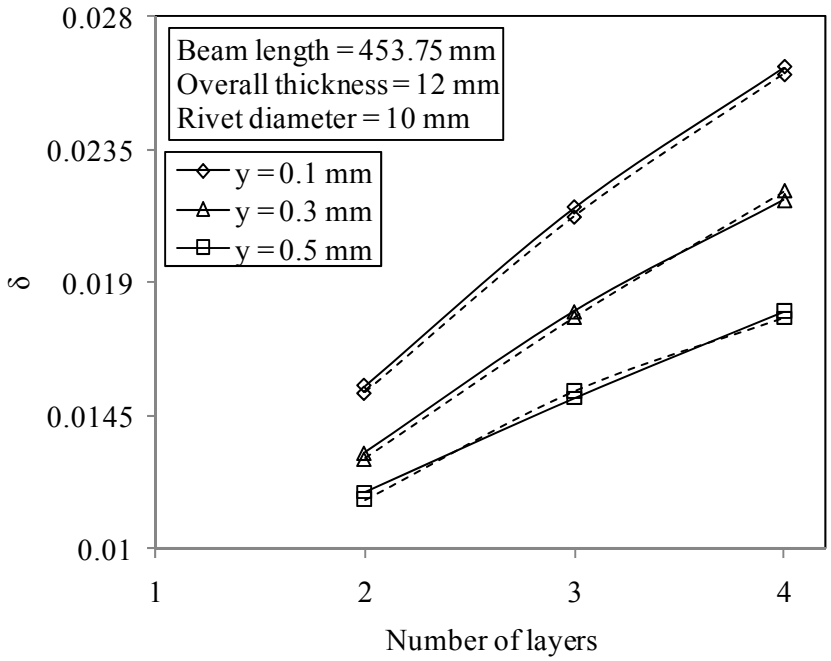

Fig. 5.74 Variation of logarithmic decrement with the number of layers for aluminium specimens with beam length 453.75 mm, overall thickness 12 mm and rivet diameter 10 mm at different amplitudes of excitation (y). The theoretical and experimental values are shown by solid and dashed lines, respectively

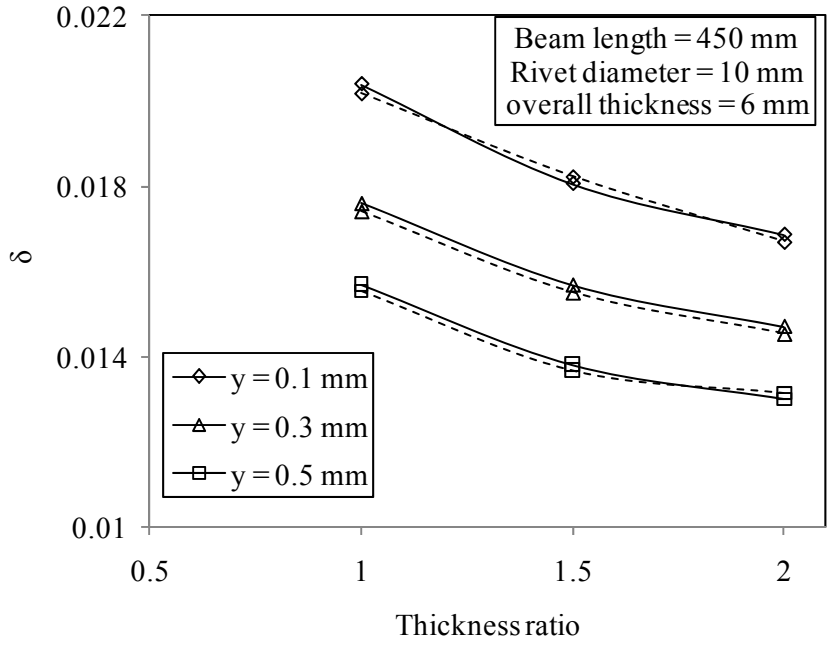

Fig. 5.75 Variation of logarithmic decrement with the thickness ratio for aluminium specimens with beam length 450 mm, overall thickness 6 mm and rivet diameter 10 mm at different amplitudes of excitation (y). The theoretical and experimental values are shown by solid and dashed lines, respectively

Some of the experimental observations using time history plots for the evaluation of logarithmic decrement have been presented in Figs. 5.76 and 5.77 as samples for mild steel and aluminium specimens, respectively. The time interval has been normalized for comparison with interval being 1 second. It is evident from these plots that the damping in jointed specimens increases with the use of more number of layers.

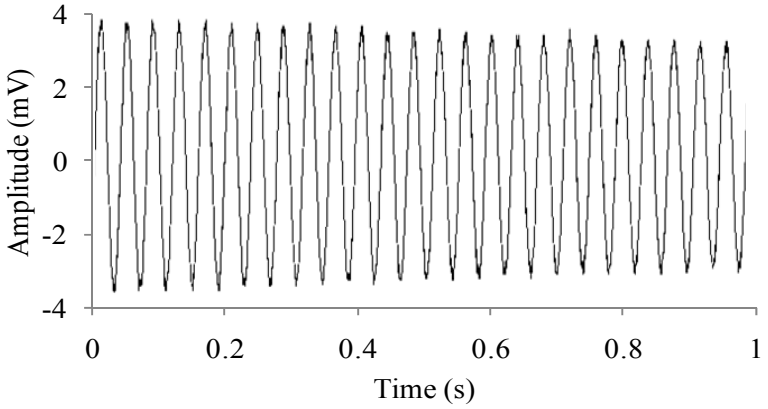

Two layered mild steel specimen (453.75x41.25x12 mm)

Amplitude of excitation = 0.1 mm, Rivet diameter = 10 mm, δ = 0.00659

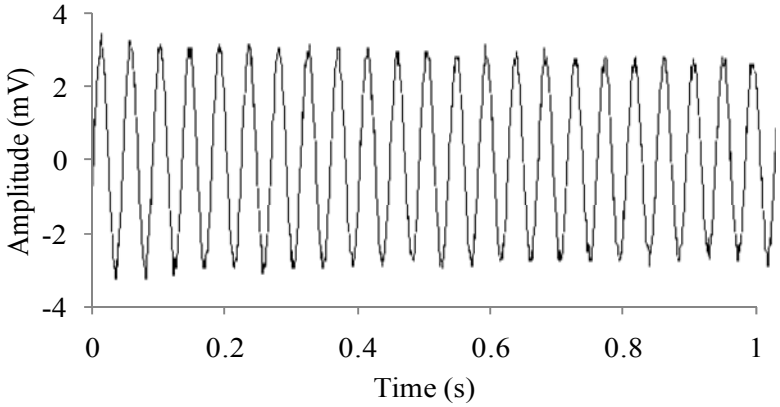

Three layered mild steel specimen (453.75x41.25x12 mm)

Amplitude of excitation = 0.1 mm, Rivet diameter = 10 mm, δ = 0.00813

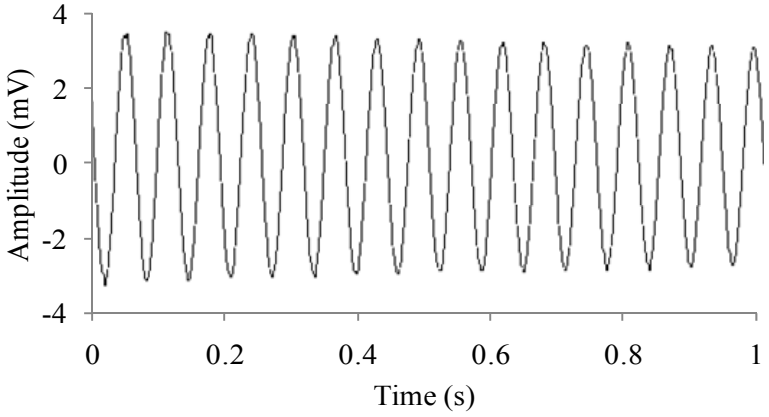

Four layered mild steel specimen (453.75x41.25x12 mm)

Amplitude of excitation = 0.1 mm, Rivet diameter = 10 mm, δ = 0.01081

Fig. 5.76 Time history curve of mild steel specimens under free vibration recorded by the digital storage oscilloscope

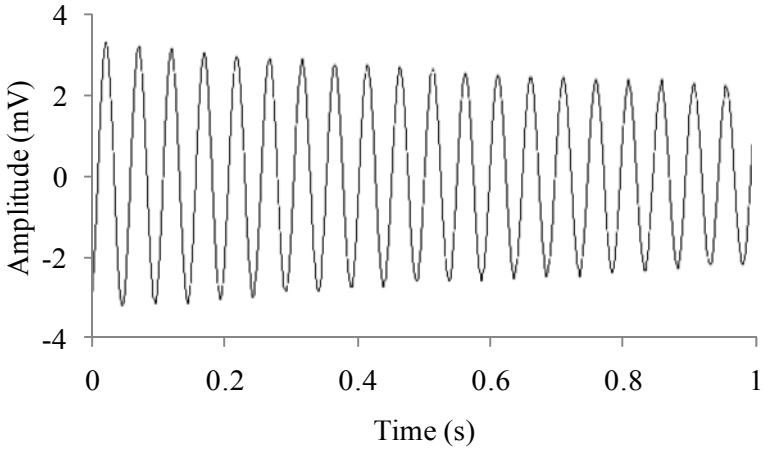

Two layered Aluminium specimen (453.75x41.25x12 mm)

Amplitude of excitation = 0.1 mm, Rivet diameter = 10 mm, δ = 0.01553

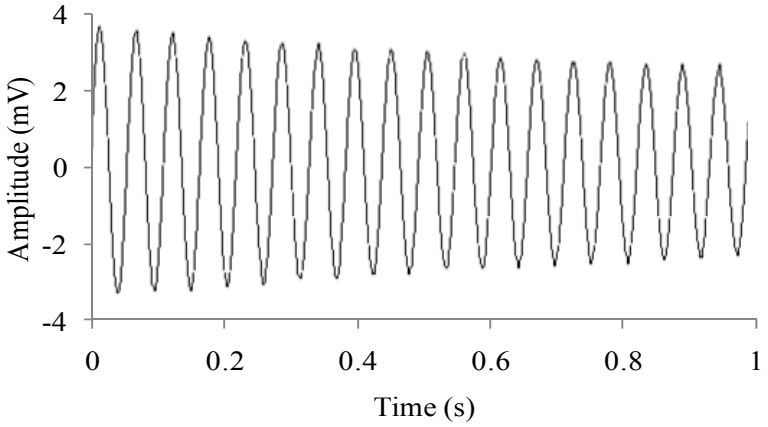

Three layered Aluminium specimen (453.75x41.25x12 mm)

Amplitude of excitation = 0.1 mm, Rivet diameter = 10 mm, δ = 0.02054

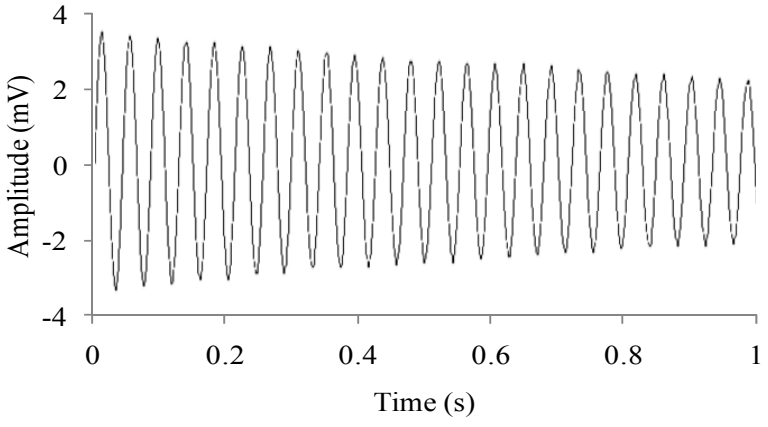

Four layered Aluminium specimen (453.75x41.25x12 mm)

Amplitude of excitation = 0.1 mm, Rivet diameter = 10 mm, δ = 0.02629

Fig. 5.77 Time history curve of Aluminium specimens under free vibration recorded by the digital storage oscilloscope

5.7 Chapter Summary

In this chapter, a number of free vibration tests have been conducted using specimens of different sizes prepared from the same stock of mild steel and aluminium commercial flats. The detailed instrumentation and necessary data for all the specimens have been presented through photographs and tables, respectively. As per the test procedure, the Young's modulus of elasticity and static bending stiffness are first found out by static deflection tests. These values are subsequently used for the theoretical evaluation of logarithmic decrement of all the specimens.

The logarithmic decrement technique, a time-response method, has been used for measuring the damping experimentally. In this method, the experimental logarithmic decrement is calculated from the time history curve of the decaying signals recorded on the screen of digital storage oscilloscope. In order to calculate the theoretical results for logarithmic decrement, the product $\alpha.\mu$ is first found out from the measured logarithmic decrement corresponding to 10 mm diameter connecting rivet. This product being the frequency and amplitude dependent, plots displaying its variation with the above two parameters have been shown in Figs. 5.10 to 5.15 for both mild steel and aluminium specimens with different thickness ratios. Then, the product $\alpha.\mu$ of a particular test specimen is found out from the corresponding plot of the above figures at specific frequency and initial excitation of vibration. This product is then utilized to evaluate the theoretical values of logarithmic decrement at different conditions of vibration. This chapter also deals with the comparison of experimental results with the corresponding theoretical ones in graphical forms for establishing the authenticity of the theory developed. It is estimated from the above comparison that the maximum variation of theoretical results through classical and finite element methods with the corresponding experimental values is 2.68 and 1.46% for mild steel and 3.62 and 2.54% for aluminium, respectively. As the results are in good agreement, the theory so developed is thus authenticated.

Further, in order to study the effects of surface roughness on the damping capacity, experiments have been conducted with a few layered and jointed beams made up of mild steel and aluminium. It is observed that the logarithmic decrement remains almost constant irrespective of roughness condition at the interfaces since the maximum deviation is found to be 0.2%.

CHAPTER 6

DISCUSSIONS

The last three chapters have elaborately discussed the theoretical analyses of the problem along with experiments. The theoretical part consists of both the classical and finite element methods for measuring the damping of the layered and jointed cantilever beams made up of mild steel and aluminium. In both the methods, the analyses assume the Euler-Bernoulli beam theory along with other assumptions as mentioned in the introduction chapter.

In the first method, an exact solution is presented considering the distributed-parameter model for the beam structure. The theoretical expression for the non-uniform pressure distribution within the influencing zone under each rivet has been found out for different beam thickness ratios from the numerical data of Minakuchi et al. [32]. This pressure distribution has been further utilized to estimate the normal and frictional forces at the interfaces, from which the expressions for product $\alpha.\mu$ for two layered beams and logarithmic decrement for two as well as multi-layered jointed beams have been formulated as given in Eq. (3.41) and (3.40), respectively.

In the second method, an approximate solution is obtained considering the beam model as a discrete system. In this method, a given beam is discretized into finite number of one-dimensional elements of equal length. Each element consists of two nodes with each node having two degrees of freedom, i.e. transverse displacement and rotation. The number of elements is taken as twice the number of rivets used in a particular specimen. It is found that no significant improvement in convergence is observed with further increase in the number of element thus establishing the optimality condition. The stiffness and mass matrices have been evaluated from the bending strain energy and kinetic energy of the beam, respectively and are further used to determine the natural frequency and mode shapes by modal analysis. Subsequently, the necessary formulations for the logarithmic decrement of two as well as multi-layered jointed beams have been developed as presented in Eq. (4.28) and (4.30), respectively. In the above derivation, the energy approach has been used to evaluate the damping in terms of logarithmic decrement. In this regard, the

expressions for dynamic slip, input strain energy and energy loss in a jointed beam have been formulated using the same stiffness matrix, shape function and displacement vector. The detailed procedure for evaluating the damping in a layered and jointed structure has been presented in Chapter 4.

Due to the assumptions made in the analyses, the theoretically computed results may be different from the actual ones. The experimental work is thus necessary for the verification of the theoretical results. For this purpose, a number of free vibration tests have been conducted using specimens of different sizes prepared from the same stock of mild steel and aluminium commercial flats. The detailed instrumentation and necessary data of all specimens have been presented through photographs and tables, respectively, in Chapter 5. The logarithmic decrement technique has been used for measuring the damping. It represents the rate at which the amplitude of a free damped vibration decreases and is calculated from the time history curve of decaying signals recorded on the screen of the digital storage oscilloscope. This method produces fairly good results when the structure is vibrated at small excitation level in the low and moderate frequency range.

The experimental results for logarithmic decrement have been compared with the corresponding numerical ones obtained in chapters 3 and 4 for establishing the authenticity of the theory developed. It is observed from the above comparison that the maximum variation of experimental results with the corresponding values from the classical and finite element methods is 2.68 and 1.46% for mild steel and 3.62 and 2.54% for aluminium specimens, respectively. This establishes the authenticity of the theory developed and the techniques used for evaluating the logarithmic decrement in mild steel and aluminium jointed specimens.

The damping action in jointed structures is influenced by the intensity of pressure distribution, micro-slip and kinematic coefficient of friction at the interfaces. All the above vital parameters are largely influenced by the thickness ratio of the beam and thereby affect the damping capacity of the structures. Both the theoretical and experimental results for different specimens with all the influencing parameters have been compared for authenticating the numerical analyses. The following observations have been made from the theoretical and experimental analyses in the process of investigation.

1. The exact nature of the interface pressure profile and its magnitude across a beam layer is necessary for the correct assessment of the damping capacity in jointed structures. This contact pressure between the surfaces is generated by the clamping action of the joints and plays a vital role in the joint properties. Although all previous analytical works have assumed a uniform pressure profile at the interfaces, but experiments have clearly shown that this is rarely the case, thereby suggesting a non-uniform pressure distribution. The theoretical expression for this non-uniform pressure distribution at the interfaces has been obtained by curve fitting the numerical data of Minakuchi et al. [32] and is given by a non-dimensional polynomial as presented in Eq. (3.29).

2. It is shown in the theory that there exists an influence zone under each connecting rivet that holds the members in contact. This zone is independent of the material of the connecting members but depends on the beam thickness ratio. As per Minakuchi et al. [32], this zone is a circle around the center of the connecting rivet with diameter equal to 4.125, 5.0 and 5.6 times the rivet diameter for beam thickness ratios of 1.0, 1.5 and 2.0, respectively. This observation has been presented in Fig. 3.7. It is shown that the pressure distribution inside this zone is parabolic in nature being maximum at the rivet hole and zero at the circumference of the influencing zone. Due to this uneven pressure distribution, a local relative motion termed as micro-slip occurs at the interfaces of the connecting members. The energy dissipation being a function of the dynamic slip and friction force as evident from Eq. (3.33) is greatly influenced by the interface pressure distribution at the contact surfaces around a connecting rivet.

3. The presence of friction in connecting joints has a strong impact on the system dynamics and largely contributes to the majority of the damping capacity of the system. The friction force in a joint arises from the shearing action between the parts and is governed by the preload on the rivet and friction coefficient. It is understood that the joint friction comes into play only when the contacting layers tend to move relatively under the action of transverse vibration and serves as a catalyst for energy dissipation. For most analyses, the Coulomb's friction law is widely used to represent the dry friction at the contacting surfaces.

4. The joints usually do not form a rigid connection and thus allow a relative motion at the interfaces of the connecting members. As the beam vibrates, it bends in the transverse direction. This beam bending causes the generation of shear stresses at the contact surfaces. When the limiting friction force is high, no slippage occurs immediately under the rivet and the damping due to joints is ignored. However, the slippage may occur quite readily away from the rivet where the clamping force is low. This slippage being of exceedingly small amount is termed as micro-slip and occurs only at the lower level of excitation. Since there is a decrease of the interface pressure with the distance away from the rivet, the magnitude of slip in regions away from the hole is larger than in regions close to the hole. This small relative displacement at the interfaces causes energy dissipation due to friction thereby contributing large amount of damping to the system. When the excitation level is increased, the macro-slip is developed due to which the entire jointed interface will slip as a whole. Usually, the macro-slip is avoided as it leads to structural damage of the joints.

5. The energy dissipation at the interfaces of jointed structures primarily depends upon the kinematic coefficient of friction (μ) and dynamic slip ratio (α). These two parameters being interdependent with each other exhibit complicated behavior under dynamic conditions. In view of the above facts, it is more appropriate to evaluate the product $\alpha.\mu$ as a single parameter from the experimental logarithmic decrement corresponding to 10 mm diameter rivet. Since this product is frequency and amplitude dependent, plots showing its variation with the above two parameters have been displayed in Figs. 5.10 to 5.15 for both mild steel and aluminium specimens. These plots have been further used for the theoretical evaluation of logarithmic decrements of layered and jointed beams with respect to other diameters and conditions of vibration. Moreover, the evaluation of the product $\alpha.\mu$ from the experimental result takes care of the effect of non-linearity, various modes of vibration, support, material and environmental damping effects in the results.

6. The average value of Young's modulus of elasticity (E) for both mild steel and aluminium specimens has been found out experimentally by conducting static deflection tests. These values are observed to be slightly less compared to their

standard values and are subsequently used in all the theoretical works. As the specimens used in all the experiments are from the same stock of commercial flats, the use of these average values of Young's modulus in the theoretical calculations is appropriate.

7. It is observed that the incorporation of joints in layered structures reduces the stiffness. It means the ratio of the stiffness of a jointed beam to that of an identical solid one is always less than one. This ratio has been calculated by carrying out the same static deflection tests as used in case of Young's modulus and is found to be decreased with the number of layers used in the jointed specimen. Few samples of the average values of the stiffness ratio for two and multi-layered mild steel and aluminium specimens are presented in Tables 5.6 to 5.9. This ratio shows how much reduction in the stiffness is produced due to the inclusion of joints and its exact assessment carries much significance in the theoretical evaluation of logarithmic decrement. It is estimated that the maximum decrease in the stiffness is approximately 15 and 13% for two layered mild steel and aluminium specimens, respectively, when compared with their equivalent solid ones. This observation is presented in Table 5.11. This stiffness decreases further by 18 and 20% for mild steel 15 and 19% for aluminium specimens with three and four layers, respectively, compared to their equivalent solid ones. It is further observed that the stiffness ratio for aluminium specimens is always more compared to that of similar mild steel ones because of the higher coefficient of interface friction for aluminium.

8. It is now a well known fact that the inclusion of joints in a fabricated structure not only damps the structure but also reduces the structural stiffness. This reduction in the stiffness brings about a slight decrease in the natural frequency. The same has been observed during experimentation by comparing the frequency between a jointed beam and an equivalent solid one. This difference in frequency is fairly close at lower modes of vibration. The maximum decrease in this frequency is found to be 7.4 and 8.1% for identical mild steel and aluminium specimens, respectively. Further, the variation in the frequency of vibration brings about a change in the product $\alpha.\mu$ as evident in Figs. 5.10 to 5.15 and hence the logarithmic decrement.

9. It is found from the experiments that the surface roughness at the jointed interfaces has no effect on the damping capacity of layered and jointed structures. In order to authenticate this, experiments are conducted with a few layered and jointed beams made up of mild steel and aluminium specimens with varying surface roughness. Usually, the kinematic coefficient of friction is more and dynamic slip ratio is less with the higher surface roughness at the interfaces and vice versa. However, it is interesting to observe that the product of the kinematic coefficient of friction and dynamic slip ratio is almost constant for any surface condition of a particular specimen at similar conditions of vibration since the maximum deviation for logarithmic decrement is found to be 0.2% as presented in Table 5.10. Hence, it is found that the logarithmic decrement remains constant irrespective of condition of roughness at the interfaces.

10. It is established that the pressure distribution varies depending on the thickness ratios. This fact is very clear from the use of different numerical values of the polynomial constants for different thickness ratios as presented in Table 3.1. It is also evident from Fig. 3.7 that the pressure distribution at the jointed interface increases with the lower thickness ratio and is maximum for thickness ratio of 1.0. Further, it may be mentioned that the distance between consecutive rivets is less in case of lower thickness ratio. These facts signify that the average pressure at the interfaces is always more in case of lower thickness ratio and the same decreases with the increase in thickness ratio. The above factors suggest that the normal force and hence the energy dissipation (damping) is more in case of lower thickness ratio. Therefore, greatest possible damping can be achieved in case of jointed structures using components of equal thickness.

11. In order to compare the damping capacity of a jointed beam with its equivalent solid one, experiments are conducted with two geometrically identical specimens. It is observed that the logarithmic decrement is always more in case of layered and jointed structures. It is estimated that the maximum increase in the logarithmic decrement is about 150 and 130% for two layered mild steel and aluminium specimens with thickness ratio 1.0, respectively, compared to its equivalent solid ones. The logarithmic decrement further increases by 26.53 and 38.42% for mild steel and 18.34 and 28.71% for aluminium structures with three and four layers

with thickness ratio 1.0, respectively, compared to similar specimens of two layered beams. This increase is due to the presence of more interface friction layers and reduction in the joint stiffness.

12. It is observed that the logarithmic decrement for aluminium specimens is always more compared to similar mild steel specimens. This is because the static bending stiffness for aluminium is always less in comparison to identical mild steel specimens resulting in the lower strain energy. Moreover, the energy loss due to friction at the interfaces of aluminium specimens is more than that of the equivalent mild steel ones because of higher kinematic coefficient of interface friction for aluminium. Thus, the net effect of the decrease in the input strain energy and increase in energy loss result in the higher logarithmic decrement for aluminium specimens compared to mild steel for similar conditions of beam dimension and vibration.

13. The friction, micro-slip, and surface roughness are many factors affecting the joint behavior and each factor will vary from joint to joint because of manufacturing tolerances. As a result, all the joints and jointed structures exhibit non-linear behavior. However, the assumption of linear vibration theory is justified when the beam is vibrated at lower amplitudes and modes of vibration.

14. The damping of jointed structures in the present work has been examined for the following variables: length of the specimen, amplitude of vibration, diameter of rivet, number of layers and beam thickness. The dependency of the damping on each of these variables is enumerated from the theoretical and experimental results in the following section:

    - The static bending stiffness decreases with an increase in the length of the specimen and thereby the strain energy introduced into the system is reduced as evident from Eq. (3.37). Since the longer specimens require more number of rivets, there will be an increase in the overall dynamic slip and hence more energy loss as evident from Eqs. (3.28) and (3.33), respectively. Moreover, the area of the interface undergoing micro-slip increases with the specimen length and also increases the energy dissipation. These facts establish that the

logarithmic decrement of a layered beam jointed with rivets increases with an increase in the cantilever length.

- The increase in the amplitude of vibration results in more input strain energy into the system as evident from the Eq. (3.37). Moreover, the product of the kinematic coefficient of friction and the dynamic slip ratio $(\alpha.\mu)$ increases with the amplitude of excitation as depicted in the Figs. 5.10 to 5.15 which will enhance the interface energy loss as seen from the Eq. (3.33). However, the combined effect of these is a net decrease in the logarithmic decrement with the higher amplitude of vibration. This is due to the introduction of more energy into the beam system compared to the interface dissipated energy. This fact suggests that the damping is amplitude dependent.

- The use of the rivets of greater diameter increases the preload on the rivets and thereby increases the normal force and the energy dissipation at the interfaces as seen from Eq. (3.33). Moreover, the increase in the diameter of the rivet is accompanied by an increase in the static bending stiffness which introduces more input energy into the system as evident from Eq. (3.37). But the energy dissipation due to interface friction occurs at a higher rate compared to the input energy and thereby the net effect is an increase in the logarithmic decrement.

- As discussed earlier, the thickness ratio of 1.0 yields maximum damping of jointed structures. This damping will further increase with the use of more number of layers with the same overall beam thickness due to more friction layers which produces higher energy loss at the interfaces. Moreover, the stiffness as well as strain energy is reduced with the increased number of layers, thereby increasing the logarithmic decrement. For example, the logarithmic decrement of a particular layered mild steel specimen increases approximately by 150, 246 and 308% whereas its stiffness decreases by 15.0, 17.7 and 20.5% for two, three and four layered beams, respectively, compared to that of an equivalent solid one. Similarly for aluminium, the increase in logarithmic decrement is found to be 130, 205 and 273% with decrease in stiffness by 13, 15 and 19% for two, three and four layered beams, respectively.

- The overall thickness of the beam influences the logarithmic decrement of the jointed structures. The larger beam thickness is accompanied by an increase in the static bending stiffness and also the input strain energy into the system. Moreover, the energy loss at the jointed interfaces increases with an increase in thickness as the product of "$\alpha.\mu$" increases due to higher natural frequency of vibration. But the input energy is increased at a higher rate compared to the energy loss resulting in a net decrease in the logarithmic decrement.

On the whole, it is established that the incorporation of joints in built-up structures produces adequate damping due to micro-slip along the frictional interfaces thereby compensating the low inherent damping of the structures. The effect of the various influencing parameters on the damping capacity of layered and jointed structures with connecting rivets have been discussed in detail in this chapter. Few salient observations on the damping capacity of layered and jointed riveted structures due to the variation of different influencing parameters have been presented in Tables 6.1 and 6.2 for mild steel and aluminium specimens, respectively.

Table 6.1 Effect of influencing parameters on the damping capacity with mild steel

Length x thickness x width (mm x mm x mm)	Influencing parameter	Variation of influencing parameter	Variation in logarithmic decrement
330x(3+3)x41.25 (with 0.1 mm amplitude)	Rivet diameter	Increases from 8 to 10 mm	Increases by 32.62%
330x(3+3)x41.25 (with 0.1 mm amplitude and 10 mm connecting rivet)	Beam length	Increases from 330 to 453.75 mm	Increases by 28.18%
330x(3+3)x41.25 (with 10 mm rivet diameter)	Amplitude of vibration	Increases from 0.1 to 0.5 mm	Decreases by 21.96%
330x6x41.25 (with 0.1 mm amplitude and 10 mm connecting rivet)	Beam thickness ratio	Increases from 1.0 to 2.0	Decreases by 19.04%
453.75x12x41.25 (with 10 mm rivet and 0.5 mm amplitude)	Number of layers	Two layers	Increase by 138.53% compared to equivalent solid one
		Three layers	Increases by 35.06% compared to that of two layers
		Four layers	Increases by 63.97% compared to that of two layers

Table 6.2 Effect of influencing parameters on the damping capacity with aluminium

Length x thickness x width (mm x mm x mm)	Influencing parameter	Variation of influencing parameter	Variation in logarithmic decrement
330x(3+3)x41.25 (with 0.1 mm amplitude)	Rivet diameter	Increases from 8 to 10 mm	Increases by 24.91%
330x(3+3)x41.25 (with 0.1 mm amplitude and 10 mm connecting rivet)	Beam length	Increases from 330 to 453.75 mm	Increases by 25.03%
330x(3+3)x41.25 (with 10 mm rivet diameter)	Amplitude of vibration	Increases from 0.1 to 0.5 mm	Decreases by 20.74%
330x6x41.25 (with 0.1 mm amplitude and 10 mm connecting rivet)	Beam thickness ratio	Increases from 1.0 to 2.0	Decreases by 17.86%
453.75x12x41.25 (with 10 mm rivet and 0.5 mm amplitude)	Number of layers	Two layers	Increase by 121.26% compared to equivalent solid one
		Three layers	Increases by 18.40% compared to that of two layers
		Four layers	Increases by 51.52% compared to that of two layers

CHAPTER 7

CONCLUSIONS AND SCOPE FOR FURTHER RESEARCH

The objectives of the present research work dealing with the damping estimation and its improvement in layered and jointed riveted structures have been outlined in chapter 1. Keeping these objectives in view, theoretical, numerical and experimental analyses have been carried out in chapters 3, 4 and 5, respectively. In-depth discussions of the theoretical and experimental results have been presented in chapter 6. This chapter summarizes some important conclusions drawn from the observations discussed in the previous chapter along with some suggestions for continuing future research in this field.

7.1 Conclusions

Extensive studies have been made to find out the effects of various influencing parameters on the damping capacity of layered and jointed structures. The damping of jointed structures in the present work has been examined for the following variables: intensity of pressure distribution, dynamic slip ratio, surface roughness and kinematic coefficient of friction at the interfaces, beam thickness ratio, length of the specimen, amplitude of vibration, diameter of rivet, number of layers and overall beam thickness. The effect of all these parameters on the damping capacity of layered and jointed riveted structures is enumerated from the theoretical and experimental results as detailed below.

1. Effect of interface pressure distribution:- The exact nature of the interface pressure profile and its magnitude across a beam layer is significant for the correct assessment of damping capacity in a structure jointed with rivets. It is established that the pressure distribution varies depending on the thickness ratios. This fact is evident from the use of different set polynomial constants for different thickness ratios as presented in Table 3.1. It is found from the theory that the interface pressure increases with the decrease in thickness ratio and is maximum for thickness ratio of 1.0 for which the average pressure at the interfaces is also more.

This signifies that the normal force and hence the energy dissipation (damping) is more in case of lower thickness ratio. Therefore, the greatest possible damping can be achieved in case of jointed structures using components of equal thickness.

2. Effect of dynamic slip ratio:- The dynamic slip ratio (α) plays an important role in estimating the damping of layered and jointed structures and is largely influenced by the surface texture of the joint interface. Therefore, it is more appropriate to consider the combined effect of both the dynamic slip ratio and coefficient of friction in the evaluation because of their interdependencies and complicated behavior under dynamic conditions as elaborated earlier. Indeed, the logarithmic decrement increases with increase in dynamic slip ratio as evident from Eq. (3.38).

3. Effect of surface roughness:- It is found from the experiments that the surface roughness at the jointed interfaces has no effect on the damping capacity of layered and jointed structures. In order to authenticate this, experiments are conducted with a few layered and jointed beams made up of mild steel and aluminium specimens with varying surface roughness. Usually, the kinematic coefficient of friction is more and dynamic slip ratio is less with the higher surface roughness at the interfaces and vice versa. However, it is interesting to observe that the product of the kinematic coefficient of friction and dynamic slip ratio is constant for any surface condition of a particular specimen under similar conditions of vibration. Hence, it is found that the logarithmic decrement remains constant irrespective of condition of roughness at the interfaces.

4. Effect of coefficient of friction:- The friction force in a joint arises from the shearing action between the parts and is governed by the preload on the rivet and friction coefficient. In the present work, the well-known Coulomb friction model has been used to quantify the friction force. It is established that the energy is dissipated through this frictional effects and is a function of both the micro-slip and friction at the interfaces. As discussed, both dynamic slip ratio *(α)* and coefficient of friction *(μ)* are interdependent and show complicated behavior under dynamic condition. In view of this, their product *($\alpha.\mu$)* is considered as a single parameter in the theory as evident from the fact that the energy dissipation is a function of the above product.

5. Effect of beam thickness ratio:- The energy dissipation mechanism at a joint is a complex phenomenon largely influenced by the interface pressure distribution which varies according to the relative thickness of the contacting members. It is quite evident from the theory that the magnitude of pressure profile increases with decrease in thickness ratio as illustrated in Fig. 3.7. This increase is accompanied by more average pressure which enhances the friction force and energy loss at the interfaces. Moreover, the energy introduced into the system is less owing to the decrease in stiffness because of reduced width of the beam in case of lower thickness ratio. The combined effect of these observations results in the increase of the logarithmic decrement with the lower thickness ratio. Therefore, the greatest possible damping can be achieved in case of jointed structures with lower thickness ratio, i.e., using components of equal thickness.

6. Effect of length of specimen:- There is a reduction in the static bending stiffness with an increase in the length of the specimen so that the strain energy introduced into the system is decreased. As the longer specimens accommodate more number of rivets, there will be an increase in the overall dynamic slip, thereby causing more energy loss as evident from Eqs. (3.28) and (3.33). Moreover, the energy dissipation is enhanced as the contact area of the interface undergoing micro-slip increases with the specimen length. The net effect of all these improves the damping with an increase in the cantilever length.

7. Effect of amplitude of vibration:- The increase in the amplitude of vibration results in more input strain energy to the system as per Eq. (3.37). However, the product of the kinematic coefficient of friction and dynamic slip ratio $(\alpha.\mu)$ increases with the amplitude of excitation as depicted in Figs. 5.10 to 5.15. This increase in the product $\alpha.\mu$ will produce an increase in the interface energy loss as evident from Eq. (3.33). It is found from the results that the energy loss occurs at a lower rate compared to the input strain energy as the amplitudes of excitation increases, thereby decreasing the logarithmic decrement.

8. Effect of diameter of rivet:- The use of rivets of larger diameter increases the preload on the rivets, thereby increasing the normal force and the energy loss at the interfaces as seen from Eq. (3.33). Moreover, the increase in the diameter of the rivet is accompanied by an increase in the static bending stiffness which introduces more input strain energy into the system as evident from Eq. (3.37).

But the energy dissipation due to interface friction occurs at a higher rate compared to the input energy, thereby causing a net increase in the logarithmic decrement.

9. Effect of number of layers:- As discussed earlier, the thickness ratio of 1.0 yields maximum damping of jointed structures. This damping will further increase with the use of more number of layers compared to the solid beam of same overall thickness due to more friction interfaces which produces higher energy loss at the interfaces. Moreover, the stiffness as well as strain energy is reduced with the increased number of layers, thereby increasing the logarithmic decrement.
10. Effect of overall beam thickness:- The overall thickness of the beam influences the logarithmic decrement of the jointed structures. The larger beam thickness is accompanied by an increase in the static bending stiffness and also the input strain energy into the system. Moreover, the energy loss at the jointed interfaces increases with an increase in thickness as the product of "$\alpha.\mu$" increases due to higher natural frequency of vibration. But the input energy is increased at a higher rate compared to the energy loss resulting in a net decrease in the logarithmic decrement.

Indeed, most damping effects encountered in real structures take place at the jointed interfaces of the connecting members. This chapter discusses the various influencing parameters affecting the damping capacity in layered and jointed structures. It is estimated from the present investigation that the maximum variation of experimental results with the corresponding values from the classical and finite element methods is 2.68 and 1.46% for mild steel and 3.62 and 2.54% for aluminium specimens, respectively. This establishes the authenticity of the theory developed and the techniques used for evaluating the logarithmic decrement in layered and jointed structures. It is found from the experimentally validated numerical results that the damping capacity of built-up structures with larger rivet diameter and specimen length having lower amplitude of vibration, thickness ratio and overall beam thickness can be improved substantially. For example, the approximate increase in the damping capacity with the above specified combinations is found to be 378.6 and 346.4% for mild steel and aluminium four layered jointed structures, respectively, compared to its equivalent solid specimens.

The main purpose of the structural design is to control the vibration of structures at a desirable level as per requirements. In fact, most monolithic structures possess low inherent damping thereby causing serious problems which will impair the function and life of structures leading to their ultimate failure. It is always desirable to keep the vibration level as low as possible by introducing damping so that the performance and useful life of structures are enhanced largely. Since many decades, it has been a biggest challenge to the practicing engineers and designers to limit this unwanted vibration in structures. In view of this, such structures must be properly designed to possess adequate damping so that the undesirable vibration levels will not build-up beyond a permitted limit. The sole contribution of the present investigation is intended in this direction only. The design concept evolved from this research work of using layered structures with riveted joints can be effectively utilized in trusses and frames, aircraft and aerospace structures, bridges, machine members, robots and many other applications where higher damping is required.

Finally, the knowledge of estimating and enhancing the damping capacity in fabricated structures jointed with rivets is very essential for the noise and vibration control engineers. The following important design guidelines have been derived from the present investigation for suppressing the undesirable effects of vibration and noise in beams with riveted joints.

- Increasing the number of layers of the cantilevers
- Increasing the diameter of the rivets
- Increasing the cantilever length
- Decreasing the thickness ratio of the beam with constant overall thickness
- Decreasing the thickness of the cantilever beam
- Decreasing the initial amplitude of excitation

7.2 Scope for Further Research

In the present investigation, the mechanism of damping and the various parameters affecting the damping capacity of layered and jointed riveted structures have been presented in detail to enable the engineers to design the structures depending upon their damping capacity in real applications. However, the present study can be extended for further research as enumerated below.

- Timoshenko beam theory can be used for analysis instead of Euler-Bernoulli beam theory.
- Higher modes of vibration can be included in the analysis.
- The problem can be studied considering the nonlinearity effects of slip, friction and joint properties.
- Frequency domain analysis can be employed.
- The analysis can be extended to other boundary conditions such as fixed-fixed, fixed-supported, supported-supported, etc.
- The analysis can be made for layered and jointed beams of dissimilar materials.

BIBLIOGRAPHY

1. Nashif, A.D., Jones, D.I.G. and Henderson, J.P., 1985, Vibration Damping, John Wiley and Sons, NY.

2. Chopra, A.K., 1995, Dynamics of Structures: Theory and Applications to Earthquake Engineering. Prentice Hall, Englewood Cliffs, NJ.

3. Chen, J.H., Hsieh, S.C. and Lee, A.C., 2005, The failure of threaded fasteners due to vibration, Proceedings of the IMechE, Part C: Journal of Mechanical Engineering Science, Vol. 219, No. 3, pp. 299-314.

4. Beards, C.F., 1986, The damping of structural vibration by controlled inter-facial slip in joints, ASME publication, 8 1-DET-86, pp. 1-5.

5. Ren, Y., 1988, Damping in structural joints, M.Sc. Thesis. Imperial College, London University.

6. Earles, S.W.E. and Mansoori, F.S., 1974, Frictional damping applied to a cantilever-beam structure: A theoretical and experimental response comparison, International Journal of Machine Tool Design and Research, Vol.14, No. 1, pp. 111-124.

7. Beards, C.F. and Imam, I.M.A., 1978, The damping of plate vibration by interfacial slip between layers, International Journal of Machine Tool Design and Research, Vol. 18, No. 3, pp. 131-137.

8. Beards, C.F. and Williams, J.L., 1977, The damping of structural vibration by rotational slip in joints, Journal of Sound and Vibration, Vo1. 53, No. 3, pp. 333-340.

9. Beards, C.F. 1975, Some effects of interface preparation on frictional damping in joints, International Journal Machine Tool Design and Research, Vol. 15, No. 1, pp. 77-83.

10. Menq, C.-H., Bielak, J. and Griffin, J.H., 1986, The influence of microslip on vibratory response, Part I: A new microslip model, Journal of Sound and Vibration, Vol. 107, No. 2, pp. 279-293.

11. Menq, C.H., Griffin, J.H. and Bielak J., 1986, The influence of microslip on vibratory response, Part II: A comparison with experimental results, Journal of Sound and Vibration, Vol. 107, No. 2, pp. 295-307.

12. Hansen, S.W. and Spies, R.D., 1997, Structural damping in laminated beams due to interfacial slip, Journal of Sound and Vibration, Vol. 204, No. 2, pp. 183-202.

13. Ungar, E.E., 1973, The status of engineering knowledge concerning the damping of built-up structures, Journal of Sound and Vibration, Vol. 26, No. 1, pp. 141-154.

14. Beards, C.F., 1992, Damping in structural joints, The Shock and Vibration Digest, Vol. 24, No. 7, pp. 3-7.

15. Ibrahim, R.A., 1994, Friction-induced vibration, chatter, squeal and chaos: Part II - Dynamics and modeling, ASME, Applied Mechanics Reviews, Vol. 47, No. 7, pp. 227-253.

16. Gaul, L. and Nitsche, R., 2000, Friction control for vibration suppression, Mechanical Systems and Signal Processing, Vol. 14, No. 2, pp. 139-150.

17. Gaul, L. and Nitsche, R., 2001, The role of friction in mechanical joints, ASME, Applied Mechanics Reviews, Vol. 54, No. 2, pp. 93-106.

18. Donnelly Jr., R.P. and Hinrichsen, R.L., 1988, The effect of energy dissipation due to friction at the joint of a simple beam structure, Mathematical and Computer Modelling, Vol. 11, pp. 1022-1027.

19. Asoor, A.A.A. and Pashaei, 2010, Experimentally study on the effects of type of joint on damping, World Applied Sciences Journal, Vol. 8, No. 5, pp. 608-613.

20. Nayfeh, A.H. and Pai, P.F., 2004, Linear and Nonlinear Structural Mechanics, John Wiley & Sons, New York.

21. Beards, C.F., 1996, Structural Vibration: Analysis and Damping, Butterworth-Heinemann, Oxford.

22. Timoshenko, S.P., 1921, On the correction for shear of the differential equation for transverse vibrations of prismatic bars, Philosophical Magazine, Vol. 41, pp. 744-746.

23. Timoshenko, S.P., 1922, On the transverse vibrations of bars of uniform cross-section, Philosophical Magazine and Journal of Science, Vol. 43, pp. 125—131.

24. Meirovitch, L., 1967, Analytical Methods in Vibrations, Macmillan, New York.

25. Bert, C.W., 1973, Material damping: An introductory review of mathematical models, measures and experimental techniques, Journal of Sound and Vibration, Vol. 29, No. 2, pp. 129–153.

26. Cremer, L., Heckl, M. and Petersson, B.A.T., 2005, Structure-Borne Sound: Structural vibrations and sound radiation at audio frequencies, Springer Berlin Heidelberg.

27. Clarence W. de Silva, 2007, Vibration Damping, Control, and Design, CRC Press, Taylor and Francis Group LLC, Boca Raton.

28. Masuko, M., Ito, Y. and Yoshida, K., 1973, Theoretical analysis for a damping ratio of a jointed cantibeam, Bulletin of JSME, Vol. 16, No. 99, pp. 1421-1432.

29. Nishiwaki, N., Masuko, M., Ito, Y. and Okumura, I., 1978, A study on damping capacity of a jointed cantilever beam, 1st Report: Experimental results, Bulletin of JSME, Vol. 21, No. 153, pp. 524-531.

30. Nishiwaki, N., Masuko, M., Ito, Y. and Okumura, I., 1980, A study on damping capacity of a jointed cantilever beam, 2nd Report: Comparison between theoretical and experimental values, Bulletin of JSME, Vol. 23, No. 177, pp. 469-475.

31. Nanda, B.K. and Behera, A.K., 1999, Study of damping in layered and jointed structures with uniform pressure distribution at the interfaces, Journal of Sound and Vibration, Vol. 226, No. 4, pp.607-624.

32. Minakuchi, Y., Koizumi, T. and Shibuya, T., 1985, Contact pressure measurement by means of ultrasonic waves using angle probes, Bulletin of JSME, Vol. 28, No. 243, pp. 1859-1863.

33. Kelly, S.G., 2000, Fundamentals of Mechanical Vibrations, McGraw-Hill International Editions, Singapore.

34. Ferri, A.A. and Heck, B.S., 1992, Analytical investigation of damping enhancement using active and passive structural joints, Journal of Guidance, Control and Dynamics, Vol. 15, No. 5, pp. 1258-1264.

35. Grandhi, R.V., 1990, Optimum design of space structures with active and passive damping, Engineering with Computers, Vol. 6, No. 3, pp. 177-183.

36. Park, Jin-Tack and Choi, Nak-Sam, 2004, Flexural vibration analysis of a sandwich beam specimen with a partially inserted viscoelastic layer, KSME Journal of Mechanical Science and Technology, Vol. 18 No. 3, pp. 347-356

37. Lazan, B.J., 1968, Damping of Materials and Members in Structural Mechanics, London, Pergamon Press.

38. Clarence W. de Silva, 2000, Vibration: Fundamentals and Practice, CRC Press LLC, Boca Raton.

39. Waterhouse, R.B., 1981, Fretting Fatigue, Applied Science Publishers, Essex, England.

40. Meirovitch, L., 2001, Fundamentals of Vibrations, Mc-Graw Hill International Editions, Mechanical Engineering Series, Singapore.

41. Thorby, D., 2008, Structural Dynamics and Vibration in Practice, Butterworth-Heinemann Publication, First Edition, Oxford, UK.

42. Ranky, M.F. and Clarkson, B.L., 1983, Frequency average loss factors of plates and shells, Journal of Sound and Vibration, Vol. 89, No.3, pp. 309-323.

43. Bies, D.A. and Hamid, S., 1980, In situ determination of loss and coupling loss factors by the power injection method, Journal of Sound and Vibration, Vol. 70, No. 2, pp. 187-204.

44. Lee, G.F. and Hartmann, B., 1998, Specific damping capacity for arbitrary loss angle, Journal of Sound and Vibration, Vol. 211, No. 2, pp. 265-272.

45. Inman, D.J., 1994, Engineering Vibration, Prentice Hall, Englewood Cliffs.

46. Sun, C.T. and Lu, Y.P., 1995, Vibration Damping of Structural Elements, Prentice Hall PTR, Englewood Cliffs, New Jersey.

47. Ross, D., Ungar, E.E. and Kerwin, E.M. Jr., 1959, Damping of plate flexural vibrations by means of viscoelastic laminate, ASME Colloquium on Structural Damping, pp. 49-87.

48. Pearce, B.K. and Baumgarten, J.R., 1971, The damping effects of viscoelastic materials, Part 2: Transverse vibration of plates with viscoelastic coatings. Transactions of ASME, Journal of Engineering for Industry, Vol. 93, pp. 645-655.

49. Reddy, C.V.R. and Narayanan, S., 1980, Response of plates with unconstrained layer damping treatment to random acoustic excitation, Part I: Damping and frequency evaluations, Journal of Sound and Vibration, Vol. 69, No. 1, pp. 35-43.

50. Parthasarathy, G., Reddy, C.V.R. and Ganesan, N., 1985, Partial coverage of rectangular plates by unconstrained layer damping treatments, Journal of Sound and Vibration, Vol. 102, No. 2, pp. 203-216.

51. Kerwin Jr., E.M., 1959, Damping of flexural waves by a constrained viscoelastic layer, Journal of the Acoustical Society of America, Vol. 31, pp. 952–962.

52. Di Taranto, R.A., 1965, Theory of vibratory bending for elastic and viscoelastic layered finite-length beams, ASME, Journal of Applied Mechanics, Vol. 32, pp.881–886.

53. Douglas, B.E. and Yang, J.C.S., 1978, Transverse compressional damping in the vibratory response of elastic–viscoelastic–elastic beams, AIAA Journal, Vol. 16, pp. 925–930.

54. Douglas, B.E., 1986, Compressional damping in three-layer beams incorporating nearly incompressible viscoelastic cores, Journal of Sound and Vibration, Vol. 104, No. 2, pp. 343–347.

55. Sylwan, O., 1987, Shear and compressional damping effects of constrained layered beams, Journal of Sound and Vibration, Vol. 118, No. 1, pp. 35–45.

56. Lee, B.C. and Kim, K.J., 1995, Consideration of both extensional and shear strain of core material in modal property estimation of sandwich plates, ASME Design Engineering Technical Conferences 3, pp. 701–708.

57. Mead, D.J. and Markus, S., 1969, The forced vibration of a three-layer, damped sandwich beam with arbitrary boundary conditions, Journal of Sound and Vibration, Vol. 10, No. 2, pp. 163–175.

58. Mead, D.J. and Markus, S., 1970, Loss factors and resonant frequencies of encastre damped sandwich beams, Journal of Sound and Vibration, Vol. 12, No. 1, pp. 99–112.

59. Mead, D.J., 1982, A comparison of some equations for the flexural vibration of damped sandwich beams, Journal of Sound and Vibration, Vol. 83, No. 3, pp. 363–377.

60. Mallik, A.K. and Ghosh, A., 1973, Improvement of damping characteristics of structural members with high damping elastic inserts, Journal of Sound and Vibration, Vol. 27, No. 1, pp. 25-36,

61. Mallik, A.K. and Ghosh, A., 1970, Improvement of damping capacity with introduced stress concentration, Indian Journal of Technology, Vol. 8, pp. 113-119.

62. Mallik, A.K. and Ghosh, A., 1971, Improvement of dynamic rigidity of structural members with introduced stress concentration, Journal of Technology, Vol. 13, pp. 19-26.

63. Rahmathullah, R. and Mallik, A.K., 1979, Damping of cantilever strips with inserts, Journal of Sound and Vibration, Vol. 66, No. 1, pp. 109-117.

64. Sextro, W., 2002, Dynamical contact problems with friction: Models, methods, experiments and applications, Lecture notes in Applied Mechanics, Vol. 3, Series editor, Pfeiffer, F., Springer.

65. Beards, C.F., 1982, Damping in structural joints, The Shock and Vibration Digest, Vol. 14, pp. 9–11.

66. Murty, A.S.R. and Padmanabhan, K.K., 1982, Effect of surface topography on damping in machine joints, Precision Engineering, Vol. 4, pp. 185-190.

67. Goodman, L.E., 1959, A review of progress in analysis of interfacial slip damping, Edited by Ruzicka, J.E., Structural Damping, New York, ASME, pp. 35–48.

68. Yoshimura, M., 1977, Measurement of dynamic rigidity and damping property for simplified joint models and simulation by computer, Annals of the CIRP, Vol. 25, No. 1, pp. 193-198.

69. Tsutsumi, M. and Ito, Y., 1979, Damping mechanism of a bolted joint in machine tools, Proceedings of the 20th International Machine Tool Design and Research Conference, Birmingham, U.K., pp. 443-448.

70. Padmanabhan, K.K. and Murty, A.S.R., 1991, Damping in structural joints subjected to tangential loads, Journal of the Structural Division, Proceedings of Institute of mechanical Engineers, Vol. 205, pp. 121–129.

71. Lenz, J. and Gaul, L., 1995, The influence of micro-slip on the dynamic behavior of bolted joints, 13th International Modal Analysis Conference, Nashville, Vol. 3, pp. 248-254.

72. Cochardt, A.W., 1954, A method for determining the internal damping of machine members, ASME, Journal of Applied Mechanics, Vol. 76, No. 9, pp. 257-262.

73. Goodman, L.E. and Klumpp, J.H., 1956, Analysis of slip damping with reference to turbine-blade vibration, ASME, Journal of Applied Mechanics, Vol. 23, pp. 421–429.

74. Groper, M., June 1985, Microslip and macroslip in bolted joints, Experimental Mechanics, pp. 171-174.

75. Hartwigsen, C.J., Song, Y., Mcfarland, D.M., Bergman, L.A. and Vakakis, A.F., 2004, Experimental study of non-linear effects in a typical shear lap joint configuration, Journal of Sound and Vibration, Vol. 277, No. 1-2, pp. 327-351.

76. Pratt, J.D. and Pardoen, G., 2002, Numerical modeling of bolted lap joint behavior, Journal of Aerospace Engineering, Vol. 15, No. 1, pp. 20-31.

77. Feeny, B., Guran, A., Hinrichs, N. and Popp, K., 1998, A historical review on dry friction and stick-slip phenomena, ASME, Applied Mechanics Reviews, Vol. 51, No. 5, pp. 321-341.

78. Williams, E.J. and Earles, S.W.E., 1974, Optimization of the response of frictionally damped beam type structures with reference to gas turbine compressor blading, ASME, Journal of Engineering for Industry, Vol. 96, pp. 471-476.

79. Beards, C.F. and Robb, D.A., July 1980, The use of frictional damping to control the vibration of the plates in structure, International Conference on Recent Advances in Structural Dynamics, Southampton, England, pp. 749-760.

80. Dowell, E.H. and Schwartz, H.B., 1983, Forced response of a cantilever beam with a dry friction damper attached, Part I: Theory, Journal of Sound and Vibration, Vol. 91, No. 2, pp. 255-267.

81. Dowell, E.H. and Schwartz, H.B., 1983, Forced response of a cantilever beam with a dry friction damper attached, Part II: Experiment, Journal of Sound and Vibration, Vol. 91, No. 2, pp. 269-291.

82. Beards, C.F. and Woodwat, A., 1985, The control of frame vibration by friction damping in joints, ASME, Journal of Vibration, Acoustics, Stress Analysis, Reliability and Design, Vol. 107, pp. 27–32.

83. Menq, C.H. and Griffin, J.H., 1985, A comparison of transient and steady state finite element analyses of the forced response of a frictionally damped beam, ASME, Journal of Vibration, Acoustics, Stress and Reliability in Design, Vol. 107, pp. 19–25.

84. Chen, S. and Sinha, A., 1990, Probabilistic method to compute the optimal slip load for a mistuned bladed disk assembly with friction dampers, ASME, Journal of Vibration and Acoustics, Vol. 112, No. 2, pp. 214–221.

85. Wang, J.H. and Chen, W.K., 1993, Investigation of the vibration of a blade with friction damper by HBM, ASME, Journal of Engineering for Gas Turbines and Power, Vol. 115, No. 2, pp. 294–299.

86. Sanliturk, K.Y., Ewins, D.J., Elliott, R. and Green, J.S., 2001, Friction damper optimization: Simulation of rainbow tests, ASME, Journal of Engineering for Gas Turbines and Power, Vol. 123, No. 4, pp. 930–939.

87. Cigeroglu, E., 2002, Nonlinear vibration analysis of bladed disks with dry friction dampers, MS Thesis, Middle East Technical University, Ankara.

88. Cigeroglu, E., Lu, W. and Menq, C.H., 2006, One-dimensional dynamic microslip friction model, Journal of Sound and Vibration, Vol. 292, pp. 881-898.

89. Lu, W., 2001, Modeling of microslip friction and design of frictionally constrained turbine blade systems, PhD Thesis, The Ohio State University.

90. Csaba, G., 1998, Forced response analysis in time and frequency domains of a tuned bladed disk with friction dampers, Journal of Sound and Vibration, Vol. 214, No. 3, pp. 395–412.

91. Sanliturk, K.Y., Imregun, M. and Ewins, D.J., 1997, Harmonic balance vibration analysis of turbine blades with friction dampers, ASME, Journal of Vibration and Acoustics, Vol. 119, No. 1, pp. 96–103.

92. Olofsson, U. and Hagman, L., 1997, A model for micro-slip between flat surfaces based on deformation of ellipsoidal elastic bodies, Tribology International, Vol. 30, No. 8, pp. 599-603.

93. Ying, R., 1992, The analysis and identification of friction joint parameters in the dynamic response of structures, Ph.D. Thesis, Imperial College, University of London, UK.

94. Thomson, W.T., 1993, Theory of Vibration with Applications, 2nd Edition, George Allen and Unwin, London.

95. Den Hartog, J.P., 1931, Forced vibrations with combined coulomb and viscous friction, Transactions of the ASME, Vol. 53, No. 9, pp. 107-115.

96. Liang, J.W. and Feeny, B.F., 1998, Identifying Coulomb and viscous friction from free-vibration decrements, Nonlinear Dynamics, Vol. 16, No. 4, pp. 337-347.

97. Ibrahim, R. A., 1994, Friction-induced vibration, chatter, squeal and chaos: Part I – Mechanics of contact and friction, ASME, Applied Mechanics Reviews, Vol. 47, No. 7, pp. 209-226.

98. Awrejcewicz, J., and Olejnik, P., 2007, Occurrence of stick-slip phenomenon, Journal of Theoretical and Applied Mechanics, Vol. 45, No. 1, pp. 33-40.

99. Motosh, N., 1975, Stress distribution in joints of bolted or riveted connections, ASME, Journal of Engineering for Industry, Vol. 97, No. 1, pp. 157-161.

100. Pian, T.H.H., 1957, Structural damping of a simple built-up beam with riveted joints in bending, ASME, Journal of Applied Mechanics, Vol. 24, pp. 35–38.

101. Sidorov, O.T., 1983, Change of the damping of vibrations in the course of operation in dependence on the parameters of bolted joints, Strength of Materials, Vol. 14, pp. 671–674.

102. El-Zahry, R.M., 1985, Investigation of the vibration behavior of pre-loaded bolted joints, Dirasat-Engineering Technology, Vol. 12, pp. 201–223.

103. Marshall, M.B., Lewis, R. and Dwyer-Joyce, R.S., 2006, Characterization of contact pressure distribution in bolted joints, Strain, Vol. 42, No. 1, pp. 31-43.

104. Kaboyashi, T. and Matsubayashi, T., 1986, Consideration on the improvement of the stiffness of bolted joints in machine tools, Bulletin of JSME, Vol. 29, pp. 3934–3937.

105. Tsai, J.S. and Chou, Y.F., 1988, Modelling of dynamic characteristics of two-bolted joints, Journal of Chinese Institute of Engineering, Vol. 11, pp. 235–245.

106. Shin, Y.S., Iverson, J.C. and Kim, K.S., 1991, Experimental studies on damping characteristics of bolted joints for plates and shells, ASME, Journal of Pressure Vessel Technology, Vol. 113, No. 3, pp. 402–408.

107. Gould, H.H. and Mikic, B.B., 1972, Areas of contact and pressure distribution in bolted joints, ASME, Journal of Engineering for Industry, Vol. 94, No. 3, pp. 864–870.

108. Ziada, H.H. and Abd, A.K., 1980, Load pressure distribution and contact areas in bolted joints, Institute of Engineers (India), Vol. 61, pp. 93–100.

109. Hisakado, T. and Tsukizoe, T., 1978, Measurent of the interface pressure distribution of flat metallic joints, Wear, Vol. 48, No. 1, pp. 209-212.

110. Damisa, O., Olunloyo, V.O.S., Osheku, C.A. and Oyediran, A.A., 2007, Static analysis of slip damping with clamped laminated beams, European Journal of Scientific Research, Vol. 17, No. 4, pp. 455-476.

111. Damisa, O., Olunloyo, V.O.S., Osheku, C.A. and Oyediran, A.A., 2008, Dynamic analysis of slip damping in clamped layered beams with non-uniform pressure distribution at the interface, Journal of Sound and Vibration, Vol. 309, No. 3-5, pp. 349-374.

112. Olunloyo, V.O.S., Damisa, O., Osheku, C.A. and Oyediran, A.A. 2007, Further results on static analysis of slip damping with clamped laminated beams, European Journal of Scientific Research, Vol. 17, No. 4, pp. 491-508.

113. Minakuchi, Y., Yoshimine, K., Koizumi, T. and Hagiwara, T., 1985, Contact pressure measurement by means of ultrasonic waves: On a method of quantitative measurement, Bulletin of JSME, Vol. 28, No. 235, pp. 40-45.

114. Minakuchi, Y., 1985, Contact pressure measurement by means of ultrasonic waves: On a bolted joint with a solid-metal flat gasket, Bulletin of JSME, Vol. 28, No. 239, pp. 792-798.

115. Earles, S.W.E., 1966, Theoretical estimation of the frictional energy dissipation in a simple lap joint, IMechE, Part C: Journal of Mechanical Engineering Science, Vol. 8, No. 2, pp. 207–214.

116. Masuko, M., Ito, Y. and Koizumi, T., 1974, Horizontal stiffness and micro-slip on a bolted joint subjected to repeated tangential static loads, Bulletin of JSME, Vol. 17, No. 113, pp. 1494-1501.

117. Richardson, R.S.H. and Nolle, H., 1977, Energy dissipation in rotary structural joints, Journal of Sound and Vibration, Vol. 54, No. 4, pp. 577–588.

118. Jezequel, L., 1983, Structural damping by slip in joints, ASME, Journal of Vibration, Acoustics Stress, Reliability and Design, Vol. 105, No. 2, pp. 497–504.

119. Hanks, B.R. and Stephens, D.G., 1967, Mechanisms and scaling of damping in a practical structural joint, Shock and Vibration Bulletin, Vol. 36, pp. 1–8.

120. Brown, C.B., 1968, Factors affecting the damping in a lap joint, ASCE, Journal of Structural Division, Vol. 94, pp. 1197–1217.

121. Beards, C.F., 1983, The damping of structural vibration by controlled interface slip in joints, ASME, Journal of Vibration, Acoustics, Stress and Reliability and in Design, Vol. 105, No. 3, pp. 369–373.

122. Hertz, T.J. and Crawley, E.F., 1985, Displacement dependent friction in space structure joints, AIAA Journal, Vol. 24, pp. 1998–2000.

123. Ferri, A.A., 1988, Modeling and analysis of nonlinear sleeve joints of large space structures, AIAA Journal of Spacecraft and Rockets, Vol. 25, No. 5, pp. 354–360.

124. Ferri, A.A. and Bindemann, A.C., 1992, Damping and vibration of beams with various types of frictional support conditions, ASME, Journal of Vibration and Acoustics, Vol. 114, No. 3, pp. 289–296.

125. Folkman, S.L. and Redd, F.J., 1990, Gravity effects on damping of a space structure with pinned joints, AIAA Journal of Guidance and Control Dynamics, Vol. 13, No. 2, pp. 228–233.

126. Folkman, S.L., Roswell, E.A. and Ferney, G.D., 1995, Influence of pinned joints on damping and dynamic behavior of a truss, AIAA Journal of Guidance and Control Dynamics, Vol. 18, No. 6, pp. 1398–1403.

127. Beards, C.F., 1985, Damping in structural joints, Shock and Vibration Digest, Vol. 17, No. 11, pp. 17–20.

128. Beards, C.F., 1989, Damping in structural joints, Shock and Vibration Digest, Vol. 21, No. 4, pp. 3–5.

129. Gregory, D.L., Smallwood, D.O., Coleman, R.G. and Nusser, M.A., 1999, Experimental studies to investigate damping in frictional shear joints, Proceedings of the 70th Shock and Vibration Symposium, NM.

130. Smallwood, D.O., Gregory, D.L. and Coleman, R.G., 2000, Damping investigations of a simplified frictional shear joint, Proceedings of the 71st Shock and Vibration Symposium, Alexandria, Virginia.

131. Heller, L., Foltete, E. and Piranda, J., 2009, Experimental identification of nonlinear dynamic properties of built-up structures, Journal of Sound and Vibration, Vol. 327, No. 1-2, pp. 183-196.

132. Walker, S.J.I., Aglietti, G.S. and Cunningham, P., 2009, A study of joint damping in metal plates, Acta Astronautica, Vol. 65, No. 1-2, pp. 184-191.

133. Ferri, A.A., 1995, Friction damping and isolation systems, ASME, Journal of vibration and acoustics, Vol. 117, pp. 196-206.

134. Ibrahim, R.A. and Pettit, C.L., 2005, Uncertainties and dynamic problems of bolted joints and other fasteners, Journal of Sound and Vibration, Vol. 279, No. 3-5, pp. 857-936.

135. Gaul, L. and Lenz, J., 1997, Nonlinear dynamics of structures assembled by bolted joints, Acta Mechanica, Vol. 125, No. 1-4, pp. 169-181.

136. Song, Y., Hartwigsen, C.J., McFarland, D.M., Vakakis, A.F. and Bergman, L.A., 2004, Simulation of dynamics of beam structures with bolted joints using adjusted Iwan beam elements, Journal of Sound and Vibration, Vol. 273, No. 1-2, pp. 249-276.

137. Miller, J.D. and Quinn, D.D., 2009, A two-sided interface model for dissipation in structural systems with frictional joints, Journal of Sound and Vibration, Vol. 321, No. 1-2, pp. 201-219.

138. Khattak, A.R., Garvey, S. and Popov, A., 2010, Proper orthogonal decomposition of the dynamics in bolted joints, Journal of Sound and Vibration, Vol. 329, No. 9, pp. 1480-1498.

139. Olunloyo, V.O.S., Osheku, C.A. and Damisa, O., 2008, Vibration damping in structures with layered viscoelastic beam-plate, ASME, Journal of Vibration and Acoustics, Vol. 130, No. 6, pp. 061002-(1-26).

140. Wang, J.H. and Chuang, S.C., 2004, Reducing errors in the identification of structural joint parameters using error functions, Journal of Sound and Vibration, Vol. 273, No. 1-2, pp. 295-316.

141. Tsai, J.S. and Chou, Y.F., 1988, The identification of dynamic characteristics of a single bolt joint, Journal of Sound and Vibration, Vol. 125, No. 3, pp. 487-502.

142. Yin, H.P., Duhamel, D. and Argoul, P., 2004, Natural frequencies and damping estimation using wavelet transform of a frequency response function, Journal of Sound and Vibration, Vol. 271, No. 3-5, pp. 999-1014.

143. Hwang, H.Y., 1998, Identification techniques of structure connection parameters using frequency response functions, Journal of Sound and Vibration, Vol. 212, No. 3, pp. 469-479.

144. Ahmadian, H. and Jalali, H., 2007, Identification of bolted lap joints parameters in assembled structures, Mechanical Systems and Signal Processing, Vol. 21, No. 2, pp. 1041-1050.

145. Sainsbury, M.G. and Zhang, Q.J., 1999, The Galerkin element method applied to the vibration of damped sandwich beams, Computers and Structures, Vol. 71, No. 3, pp. 239-256.

146. Lee, S.Y., Ko, K.H. and Lee, J.M., 2000, Analysis of dynamic characteristics of structural joints using stiffness influence coefficients, KSME International Journal, Vol. 14, No. 12, pp. 1319-1327.

147. Chen, W. and Deng, X., 2005, Structural damping caused by micro-slip along frictional interfaces, International Journal of Mechanical Sciences, Vol. 47, No. 8, pp. 1191-1211.

148. Oldfield, M., Ouyang, H. and Mottershead, J.E., 2005, Simplified models of bolted joints under harmonic loading, Computers and Structures, Vol. 84, No. 1-2, pp. 25-33.

149. Pian, T.H.H. and Hallowell, F.C., 1950, Investigation of structural damping in simple built-up beams, Technical Report, Aeroelastic and Structures Laboratory, Massachusetts Institute of Technology, Cambridge, Mass.

150. Nanda, B.K., 2006, Study of the effect of bolt diameter and washer on damping in layered and jointed structures, Journal of Sound and Vibration, Vol. 290, No. 3-5, pp. 1290-1314.

151. Shigley, J.E., Mischke, R. and Brown Jr., T.H., 2004, Standard Handbook of Machine Design, 3rd edition, Mc-Graw Hill Book Company, pp. 24.6.

152. Maitra, G. M., and Prasad, L. V., 1995, Handbook of Mechanical Design, 2nd edition, Tata Mc-Graw Hill Publication, pp. 5.79-5.80.

153. Clough, R.W. and Penzien, J., 2003, Dynamics of Structures, 3rd edition, Computers and Structures, Inc., Berkeley, USA.

Curriculum Vitae

Name:	RAMESH CHANDRA MOHANTY
E-mail:	mohanty29@gmail.com
Date of birth:	12th March 1967
Nationality:	Indian
Permanent Address:	At: Sanakusumi, Po: Chandeswar, Dist: Khurda PIN: 752023 (Orissa), India

Education: Bachelor Degree in Mechanical Engineering,
Institution of Engineers (India), 1992

M. Tech., Biju Pattanaik University of Technology,
Rourkela, Orissa, India, 2005

Publications

1. Mohanty, R.C. and Nanda, B.K., 2009, Damping in layered and jointed riveted structures with equal thickness, Journal of Mechanical Engineering Science, Part C, IMechE, Vol. 223, No. C2, pp. 319-328.
2. Mohanty, R.C. and Nanda, B.K., 2010, Effect of micro-slip on the damping capacity of jointed riveted structures with unequal thickness, Journal of Vibration and Control. (**In Press**)
3. Mohanty, R.C. and Nanda, B.K., 2010, Investigation into the dynamics of layered and jointed cantilevered beams, Journal of Mechanical Engineering Science, Part C, IMechE, Vol. 224. (**In Press)**
4. Mohanty, R.C. and Nanda, B.K., Damping in layered and riveted structures, Proceedings of the International Conference on Frontiers in Design and Manufacturing Engineering (ICDM ’08), February 1-2, 2008, Coimbatore, India.
5. Mohanty, R.C. and Nanda, B.K., Damping in jointed riveted structural members of unequal thickness, Proceedings of the International Conference on Advances in Mechanical Engineering (ICAME ’08), December 15-17, 2008, Surat, India.

6. Mohanty, R.C. and Nanda, B.K., Damping analysis in built-in structures assembled by riveted joints, Proceedings of the International Conference on Emerging Research and Advances in Mechanical Engineering (ERA'09), March 19-21, 2009, Chennai, India.
7. Mohanty, R.C. and Nanda, B.K., Finite element analysis of transverse vibration of a jointed beam, Proceedings of the International Conference on Advances in Mechanical Engineering (ICAME '09), August 3-5, 2009, Surat, India.
8. Mohanty, R.C. and Nanda, B.K., Damping capacity of riveted structures with unequal thickness, Proceedings of the National Conference on Mechanism Science and Technologies: From Theory to Applications (NCMSTA '08), November 13-14, 2008, Hamirpur, India.

Papers Communicated

1. Mohanty, R.C. and Nanda, B.K., Determination of slip damping in jointed riveted beams by finite element approach, Structural Engineering and Mechanics (SEM).
2. Mohanty, R.C. and Nanda, B.K., Finite element analysis of slip damping in a riveted built-up structure, International Journal of Acoustics and Vibration (IJAV).
3. Mohanty, R.C. and Nanda, B.K., Effect of structural joints on the damping of built-up structures, Journal of Applied Mechanics, ASME.
4. Mohanty, R.C. and Nanda, B.K., Mechanism of energy dissipation in riveted joints, Journal of Vibration and Acoustics, ASME.
5. Mohanty, R.C. and Nanda, B.K., Investigation into the Slip Damping of Layered and Jointed Aluminium Structures, Journal of the Brazilian Society of Mechanical Science and Engineering.
6. Mohanty, R.C. and Nanda, B.K., Effect of thickness ratio on the slip damping of jointed aluminium cantilever beams, International Journal of Design Engineering, Inderscience.